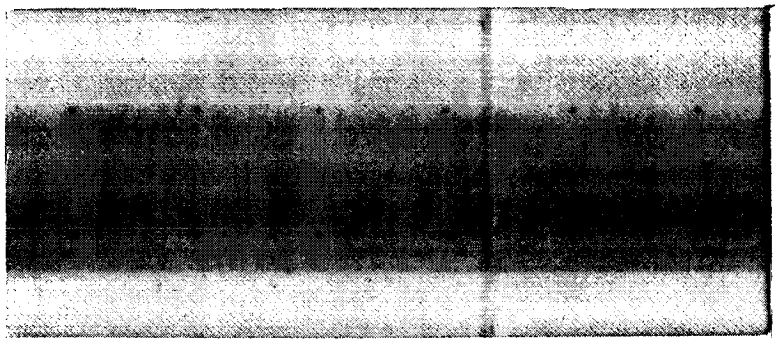

(NASA-CR-181343) VARIATIONAL APPROACH TO PROBABILISTIC FINITE ELEMENTS Final Report, 1 May 1984 - 31 Aug. 1987 (Northwestern Univ.) 178 p Avail: NTIS HC A09/MF A01
CSCL 12A G3/64

N87-29212

Unclas
0097606

Technological Institute
NORTHWESTERN UNIVERSITY
EVANSTON, ILLINOIS

VARIATIONAL APPROACH TO PROBABILISTIC FINITE ELEMENTS

Final Report to NASA Lewis Research Center
Grant No. NAG 3-535
May 1, 1984 to August 31, 1987

By

T. Belytschko, W. K. Liu,
A. Mani and G. Besterfield

Department of Mechanical Engineering
The Technological Institute
Northwestern University
Evanston, Illinois 60208

Publications Under NASA Lewis Grant

Liu, W. K., Belytschko, T. and Mani, A., "A Computational Method for the Determination of the Probabilistic Distribution of the Dynamic Response of Structures," Computer-Aided Engineering, ASME PVP-Vol. 98-5, pp. 243-248, 1985.

Liu, W. K., Belytschko, T. and Mani, A., "Probabilistic Finite Elements for Transient Analysis," presented at the ASME Winter Annual Meeting, Miami, November 1985.

Liu, W. K., Belytschko, T. and Mani, A., "Random Field Finite Elements," International Journal of Numerical Methods in Engineering, Vol. 23, pp. 1831-1845, 1986.

Liu, W. K., Belytschko, T. and Mani, A., "Probabilistic Finite Element Methods for Nonlinear Structural Dynamics," Computer Methods in Applied Mechanics and Engineering, Vol. 56, pp. 61-81, 1986.

Liu, W. K., Belytschko, T., Mani, A. and Besterfield, G. H., "A Variational Principle for Probabilistic Mechanics," Finite Element Methods for Plate and Shell Structures, Vol. 2: Formulations and Algorithms, eds. T. J. R. Hughes and E. Hinton, Pineridge Press, Swansea, U.K., pp. 285-311, 1986.

Liu, W. K., Belytschko, T., Besterfield, G. H. and Mani, A., "Probabilistic Finite Elements and Potential Applications to Fractures," presented at the 4th Army Conference on Applied Mathematics and Computing, May 1986.

Liu, W. K., Belytschko, T. and Besterfield, G. H., "Transient Probabilistic Systems," presented at First World Congress on Computational Mechanics, Austin, Texas, September 1986.

Liu, W. K., Belytschko, T. and Mani, A., "Applications of Probabilistic Finite Element Methods in Elastic/Plastic Dynamics," Journal of Engineering for Industry, ASME, Vol. 109, pp. 2-8, 1987.

Liu, W. K., Mani, A. and Belytschko, T., "Finite Element Methods in Probabilistic Mechanics," to appear in Probabilistic Engineering Mechanics, 1987.

Liu, W. K., Besterfield, G. H. and Belytschko, T., "Transient Probabilistic Systems," to appear in Computer Methods in Applied Mechanics and Engineering, 1987.

Liu, W. K., Besterfield, G. H. and Belytschko, T., "Variational Approach to Proabilistic Finite Elements," submitted to Journal of Engineering Mechanics Division, ASCE, 1987.

Liu, W. K., Besterfield, G. H. and Belytschko, T., "Probabilistic Hu-Washizu Variational Principle," presented at 28th AIAA Structural Dynamics and Materials Conference, Monterey, California, April 1987.

Liu, W. K., Belytschko, T., Mani, A. and Besterfield, G. H., "Probabilistic Finite Elements and Its Applications," presented at Fifth International Conference on Applications of Statistics and Probability in Soil and Structural Engineering (ICASP5), Vancouver, Canada, May 1987.

Probabilistic Finite Element Methods

Probabilistic finite element methods (PFEM), synthesizing the power of finite element methods with second-moment techniques, are formulated for various classes of problems in structural and solid mechanics. Time-invariant random materials, geometric properties and loads are incorporated in terms of their fundamental statistics viz. second-moments. Analogous to the discretization of the displacement field in finite element methods, the random fields are also discretized. Preserving the conceptual simplicity, the response moments are calculated with minimal computations. By incorporating certain computational techniques, these methods are shown to be capable of handling large systems with many sources of uncertainties.

By construction, these methods are applicable when the scale of randomness is not very large and when the probabilistic density functions have decaying tails. The accuracy and efficiency of these methods, along with their limitations, are demonstrated by various applications. Results obtained are compared with those of Monte Carlo simulation and it is shown that good accuracy can be obtained for both linear and nonlinear problems. The methods are amenable to implementation in deterministic FEM based computer codes.

ACKNOWLEDGEMENT

The support of NASA Lewis Grant No. NAG3-535 for this research and the encouragement of Dr. Christos Chamis are gratefully acknowledged.

TABLE OF CONTENTS

LIST OF FIGURES

Page

CHAPTER 2

CHAPTER 4

CHAPTER 5

CHAPTER 1

INTRODUCTION

Traditionally, engineering analysis has been based on deterministic models with well-defined parameters. However, it is increasingly being recognized that uncertainties are often associated with parameters such as material and geometric properties, forces and boundary conditions and that these should be adequately modeled. An example is the degradation of material properties with time as a result of fatigue, wear and long-term creep; such changes in material properties can be treated as uncertainties. In general, the random uncertainties which are included in a stochastic process can be classified into three major categories: (1) physical uncertainty, (2) statistical uncertainty and (3) uncertainty in the model. A detailed discussion of these topics can be found in, for example, Refs. [1-4]. Theoretically, these uncertainties can be modeled as random variables or random fields governed by joint probability density or distribution functions. In practice, the exact joint probability density functions are not always available; it is more likely that only the first few moments such as the mean and covariance are known.

Uncertainty analysis in structural mechanics has concentrated on problems of an almost totally stochastic nature. Within this setting, even a single degree of freedom system with nonlinearities poses a formidable challenge and has not been solved satisfactorily. The most commonly employed solution technique is Monte Carlo simulation (see e.g. [3]). In general, these simulation procedures are computationally

expensive, even though they are easily applicable to both linear and nonlinear systems. For linear systems, nonstatistical methods such as "second-moment analysis", are available [2]. A related second order perturbation technique applied to a special class of linear structural vibrations is discussed in [5]. The emphasis is on the modal decoupling of the equations of motion with uncertain damping. The "second-moment analysis" has also been extended in [6] to define the mean and variance of vector functions. This formulation is mathematically elegant and Kronecker algebra and matrix calculus are employed. While this formulation has also been extended in [7] to linear stochastic systems with colored multiplicative noise, the direct application of this technique to nonlinear structural dynamics is not feasible, because in most nonlinear structural analysis, concern lies more with deviations in loads from a deterministic path and in uncertainties in material properties to which a value can be assigned rather than completely stochastic loads or systems.

The research reported here can be subdivided into two parts: (1) development of a variational principle to embed the probabilistic character of the constitutive properties and loads (which are part of the boundary conditions and body forces) and to obtain the corresponding probabilistic character of the nodal forces; (2) the determination of the probabilistic distribution of the response (displacement and stress) from the probabilistic description of the nodal forces.

The main thrust of this research has been to integrate second-moment based techniques with finite element methods in a method called

probabilistic finite elements (PFEM); finite elements are currently the most versatile tools of analysis in large-scale structural and solid mechanics. Through this synthesis, we have developed versatile and efficient techniques for probabilistic analysis. The investigation is restricted to time invariant uncertainties which may be present as discrete random variables or random fields in material, geometric properties and/or forces. These methods are applicable when the uncertainties are not very large and when the probabilistic density functions or histograms have decaying tails. The most appealing features about PFEM are its conceptual simplicity, ease of computer implementation and the flexibility to accommodate efficient numerical techniques at every stage of the methodology.

PFEM has been formulated for various classes of problems in structural and solid mechanics. In the next chapter, methods are developed for nonlinear structural dynamics with discrete random variables. In Chapter 3, random fields are modeled, essentially by discretization. The encumberances of correlated random variables are avoided by an eigenvalue transformation to the space of uncorrelated random variables. In Chapter 4, these methods are derived from variational principles. The linear formulation is obtained from the potential energy variational principle and the nonlinear counterpart is derived from the principle of virtual work with appropriate stress and strain measures to account for the large deformation. In Chapter 5, numerical applications in elastoplastic mechanics are studied in detail, along with improved computational techniques. The summary and conclusions are presented in Chapter 6.

CHAPTER 2

PROBABILISTIC FINITE ELEMENTS FOR NONLINEAR STRUCTURAL DYNAMICS

2.1 Introduction

It is important to be able to treat the effects of uncertainties in a reasonably economical manner; standard Monte Carlo procedures are simply too expensive. Furthermore, the methods should be designed so that they can be incorporated into widely used finite element programs in a natural and concise manner. Thus, the approach should be integrable with the elemental discretization and nodal assembly procedures that characterize finite element theory and software implementation.

In the next section, the formulation of the probabilistic finite element method (PFEM) is presented. The method is applicable in structural dynamics with discrete random variables with or without correlation. In Section 2.3, the computational aspects of PFEM are discussed. In Section 2.4, the analysis of a two degree of freedom spring-mass probabilistic system is then given. Results are also presented for a ten-bar probabilistic system with nonlinearities. The proposed PFEM method is compared to (1) Monte Carlo simulations (MCS) and (2) Hermite-Gauss Quadrature (HGQ) schemes. All these methods are schematically depicted in Fig. 1, highlighting the major computational steps. In Section 2.5, the relative performance of the PFEM as compared to the other two methods is discussed. The reason for the limitation of each solution technique is also presented.

2.2 Formulation of the Probabilistic Finite Element Method (PFEM)

We consider the structural system to be governed by the following system of nonlinear algebraic equations which arises from a finite element discretization:

$$\underset{\sim}{M}\,\ddot{\underset{\sim}{d}} + \underset{\sim}{f}(\underset{\sim}{b}, \underset{\sim}{d}, \dot{\underset{\sim}{d}}) = \underset{\sim}{F}(t) \tag{2.2.1}$$

where $\underset{\sim}{M}$, $\underset{\sim}{f}$, $\underset{\sim}{d}$ and $\underset{\sim}{F}$ are the generalized mass, internal force, displacement and external force respectively; and a superscript dot represents material time (t) derivative. While the internal and external nodal forces are obtained from one variational statement, they are segregated for convenience. The probabilistic effects are described through the q-dimensional random vector $\underset{\sim}{b}$; this can include the probabilistic distributions of the material properties; the mass $\underset{\sim}{M}$ is assumed to be deterministic. All these probabilistic distributions, as reflected in the variance of the material properties, the composite load spectra, etc. are represented by the generalized variance vector, $\mathrm{Var}(\underset{\sim}{b})$. We shall denote the expected value operator by E[ ] and use second order expansions so E[ ] is given by

$$E[\underset{\sim}{\phi}(\underset{\sim}{b})] \simeq \overline{\underset{\sim}{\phi}} + \frac{1}{2}\frac{\partial^2 \overline{\underset{\sim}{\phi}}}{\partial b_i\, \partial b_j}\,\mathrm{Cov}(b_i, b_j) \tag{2.2.2}$$

where $\underset{\sim}{\phi}$ is a vector function of the random variables. The superposed bar denotes "at the mean value of $\underset{\sim}{b}$" and the symbol Cov represents the covariance; summations on i and j from 1 to q are assumed. If b_i is

uncorrelated to b_j for $i \neq j$, then

$$\mathrm{Cov}(b_i, b_j) = 0 \qquad \text{for } i \neq j \tag{2.2.3a}$$

and

$$\mathrm{Cov}(b_i, b_i) = \mathrm{Var}(b_i) \qquad \text{no sum on } i \tag{2.2.3b}$$

Applying the expected value operator to Eq. (2.2.1) yields

$$E[\underset{\sim}{M}\,\ddot{\underset{\sim}{d}}] + E[\underset{\sim}{f}(\underset{\sim}{b}, \underset{\sim}{d}, \dot{\underset{\sim}{d}})] = E[\underset{\sim}{F}(t)] \tag{2.2.4}$$

Employing Eq. (2.2.2) and the chain rules:

$$E[\underset{\sim}{M}\,\ddot{\underset{\sim}{d}}] \simeq \underset{\sim}{M}\,\bar{\underset{\sim}{a}} + \frac{1}{2}\,\underset{\sim}{M}\,\frac{\partial^2 \bar{\underset{\sim}{a}}}{\partial b_i \partial b_j}\,\mathrm{Cov}(b_i, b_j) \tag{2.2.5a}$$

$$\begin{aligned} E[\underset{\sim}{f}] \simeq\ & \bar{\underset{\sim}{f}} \\ & + \frac{1}{2}\,\frac{\partial^2 \bar{\underset{\sim}{f}}}{\partial b_i \partial b_j}\,\mathrm{Cov}(b_i, b_j) \\ & + \left\{\frac{\partial \bar{\underset{\sim}{C}}}{\partial b_i}\,\frac{\partial \bar{\underset{\sim}{v}}}{\partial b_j} + \frac{\partial \bar{\underset{\sim}{K}}}{\partial b_i}\,\frac{\partial \bar{\underset{\sim}{d}}}{\partial b_j}\right\}\,\mathrm{Cov}(b_i, b_j) \\ & + \frac{1}{2}\left[\bar{\underset{\sim}{C}}\,\frac{\partial^2 \bar{\underset{\sim}{v}}}{\partial b_i \partial b_j} + \bar{\underset{\sim}{K}}\,\frac{\partial^2 \bar{\underset{\sim}{d}}}{\partial b_i \partial b_j}\right\}\,\mathrm{Cov}(b_i, b_j) \end{aligned} \tag{2.2.5b}$$

and

$$E[\underset{\sim}{F}(t)] = \underset{\sim}{F}(t) \tag{2.2.5c}$$

where $\dot{\underset{\sim}{d}}$ and $\ddot{\underset{\sim}{d}}$ have been replaced by $\underset{\sim}{v}$ and $\underset{\sim}{a}$ respectively. The $\underset{\sim}{C}$ and $\underset{\sim}{K}$ matrices are the damping and stiffness matrices, respectively. They are

$$\underset{\sim}{C} = \frac{\partial \underset{\sim}{f}}{\partial \underset{\sim}{v}} \tag{2.2.6a}$$

and

$$\underset{\sim}{K} = \frac{\partial \underset{\sim}{f}}{\partial \underset{\sim}{d}} \tag{2.2.6b}$$

In the case of a linear structure, $\underset{\sim}{f}$ is given by

$$\underset{\sim}{f} = \underset{\sim}{C}\,\underset{\sim}{v} + \underset{\sim}{K}\,\underset{\sim}{d} \tag{2.2.6c}$$

For simplicity, let us assume that Eqs. (2.2.3) holds. This assumption is quite suitable for finite element models which are built up from discrete structural elements, such as bars and beams. Using this simplification and applying perturbation techniques on Eqs. (2.2.5), Eq. (2.2.4) can be shown to yield

$$\underset{\sim}{M}\,\overline{\underset{\sim}{a}} + \overline{\underset{\sim}{f}} = \underset{\sim}{F}(t) \tag{2.2.7a}$$

and

$$\underset{\sim}{M}\,\Delta\underset{\sim}{\bar{a}} + \underset{\sim}{\bar{C}}\,\Delta\underset{\sim}{\bar{v}} + \underset{\sim}{\bar{K}}\,\Delta\underset{\sim}{\bar{d}} = \Delta\underset{\sim}{\bar{F}} \tag{2.2.7b}$$

where

$$\Delta\underset{\sim}{\bar{F}} = -\sum_{j=1}^{q}\left\{\left(\frac{\partial\underset{\sim}{\bar{C}}}{\partial b_j}\frac{\partial\underset{\sim}{\bar{v}}}{\partial b_j} + \frac{\partial\underset{\sim}{\bar{K}}}{\partial b_j}\frac{\partial\underset{\sim}{\bar{d}}}{\partial b_j}\right)\mathrm{Var}(b_j) + \frac{1}{2}\frac{\partial^2\underset{\sim}{\bar{f}}}{\partial b_j^2}\mathrm{Var}(b_j)\right\} \tag{2.2.8a}$$

$$\Delta\underset{\sim}{\bar{a}} = \frac{1}{2}\sum_{j=1}^{q}\frac{\partial^2\underset{\sim}{\bar{a}}}{\partial b_j^2}\mathrm{Var}(b_j) \tag{2.2.8b}$$

$$\Delta\underset{\sim}{\bar{v}} = \frac{1}{2}\sum_{j=1}^{q}\frac{\partial^2\underset{\sim}{\bar{v}}}{\partial b_j^2}\mathrm{Var}(b_j) \tag{2.2.8c}$$

and

$$\Delta\,\underset{\sim}{\bar{d}} = \frac{1}{2}\sum_{j=1}^{q}\frac{\partial^2\underset{\sim}{\bar{d}}}{\partial b_j^2}\mathrm{Var}(b_j) \tag{2.2.8d}$$

Once $\Delta\underset{\sim}{\bar{a}}$, $\Delta\underset{\sim}{\bar{v}}$ and $\Delta\underset{\sim}{\bar{d}}$ are obtained by solving Eq. (2.2.7b), the second-order means are

$$E[\underset{\sim}{\ddot{d}}] = E[\underset{\sim}{a}] \approx \underset{\sim}{\bar{a}} + \Delta\underset{\sim}{\bar{a}} \tag{2.2.9a}$$

$$E[\dot{\underset{\sim}{d}}] = E[\underset{\sim}{v}] \simeq \overline{\underset{\sim}{v}} + \Delta\overline{\underset{\sim}{v}} \tag{2.2.9b}$$

and

$$E[\underset{\sim}{d}] = \overline{\underset{\sim}{d}} + \Delta\overline{\underset{\sim}{d}} \tag{2.2.9c}$$

If one is interested in the deviations in response from a deterministic path due to the uncertainties in material properties to which a value can be assigned, the number of time integrations (simulations) reduces to only two. These two simulations are

$$\underset{\sim}{M}\,\overline{\underset{\sim}{a}} + \overline{\underset{\sim}{f}} = \underset{\sim}{F} \tag{2.2.10a}$$

and

$$\underset{\sim}{M}\,\Delta\underset{\sim}{a} + \overline{\underset{\sim}{C}}\,\Delta\underset{\sim}{v} + \overline{\underset{\sim}{K}}\,\Delta\underset{\sim}{d} = \Delta\underset{\sim}{F} \tag{2.2.10b}$$

where

$$\Delta\underset{\sim}{a} = \sum_{j=1}^{q} \frac{\partial\overline{\underset{\sim}{a}}}{\partial b_j}\,\Delta b_j \tag{2.2.10c}$$

$$\Delta\underset{\sim}{v} = \sum_{j=1}^{q} \frac{\partial\overline{\underset{\sim}{v}}}{\partial b_j}\,\Delta b_j \tag{2.2.10d}$$

$$\Delta \underset{\sim}{d} = \sum_{j=1}^{q} \frac{\partial \underset{\sim}{\bar{d}}}{\partial b_j} \Delta b_j \qquad (2.2.10e)$$

$$\Delta \underset{\sim}{F} = -\sum_{j=1}^{q} \left(\frac{\partial \underset{\sim}{\bar{f}}}{\partial b_j} \Big|_{\underset{\sim}{d},\ \underset{\sim}{v} = \text{constant}} \right) \Delta b_j \qquad (2.2.10f)$$

and Δb_j is equal to the preassigned value of b_j. It is also necessary to obtain the sensitivity vectors, i.e. $\partial(\ )/\partial b_i$; see Section 3.

Finally, once the means and the sensitivity vectors are determined, the variance vectors can be computed easily by the following first order formulas

$$\mathrm{Var}(\underset{\sim}{a}) \simeq \sum_{i,j=1}^{q} \left(\frac{\partial \underset{\sim}{\bar{a}}}{\partial b_i}\right)\left(\frac{\partial \underset{\sim}{\bar{a}}}{\partial b_j}\right) \mathrm{Cov}(b_i, b_j) \qquad (2.2.11a)$$

$$\mathrm{Var}(\underset{\sim}{v}) \simeq \sum_{i,j=1}^{q} \left(\frac{\partial \underset{\sim}{\bar{v}}}{\partial b_i}\right)\left(\frac{\partial \underset{\sim}{\bar{v}}}{\partial b_j}\right) \mathrm{Cov}(b_i, b_j) \qquad (2.2.11b)$$

$$\mathrm{Var}(\underset{\sim}{d}) \simeq \sum_{i,j=1}^{q} \left(\frac{\partial \underset{\sim}{\bar{d}}}{\partial b_i}\right)\left(\frac{\partial \underset{\sim}{\bar{d}}}{\partial b_j}\right) \mathrm{Cov}(b_i, b_j) \qquad (2.2.11c)$$

In the case of uncorrelated $\underset{\sim}{b}$'s, the covariance matrix becomes a diagonal matrix and the diagonal terms are denoted by

$$\mathrm{Var}(\underset{\sim}{a}) \simeq \sum_{j=1}^{q} \left(\frac{\partial \underset{\sim}{\bar{a}}}{\partial b_j}\right)^2 \mathrm{Var}(b_j) \qquad (2.2.12a)$$

$$\mathrm{Var}(\underset{\sim}{v}) \simeq \sum_{j=1}^{q} \left(\frac{\partial \underset{\sim}{\bar{v}}}{\partial b_j}\right)^2 \mathrm{Var}(b_j) \qquad (2.2.12b)$$

$$\mathrm{Var}(\underset{\sim}{d}) \simeq \sum_{j=1}^{q} \left(\frac{\partial \overline{\underset{\sim}{d}}}{\partial b_j}\right)^2 \mathrm{Var}(b_j) \qquad (2.2.12c)$$

Similar procedures can also be developed for the probabilistic distributions of stresses. However, this direct approach can be very expensive if the number of random variables is greater than the number of requested probabilistic distributions of stresses. For this situation, an alternative approach, termed an adjoint probabilistic stress analysis, is developed. This is described in [12].

Remark 1 The uncertainties discussed here are described by discrete random variables. Physical parameters, such as material properties, are often continuous functions in space. When there are uncertainties associated with these parameters, we have random fields. The probabilistic distributions at any two points can be represented by a "correlation function." One way to adapt the above procedures to "random fields" is to first do a finite element discretization of the correlation function and thus obtain the covariance matrix. Once this matrix is obtained the PFEM method as developed here could be used with minor modifications.

Remark 2 To the author's knowledge, Eqs. (2.2.7) through (2.2.12) represent the first consistently derived second moment probabilistic finite element method (PFEM) which can readily be adapted to existing deterministic finite element computer programs. The second order

terms $\overline{\Delta \underset{\sim}{a}}$, $\overline{\Delta \underset{\sim}{v}}$ and $\overline{\Delta \underset{\sim}{d}}$ are computed directly from the second moment mean Eq. (2.2.7b). Consequently Eqs. (2.2.9) are second order accurate and Eqs. (2.2.11) are first order accurate.

Remark 3 The complete probability distributions are not available for most random variables except perhaps the first two moments. Methods such as MCS or HGQ usually require knowledge of probability density functions. The PFEM method requires only the first two moments and is therefore widely applicable.

2.3 Computational Aspects of PFEM

The computing procedures essentially involve time integrations of the various equations derived in the previous section. In general, the sensitivity vectors can be obtained directly by integrating the sensitivity equations in time. However, this is not possible for some nonlinear systems. In such cases, the usual procedure is to calculate the derivatives by finite differences [1]. Calculating the finite difference derivatives increases the computation for a probabilistic system. However, results obtained are excellent when compared to the solutions obtained by other methods. The computing procedures for linear and nonlinear systems are described separately below.

Linear Systems

For a linear system, Eqs. (2.2.7) become

$$\underset{\sim}{M}\,\bar{\underset{\sim}{a}} + \bar{\underset{\sim}{C}}\,\bar{\underset{\sim}{v}} + \bar{\underset{\sim}{K}}\,\bar{\underset{\sim}{d}} = \underset{\sim}{F}(t) \tag{2.3.1a}$$

$$\underset{\sim}{M}\,\Delta\bar{\underset{\sim}{a}} + \bar{\underset{\sim}{C}}\,\Delta\bar{\underset{\sim}{v}} + \bar{\underset{\sim}{K}}\,\Delta\bar{\underset{\sim}{d}} = \Delta\bar{\underset{\sim}{F}} \tag{2.3.1b}$$

The solutions of Eq. (2.2.7a) and (2.2.7b) are obtained in sequence so that the additional computation due to the latter is minimized. The solution algorithms, such as implicit and/or explicit time integration, used in Eq. (2.3.1a) can be applied directly to Eq. (2.3.1b) with the formulation of only one additional vector function $\Delta\bar{\underset{\sim}{F}}$.

If we examine Eq. (2.2.8a) closely, it can be shown that $\overline{\Delta F}$ can be computed element-wise once $\overline{v}$, $\overline{d}$, $\frac{\partial \overline{v}}{\partial b_j}$ and $\frac{\partial \overline{d}}{\partial b_j}$ are given. In addition, the corresponding variation of the elemental nodal forces can then be assembled into a description of the probabilistic distribution of the elemental nodal forces for the complete finite element model.

It can be easily shown that the governing equations for the sensitivity vectors are obtained by differentiating Eq. (2.2.1) with respect to b_j. They are

$$\underset{\sim}{M} \frac{\partial \overline{a}}{\partial b_j} + \underset{\sim}{\overline{C}} \frac{\partial \overline{v}}{\partial b_j} + \underset{\sim}{\overline{K}} \frac{\partial \overline{d}}{\partial b_j} = \frac{\partial \hat{F}}{\partial b_j} \tag{2.3.2a}$$

where

$$\frac{\partial \hat{F}}{\partial b_j} = - \frac{\partial \overline{f}}{\partial b_j} \Bigg|_{\underset{\sim}{d},\underset{\sim}{v} = \text{constant}} \tag{2.3.2b}$$

or

$$\frac{\partial \hat{F}}{\partial b_j} = - \frac{\partial \overline{C}}{\partial b_j} \overline{v} - \frac{\partial \overline{K}}{\partial b_j} \overline{d} \tag{2.3.2c}$$

From Eqs. (2.3.1a-b) and (2.3.2a); it can be seen that the whole procedure uses the same effective stiffness matrix so only one matrix needs to be triangulated.

To evaluate the mean and variance from Eqs. (2.2.9) and (2.2.12), the total number of time integrations required is q + 2. These are: one integration to evaluate the displacement, velocity and acceleration

at the mean value of $\underset{\sim}{b}$ (Eq. 2.3.10a); 'q' integrations to evaluate the sensitivity vectors (Eq. 3.2a); and one more integration to evaluate the second order variations (Eq. 2.3.1b). The computational steps involved in PFEM are shown in Fig. 2. Notice that all time integrations employ the same effective stiffness matrix; parallel computation procedures could be employed, thereby increasing the efficiency tremendously.

Systems with Material and Geometrical Nonlinearities

As in the linear case, the displacement, velocity and acceleration, at the mean value of $\underset{\sim}{b}$ is obtained by integrating Eq. (2.2.7a). The relative merits between implicit and explicit time integrations are considered here for a probabilistic nonlinear system.

By total differentiation of Eq. (2.2.10a) with respect to B_j, i.e. d/db_j, we have:

$$\underset{\sim}{M} \frac{d\overline{\underset{\sim}{a}}}{db_j} + \frac{d\overline{\underset{\sim}{f}}}{db_j} = \underset{\sim}{0} \tag{2.3.3a}$$

and

$$\underset{\sim}{M} \frac{d^2\overline{\underset{\sim}{a}}}{db_j^2} + \frac{d^2\overline{\underset{\sim}{f}}}{db_j^2} = \underset{\sim}{0} \tag{2.3.3b}$$

Equations (2.2.7a) and (2.3.3a) can be written as

$$\underset{\sim}{M}\, \overline{\underset{\sim}{a}}_{n+1} + \overline{\underset{\sim}{f}}_{n+1} = \underset{\sim}{F}(t_{n+1}) \tag{2.3.4a}$$

and

$$\underset{\sim}{M}\frac{\partial \overline{\underset{\sim}{a}}_{n+1}}{\partial b_j} + \overline{\underset{\sim}{K}}\frac{\partial \overline{\underset{\sim}{d}}_{n+1}}{\partial b_j} = -\frac{\partial \overline{\underset{\sim}{f}}}{\partial b_j}(\underset{\sim}{b}, \underset{\sim}{d}_{n+1}) \tag{2.3.4b}$$

where $\overline{\underset{\sim}{f}}_{n+1}$ and $\overline{\underset{\sim}{K}}$ are the internal force vector and the "tangent stiffness matrix", respectively, evaluated at $\overline{\underset{\sim}{b}}$, $\overline{\underset{\sim}{d}}_{n+1}$ and t_{n+1}. Equations (2.3.4a) and (2.3.4b) can be solved by the implicit Newmark-β algorithm [10]. The "mean value" equation (2.3.4a) can be solved by Newton-Raphson iteration

$$\overline{\underset{\sim}{K}}^{*}\,\Delta\underset{\sim}{a}_{n+1}^{\nu+1} = \overline{\underset{\sim}{r}}_{n+1}^{\nu} \tag{2.3.5a}$$

where the residual vector is given by

$$\overline{\underset{\sim}{r}}_{n+1}^{\nu} = \left[\underset{\sim}{F}_{n+1} - \overline{\underset{\sim}{f}}_{n+1} - \underset{\sim}{M}\,\overline{\underset{\sim}{a}}_{n+1}\right]^{\nu} \tag{2.3.5b}$$

and the effective stiffness matrix is

$$\overline{\underset{\sim}{K}}^{*} = \left\{\underset{\sim}{M} + \beta\Delta t^2\,\overline{\underset{\sim}{K}}\right\}^{\nu} \tag{2.3.5c}$$

The symbol ν represents the equilibrium iteration counter at time step n+1 and iterations are repeated until $\Delta\underset{\sim}{a}_{n+1}^{\nu+1}$ approaches zero.

Similarly, the first order sensitivity equation (2.3.4b) can be written as

$$\overline{\underset{\sim}{K}}^{*} \frac{\partial \overline{\underset{\sim}{d}}_{n+1}}{\partial b_j} = -\beta \Delta t^2 \frac{\partial \overline{\underset{\sim}{f}}_{n+1}}{\partial b_j} + \underset{\sim}{M} \frac{\partial \hat{\underset{\sim}{d}}_{n+1}}{\partial b_j} \tag{2.3.6a}$$

where

$$\frac{\partial \hat{\underset{\sim}{d}}_{n+1}}{\partial b_j} = \frac{\partial \overline{\underset{\sim}{d}}_{n}}{\partial b_j} + \Delta t \frac{\partial \overline{\underset{\sim}{v}}_{n}}{\partial b_j} + (\tfrac{1}{2} - \beta)\Delta t^2 \frac{\partial \overline{\underset{\sim}{a}}_{n}}{\partial b_j} \tag{2.3.6b}$$

It is observed here that the effective stiffness matrix $\overline{\underset{\sim}{K}}^{*}$ is <u>identical</u> in both Eq. (2.3.5a) and Eq. (2.3.6a). Since the triangulated $\overline{\underset{\sim}{K}}^{*}$ is given during the iteration procedures, $\frac{\partial \overline{\underset{\sim}{d}}_{n+1}}{\partial b_j}$ can be obtained simply by forward reductions and back substitutions; therefore, the number of time integrations is still q + 2.

The main advantage of employing implicit time integration is its unconditional stability. Therefore, the above methods are best suited for structural dynamics problems dominated by low frequency response. For impulsive and short duration transient problems, Eq. (2.2.7a), (2.3.3a) and (2.3.3b) can alternatively be solved by explicit integrations. Since $\underset{\sim}{f}(\underset{\sim}{b}, \underset{\sim}{d})$ is nonlinear, the sensitivity vectors can be obtained by central-differences. Equations (2.3.3a) and (2.3.3b) are approximated by

$$\underset{\sim}{M} \left(\frac{\underset{\sim}{a}^{+} - \underset{\sim}{a}^{-}}{2\Delta b_j}\right) + \left(\frac{\underset{\sim}{f}^{+} - \underset{\sim}{f}^{-}}{2\Delta b_j}\right) = \underset{\sim}{0} \tag{2.3.7a}$$

and

$$\underset{\sim}{M} \left(\frac{\underset{\sim}{a}^{+} - 2\overline{\underset{\sim}{a}} + \underset{\sim}{a}^{-}}{\Delta b_j^2}\right) + \left(\frac{\underset{\sim}{f}^{+} - 2\overline{\underset{\sim}{f}} + \underset{\sim}{f}^{-}}{\Delta b_j^2}\right) = \underset{\sim}{0} \tag{2.3.7b}$$

where

$$\underset{\sim}{a}^{+} = \underset{\sim}{a}(\overline{\underset{\sim}{b}} + \Delta\underset{\sim}{b}_j) \tag{2.3.7c}$$

$$\underset{\sim}{a}^{-} = \underset{\sim}{a}(\overline{\underset{\sim}{b}} - \Delta\underset{\sim}{b}_j) \tag{2.3.7d}$$

and

$$\underset{\sim}{f}^{+} = \underset{\sim}{f}(\overline{\underset{\sim}{b}} + \Delta\underset{\sim}{b}_j, \underset{\sim}{d}^{+}) \tag{2.3.7e}$$

$$\underset{\sim}{f}^{-} = \underset{\sim}{f}(\overline{\underset{\sim}{b}} - \Delta\underset{\sim}{b}_j, \underset{\sim}{d}^{-}) \tag{2.3.7f}$$

$\underset{\sim}{d}^{+}$ and $\underset{\sim}{d}^{-}$ are similarly defined and $\Delta\underset{\sim}{b}_j$ is defined by

$$\Delta\underset{\sim}{b}_j = (0, 0, \ldots, \Delta b_j, 0, \ldots, 0)^T \tag{2.3.7g}$$

where T denotes the transpose. With this computational procedure, the total number of time integrations would still be q + 2. However, the number of internal force calculations would be 2q + 1. These are: one integration for the mean Eq. (2.2.7a) and 2q integrations with finite differencing for Eq. (2.3.7a) and Eq. (2.3.7b). Apart from purely implicit or purely explicit algorithms, mixed time implicit-explicit algorithms [4] could also be employed so that the attributes of each of the algorithms can be achieved.

2.4 Numerical Examples

Example 1: A Two-Degree-of-Freedom Spring-Mass System.

The performance of PFEM, the new method developed here, is evaluated via a two-degree-of-freedom spring-mass system. The mean is second order accurate and the variance is first order accurate in this example. The computed results are compared with those obtained employing (1) Monte Carlo Simulation (MCS) and (2) Hermite-Gauss Quadrature (HGQ) schemes. The two latter methods as implemented here are reviewed in Appendix A.

The problem statement is depicted in Fig. 3. A sinusoidal vector forcing function is used:

$$\underset{\sim}{F}(t) = \begin{bmatrix} 0.0 \\ 25.0 \times 10^6 \sin 2000t \end{bmatrix} \qquad (2.4.1)$$

The random spring constants K_1 and K_2 are normally distributed with a coefficient of variation (i.e. σ/μ) equal to 0.05. The mean spring constants are 24×10^6 and 12×10^6 respectively. The deterministic masses m_1 and m_2 are 0.372 and 0.248 respectively. A stiffness-proportional damping of 3% is included. The probabilistic equations derived earlier are solved by the implicit Newmark-β method [3]. The mean amplitude $\bar{d}_1$ is depicted in Fig. 4, for all the three numerical methods -- PFEM, HGQ and MCS. The PFEM solution compares very well with the other two methods. For the variance of d_1 the PFEM solution plotted

in Fig. 5, seems to overshoot the variance at large times. The mean and variance of d_2 are similarly compared and depicted in Figs. 6 and 7. The maximum coefficient of variation of the displacements d_1 and d_2 are found to 0.13 and 0.10 respectively. The $\pm 3\sigma$ bounds for the displacements d_1 and d_2 are plotted in Figs. 8 and 9 respectively.

Example 2: A Ten-Bar Probabilistic System with Material and Geometrical Nonlinearities.

The problem statement is depicted in Fig. 10. The load time function, which is also shown in Fig. 10, is applied at node 3. This particular load-time history is chosen such that only four of the ten bars, elements 1, 3, 7 and 8, will yield. Therefore the probabilistic model can be simplified by choosing the yield stresses of these four elements as the normal random variables which have the major impact on the response. The coefficient of variation is 0.05. Since the other six elements do not come close to yield, they are considered deterministic variables. With this approach, instead of 59049 analyses, only 81 analyses are required for the Hermite Gauss Quadrature method. The justification for this drastic simplification is explained in detail in Appendix A.

For the PFEM method, the finite difference derivatives are evaluated with an interval Δb_j equal to $0.05\ \bar{b}_j$ and the equations are solved by explicit time integration. The mean is second-order accurate whereas the variance is first-order accurate. The Monte Carlo Simulation results are obtained with 400 simulations.

The probabilistic displacement and stress solutions at selected

locations are given in Figs. 11 through 14. The maximum coefficient of variation of the displacement of node 1 is found to be 0.13 and that of the stress in element 1 is 0.11. For this example, the three methods (PFEM, HGQ and MCS) have been employed and they all compare quite well.

The bounds of the displacement and stress can be estimated based on the Chebyschev inequality

$$P(|x - \mu| > n\sigma) < \frac{1}{n^2} \quad , \qquad n > 0 \tag{2.4.2}$$

where $\mu = E(x)$ and $\sigma^2 = Var(x)$. The $\pm 3\sigma$ bounds (i.e., $n = 3$) for the displacement and stress are plotted in Figs. 15 and 16, and the solutions can be expected to be within these bounds with 89% confidence level.

2.5 Comparisons Among the Three Methods and Conclusions

Based on these numerical studies, we have drawn the following tentative conclusions:

1) Although all three methods agree very well and are evidently comparable in accuracy, PFEM is the most efficient solution procedure for small to medium size problems. The relative computational efficiency of the three methods is summarized in Figure 17.

Relative Computational Efficiency of Three Probabilistic Methods.

	PFEM	HGQ	MCS
2 bar Structure	1	8	400
10 bar Structure	1	4	60

Figure 17

The number of time integrations required for a general structure with q random variables can be summarized as follows:

i) PFEM with partial derivatives evaluated directly: $q + 2$

ii) PFEM with partial derivatives evaluated by finite difference: $2q + 1$

iii) HGQ with three-point quadrature : 3^q

iv) MCS with simple Monte Carlo Simulation of sample size N : N

2) Although PFEM is expected to be most accurate when the variances are small, it performs quite well even when the response shows a large coefficient of variation (e.g., 0.13 for the displacement at Node 1 in the ten-bar structure). This could be attributed partly to the nature of the probabilistic distribution. For most distributions, values of response far- away from the mean are less likely to be found than those near the mean. Hence second moment analysis about the mean turns out to be quite accurate.

3) The three methods are applicable to linear and nonlinear systems. In linear systems the partial derivatives can be obtained directly. In nonlinear system the brute force method is to obtain these derivatives by finite differences. We are currently investigating ways to compute these derivatives efficiently. However, the methods are problem dependent.

4) A minor drawback of PFEM is that its accuracy deteriorates for large times even with structural damping. An explanation is given in Appendix B. We are currently investigating several ways of improving this.

5) PFEM can be easily incorporated into widely used finite element programs.

6) A PFEM analysis can be obtained with $q + 2$ simulations if $Cov(b_i, b_j) \neq 0$ for $i \neq j$. For this purpose the b_i must be transformed into

another set of random variables c_j through an eigenproblem such that $Cov(c_i, c_j) = 0$ for $i \neq j$ and in most cases only a few modes are sufficient [13].

7) Currently the PFEM is being extended to the transient analysis of nonlinear continua. The details of the method can be found in [5].

Since this method involves only matrix and vector assembly it can be incorporated in a natural and concise manner in general purpose finite element programs.

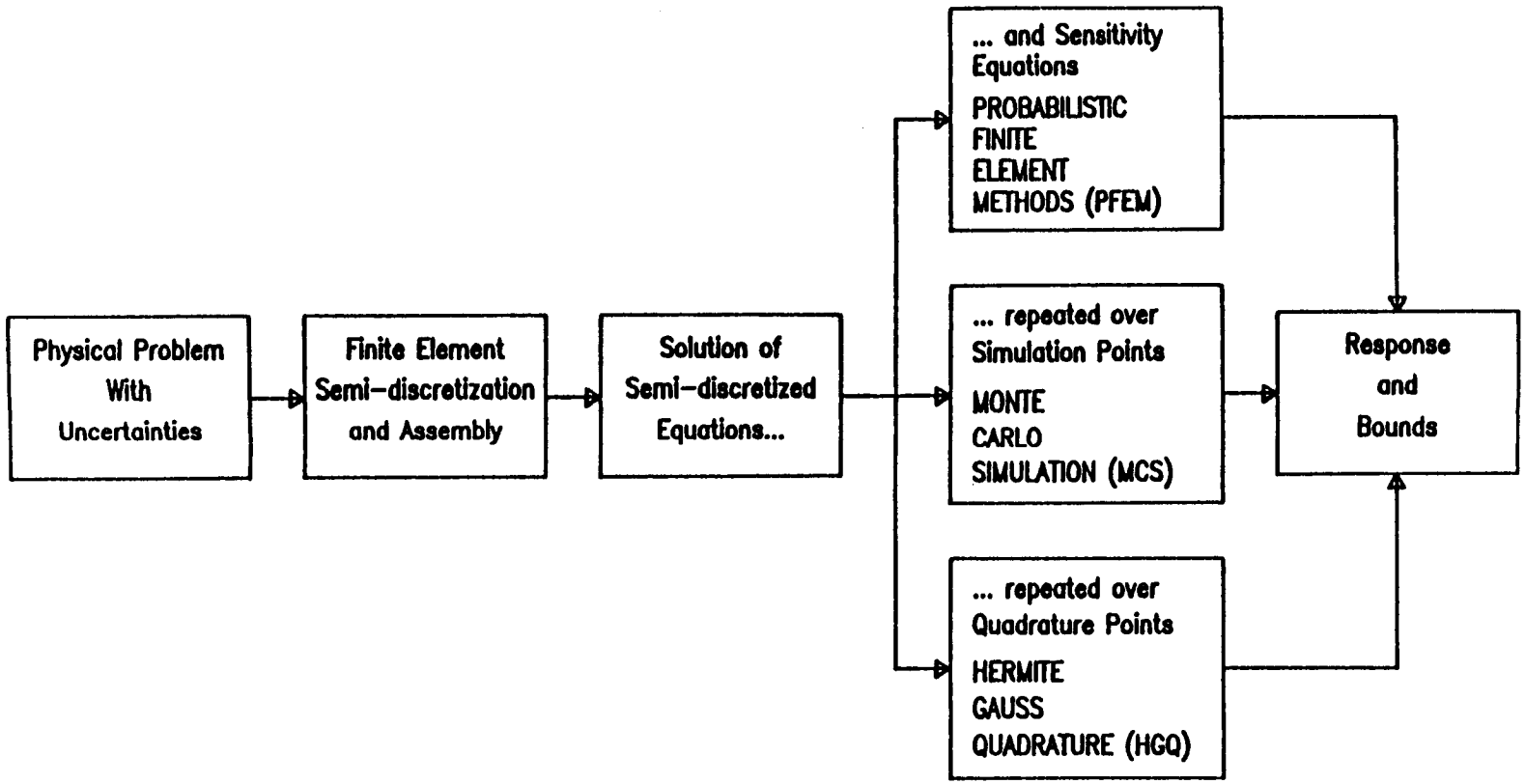

Schematic of Probabilistic Methods

Figure 1

ITEM	CALCULATED QUANTITIES	EQUATION NUMBERS	NUMBERS OF INTEGRATIONS
1	The mean values i.e. $\bar{\underline{d}}$, $\bar{\underline{v}}$ and $\bar{\underline{a}}$	(3.1a)	1
2	The sensitivity derivatives for each random variable b_j, $j = 1, \ldots, q$ i.e., $\frac{\partial \bar{\underline{d}}}{\partial b_j}$, $\frac{\partial \bar{\underline{v}}}{\partial b_j}$ and $\frac{\partial \bar{\underline{a}}}{\partial b_j}$	(3.2a)	q
3	The second order variations i.e., $\Delta\bar{\underline{d}}$, $\Delta\bar{\underline{v}}$ and $\Delta\bar{\underline{a}}$	(3.1b)	1
			Total = q + 2

Computational Steps in PFEM

Figure 2

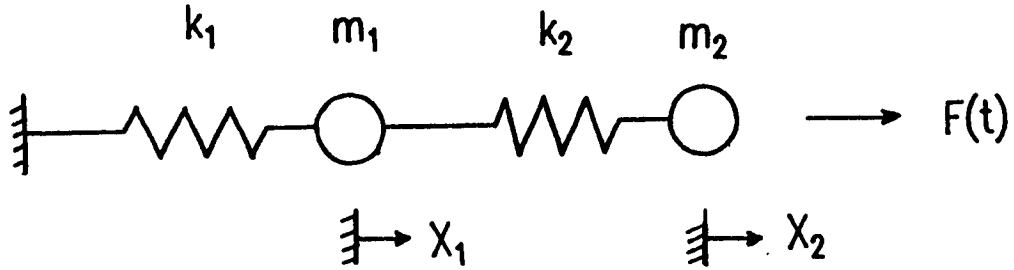

$$F(t)=25.0 \times 10^6 \sin(2000t)$$

$m_1=0.372$ $\quad k_1=24.0 \times 10^6$

$m_2=0.248$ $\quad k_2=12.0 \times 10^6$

A Two Degree of Freedom Example

Figure 3

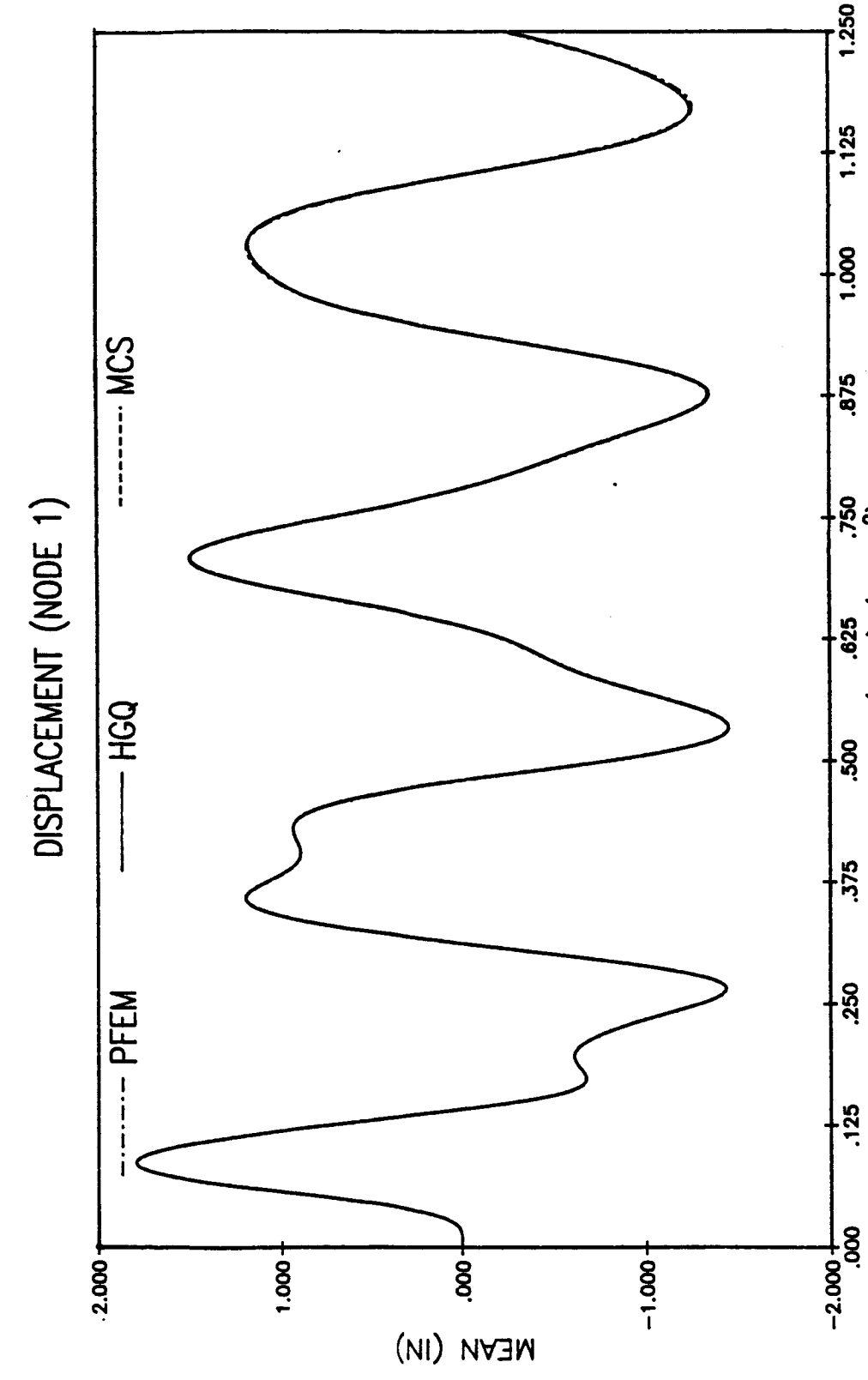

Comparison of the Mean Displacement at Node 1

Figure 4

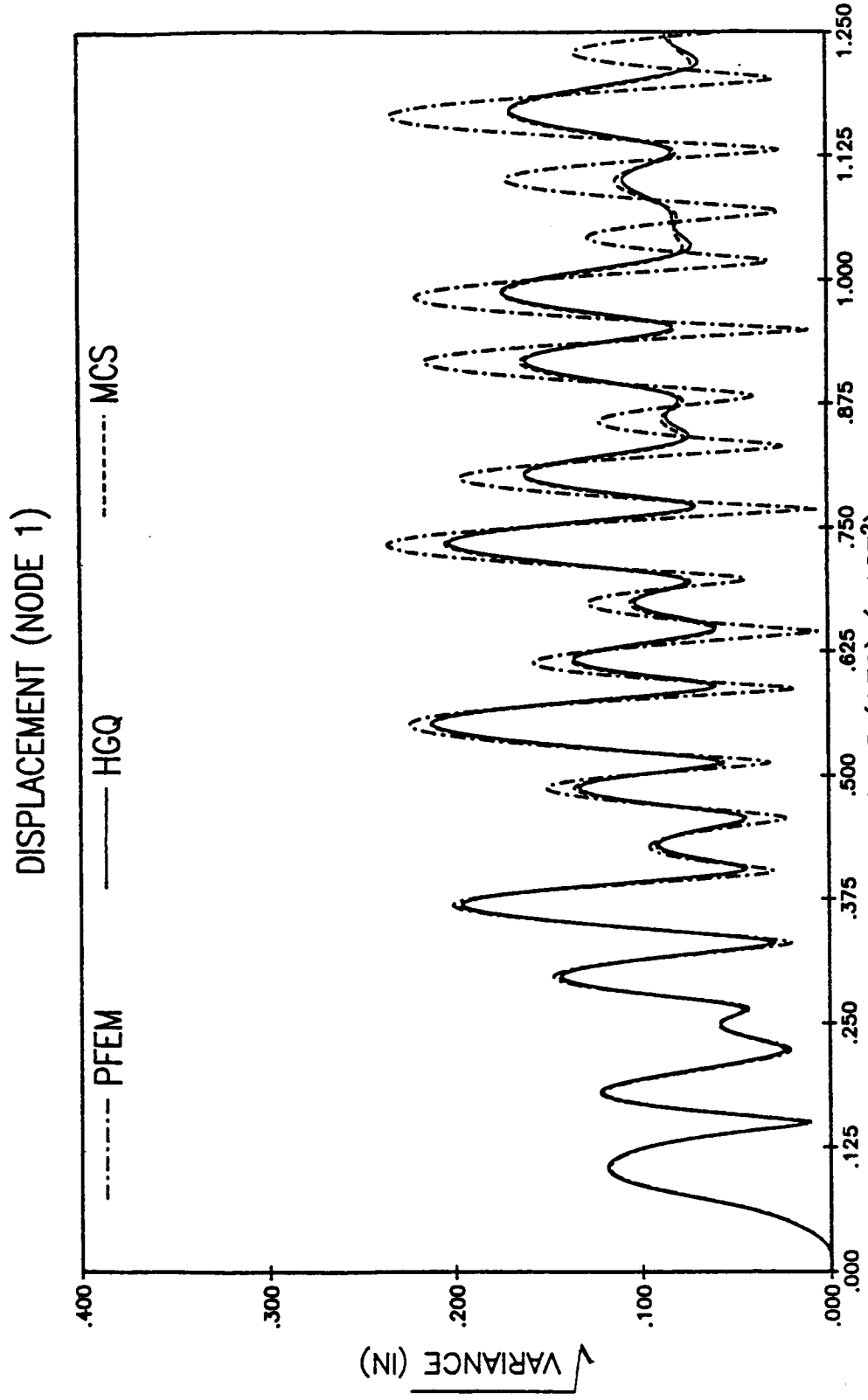

Comparison of the Variance of Displacement at Node 1

Figure 5

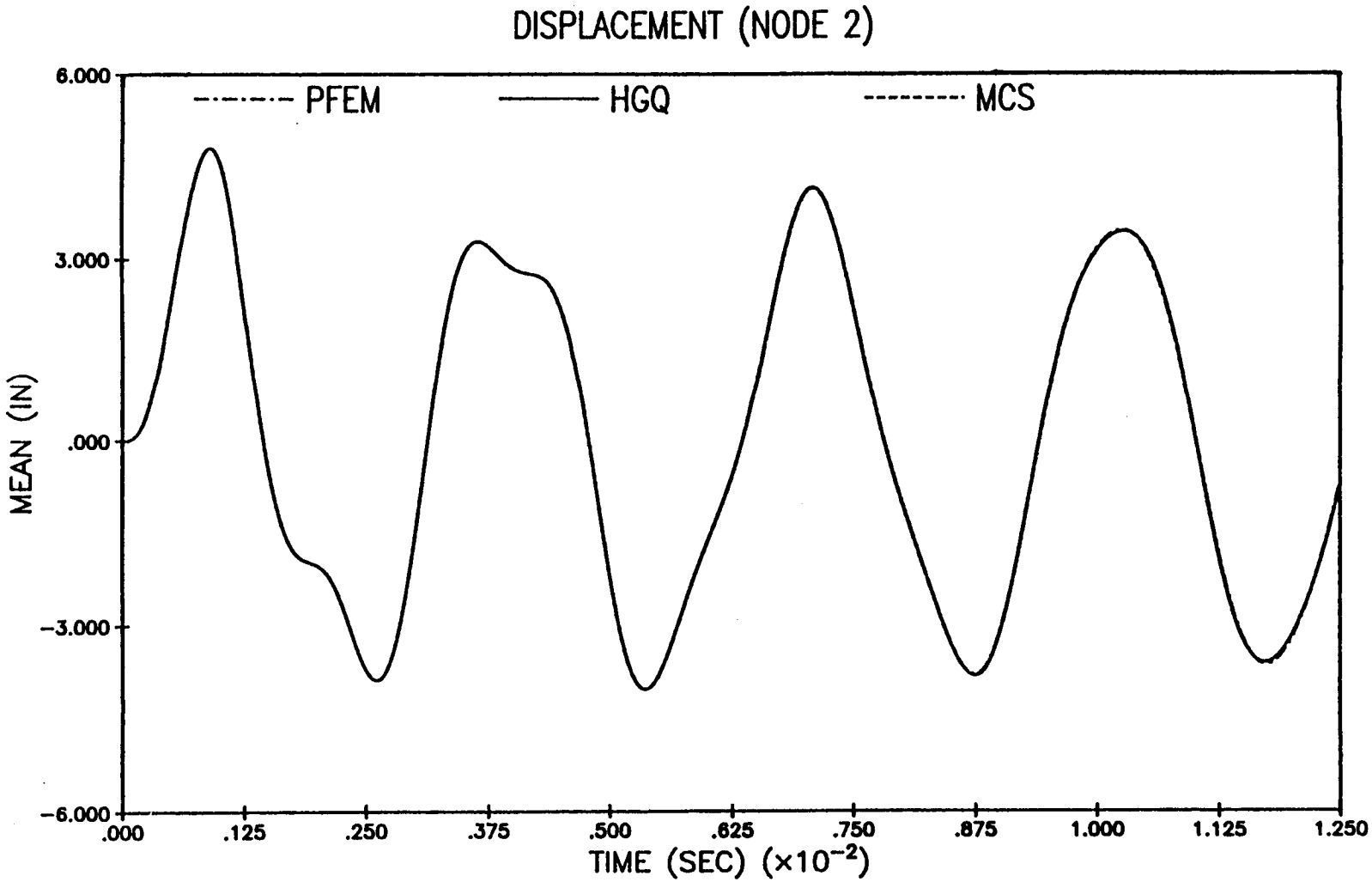

Comparison of the Mean Displacement at Node 2
Figure 6

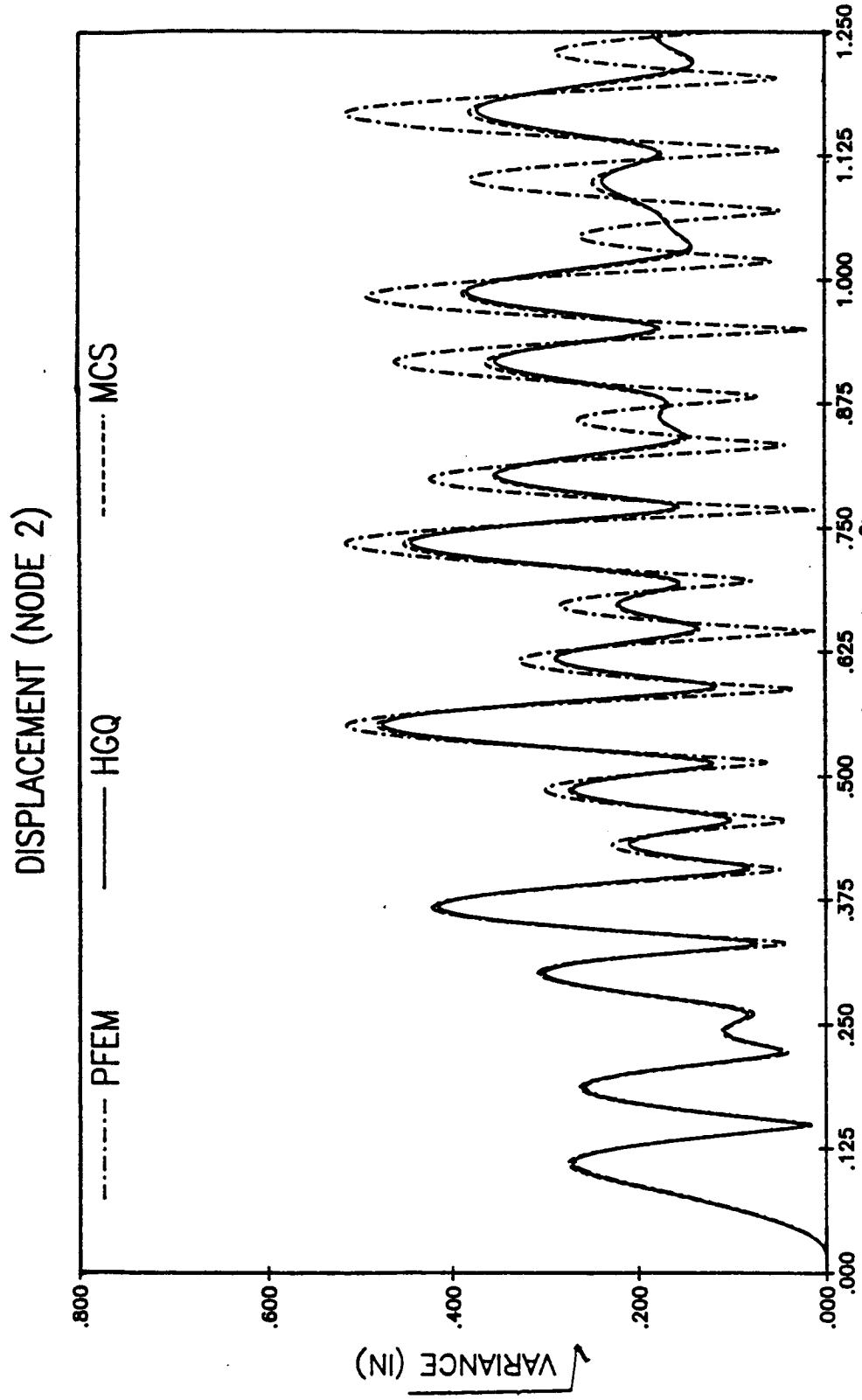

Comparison of the Variance of Displacement at Node 2

Figure 7

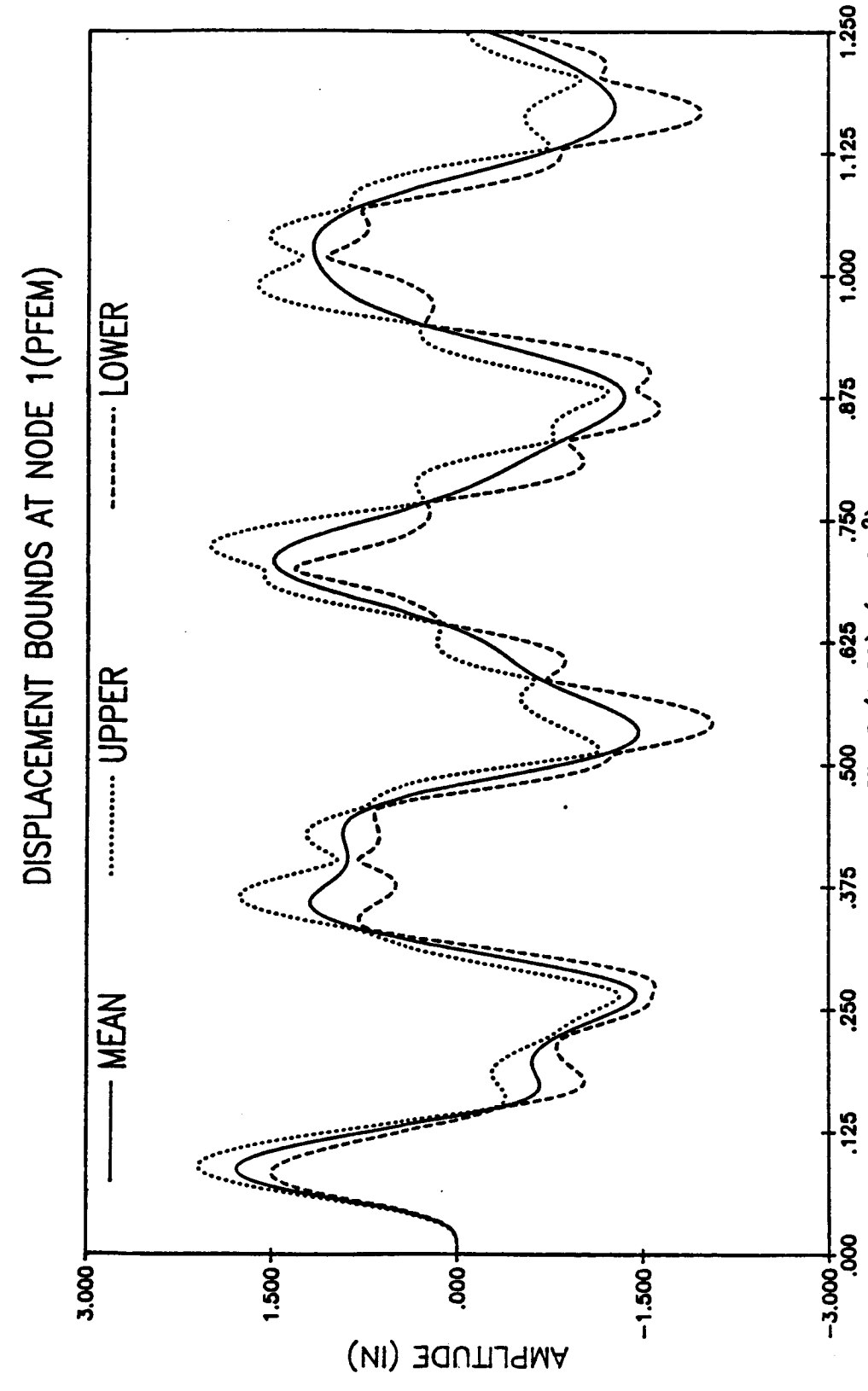
DISPLACEMENT BOUNDS AT NODE 1(PFEM)
MEAN
UPPER
LOWER
AMPLITUDE (IN)
3.000
1.500
.000
-1.500
-3.000
.000
.125
.250
.375
.500
.625
.750
.875
1.000
1.125
1.250
TIME (SEC) (×10⁻²)

Figure 8

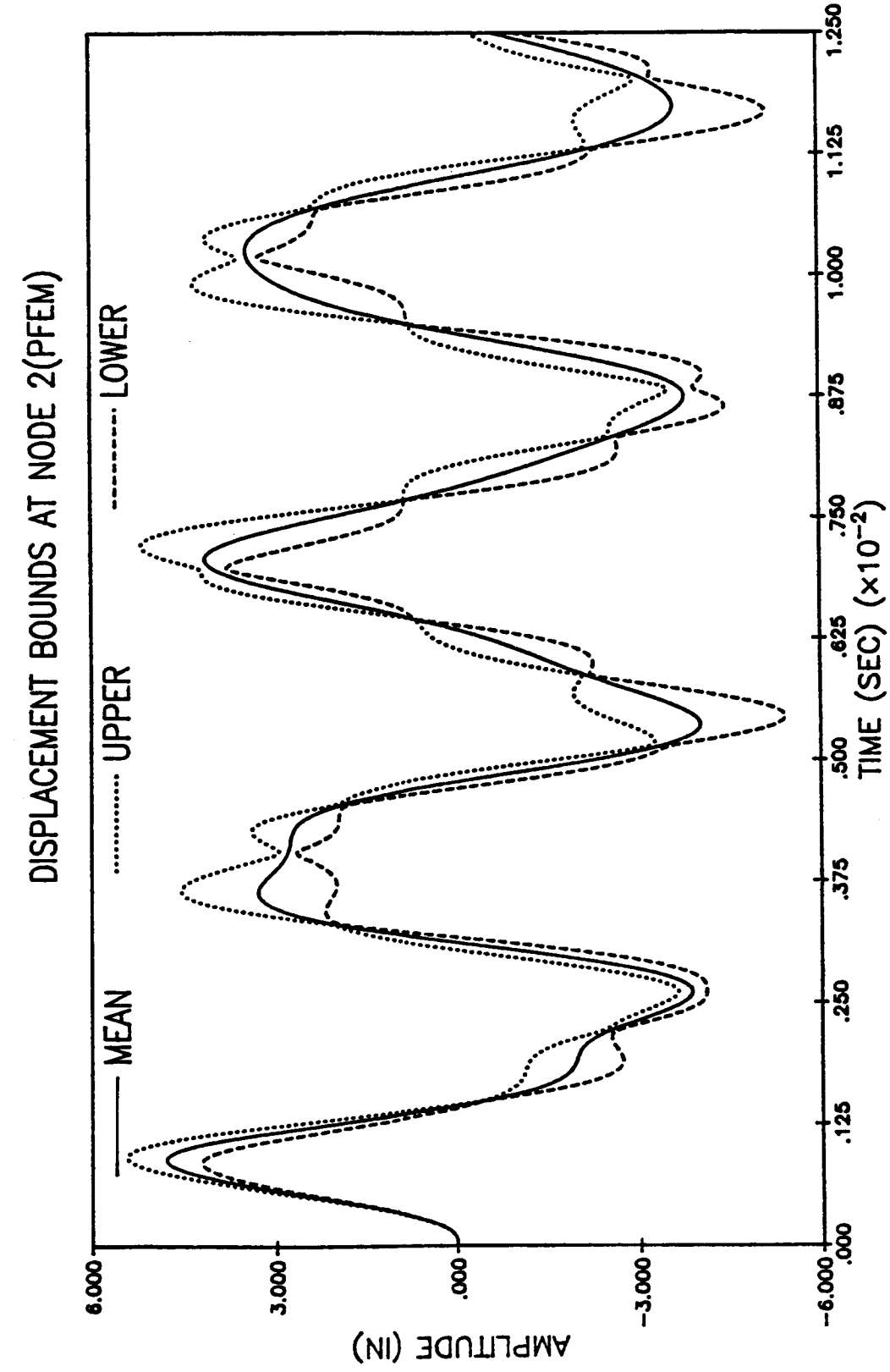
DISPLACEMENT BOUNDS AT NODE 2(PFEM)
MEAN
UPPER
LOWER
AMPLITUDE (IN)
6.000
3.000
.000
-3.000
-6.000
.000
.125
.250
.375
.500
.625
.750
.875
1.000
1.125
1.250
TIME (SEC) (×10⁻²)

Figure 9

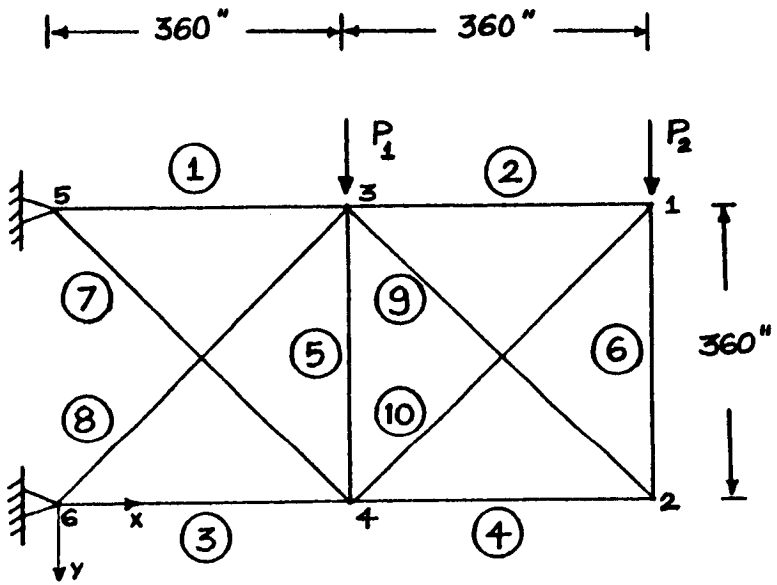

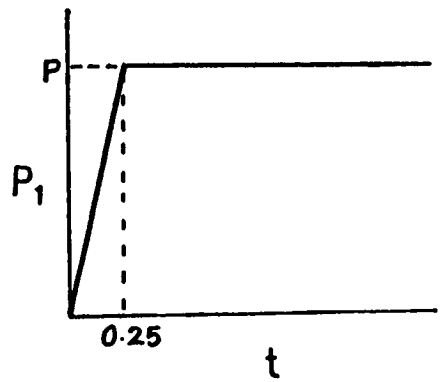

$E = 30.0 \times 10^6$

$E_T = 30.0 \times 10^4$

$A = 6.0$

$\rho = 0.30$

$\sigma_Y = 15000.0$

$P = 175.0 \times 10^3$

$P_2 = 0.0$

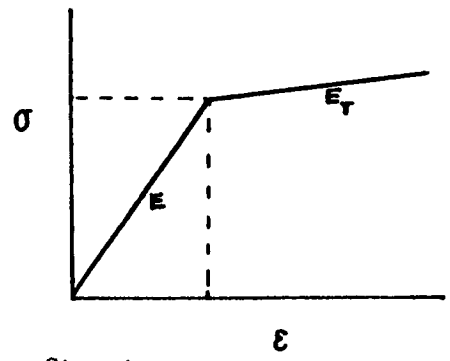

Problem Statement: Ten-Bar Nonlinear Structure

Figure 10

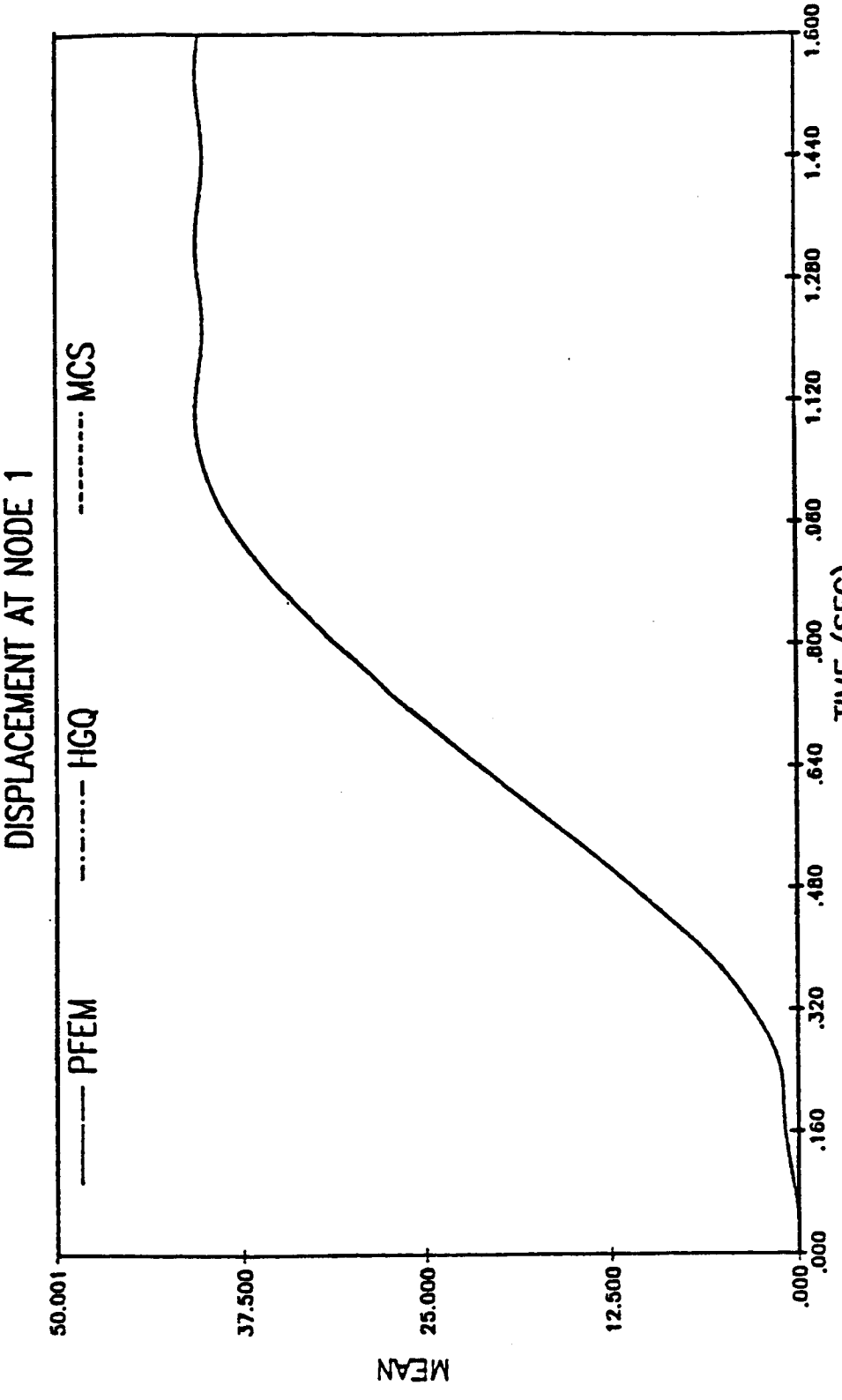

Comparison of the Mean y-Displacement of Node 1

Figure 11

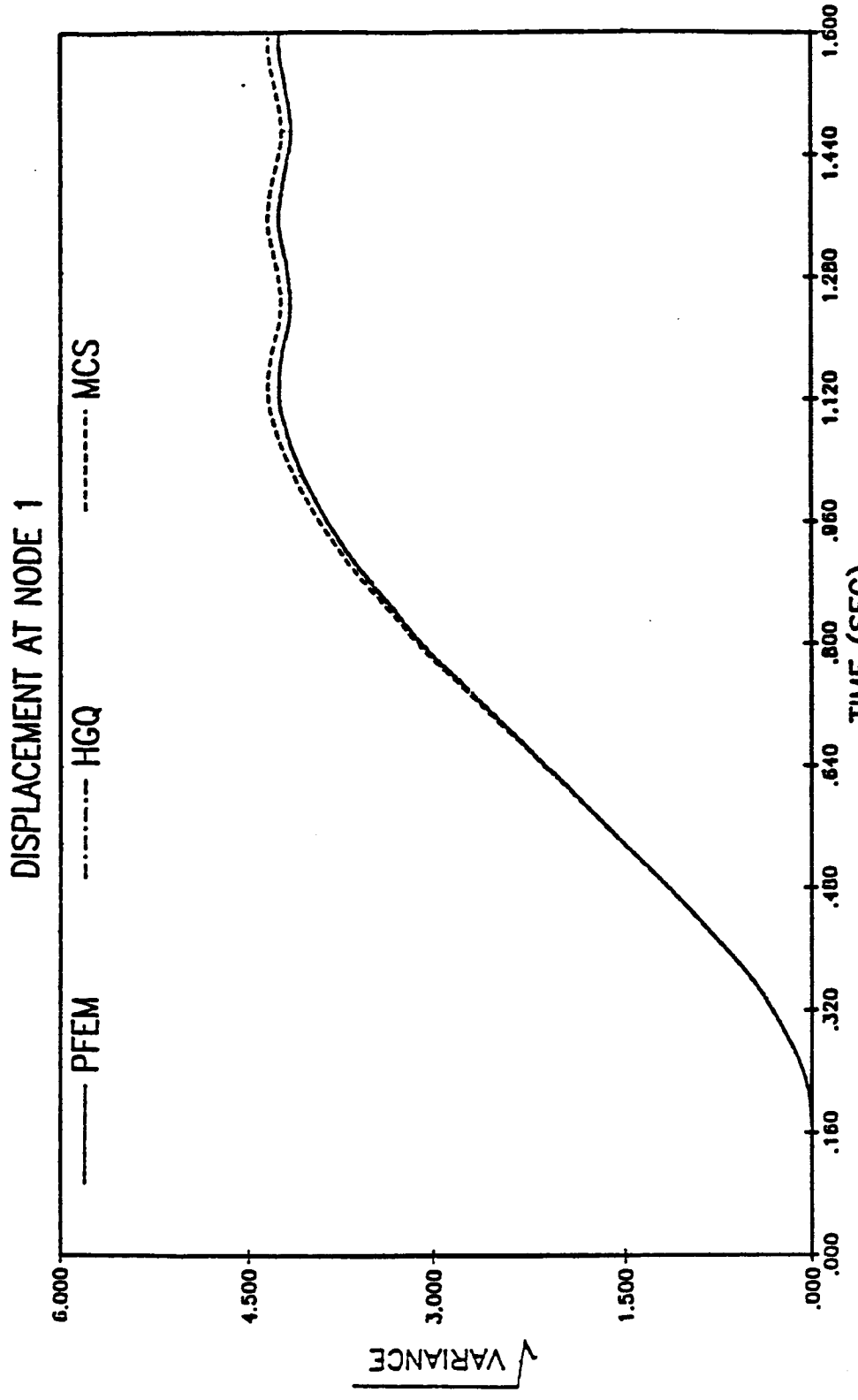

Comparison of the Variance of the y-Displacement of Node 1

Figure 12

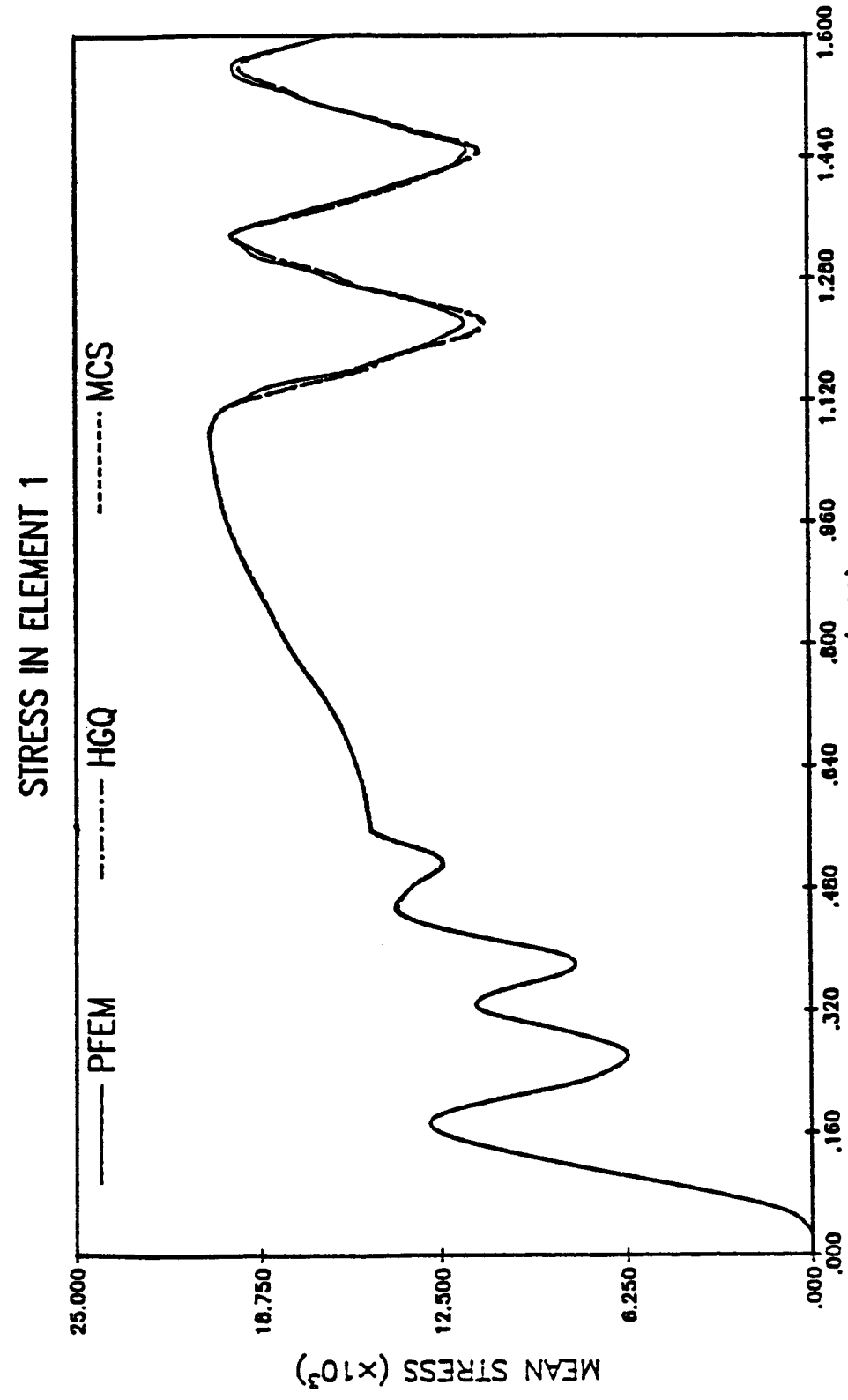

Comparison of the Mean Stress of Member 1

Figure 13

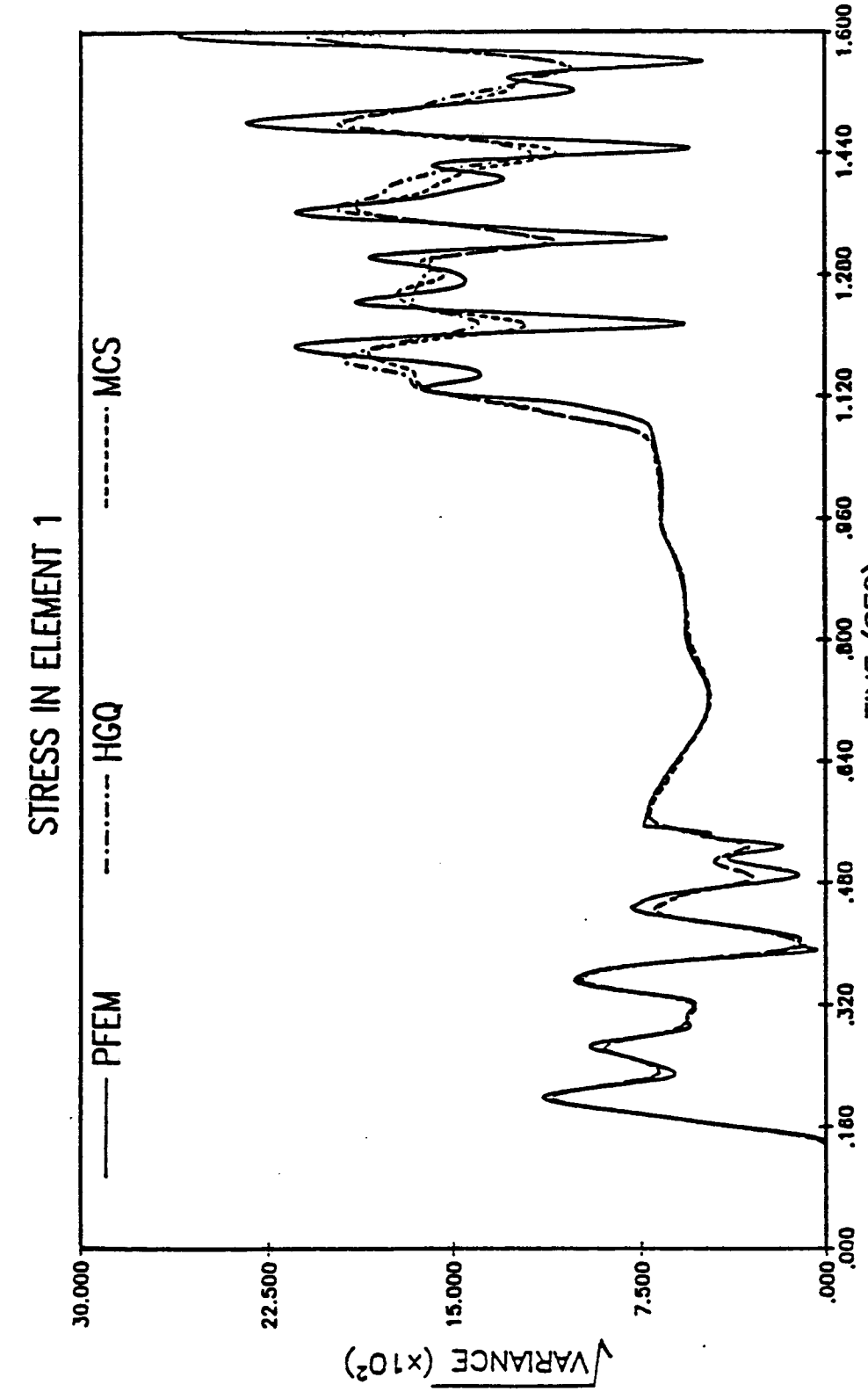

Comparison of the Variance of Stress in Member 1

Figure 14

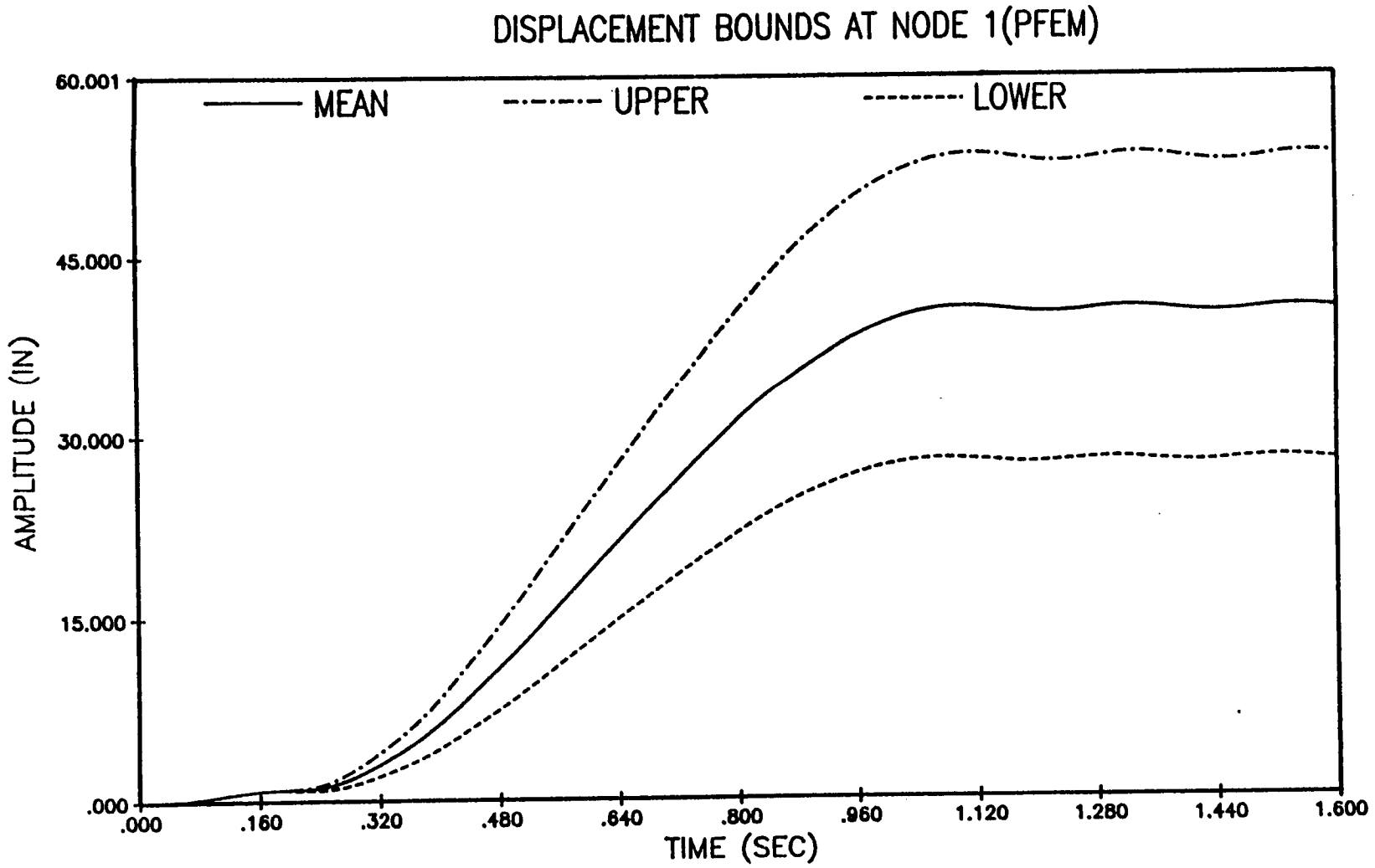
DISPLACEMENT BOUNDS AT NODE 1(PFEM)
MEAN
UPPER
LOWER
60.001
45.000
30.000
15.000
.000
AMPLITUDE (IN)
.000
.160
.320
.480
.640
.800
.960
1.120
1.280
1.440
1.600
TIME (SEC)

Figure 15

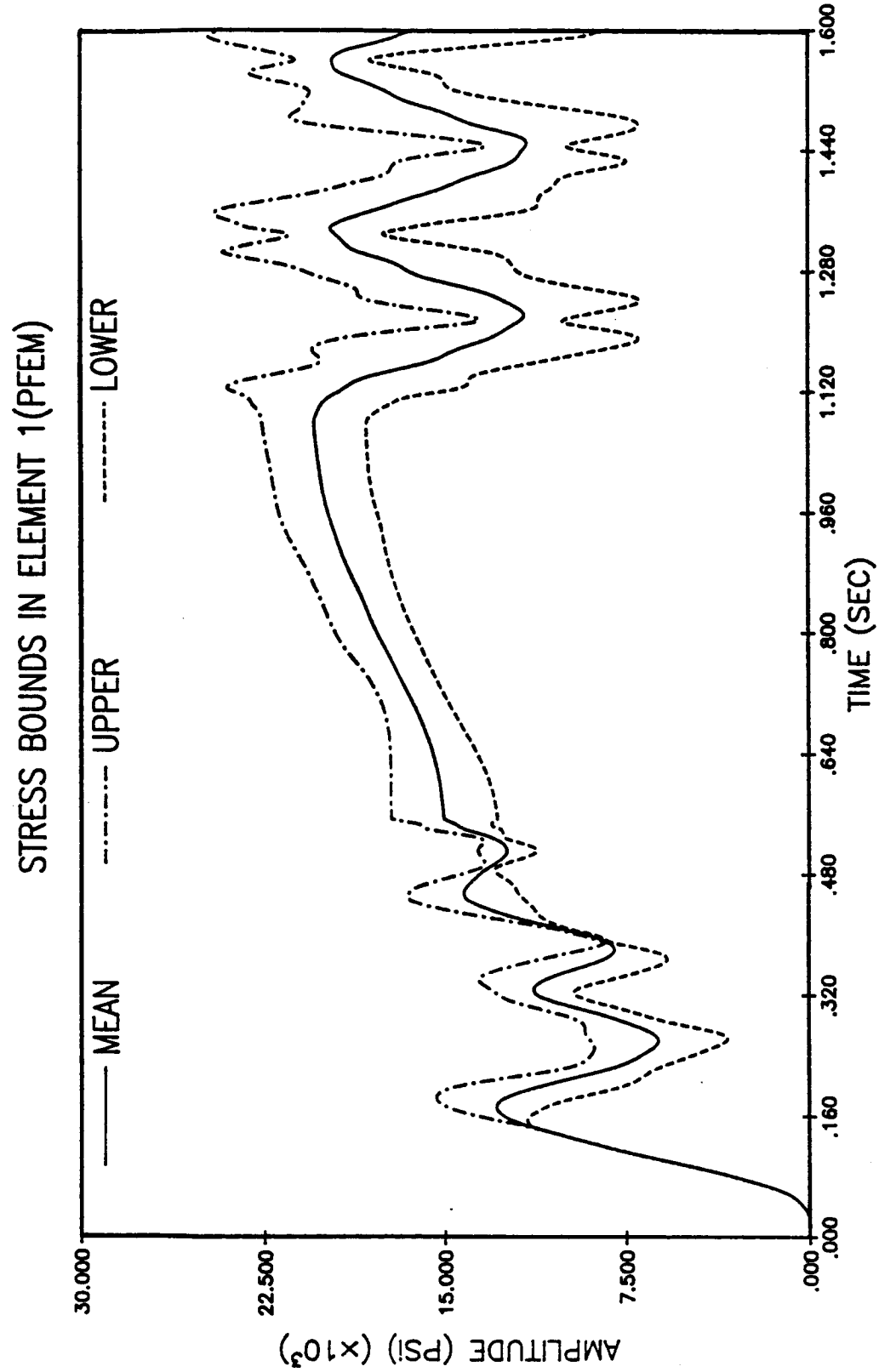
STRESS BOUNDS IN ELEMENT 1(PFEM)
MEAN
UPPER
LOWER
AMPLITUDE (PSI) (x10³)
30.000
22.500
15.000
7.500
.000
.000
.160
.320
.480
.640
.800
.960
1.120
1.280
1.440
1.600
TIME (SEC)

Figure 16

CHAPTER 3

RANDOM FIELD FINITE ELEMENTS

3.1 Introduction

At the present time, probabilistic methods in mechanics, for problems involving time-independent uncertainties, can be broadly classified into two major categories: (1) methods using a statistical approach and (2) methods using a non-statistical approach. The literature in these areas is quite considerable and so only a few sample references are indicated below.

Simulation, involving sampling and estimation, is the most prevalent statistical approach. Direct Monte Carlo simulation, stratified sampling and Latin Hypercube sampling are some of the frequently employed simulation techniques. A comparative discussion of these techniques can be found in, for example, Refs. [1,2,3,6]. These techniques, however, have their limitations. Transformations of the distributions are necessary before simulation can be done [4,5,8,9]. This implies, of course, that the multivariate distribution function needs to be known for simulation. The topic of transformation techniques is still an area of current research. Furthermore, since the accuracy of sampling techniques depends on the sample size, in accordance with the "Weak Law of Large Numbers" [4,11], simulations can become prohibitively expensive; hence the interest in non-statistical methods.

Non-statistical approaches include numerical integration [10,15,16], second-moment analysis [4,5,7,9,14-17], and stochastic

finite element methods [11-13,15,16]. Particularly, second-moment techniques have proven to be accurate and efficient in structural mechanics. A major advantage of these techniques is that the multivariate distribution function need not be known but only the first two moments. An inherent limitation of second moment analysis is that the uncertainties cannot be too large, i.e., variances of the random variables cannot be large when compared with their mean values. Typically, the maximum coefficient of variation is around 10% although it has been shown that it could be as high as 20% for acceptable results to be obtained [5,14].

Linear problems in structural mechanics with uncertain parameters have been solved by second-moment analysis [11-13]. However, similar solution techniques for nonlinear problems in structural dynamics are, to the authors' knowledge, nonexistent. Recently, the authors have developed probabilistic finite element methods for nonlinear structural dynamics [15,16]. The methods are applicable to correlated and uncorrelated discrete random variables, though they are limited to discrete structures such as spring-mass systems and nonlinear truss structures.

The herein proposed method is applicable to nonlinear structural dynamics problems with random fields — both homogeneous and inhomogeneous. In the next section, the formulation of the probabilistic finite element methods for linear continua is outlined. In Section 3.3, the procedures for the transformation of the full covariance matrix to a diagonal matrix are discussed. In Section 3.4,

the computational procedures using the transformed random variables are given. The PFEM, as applied to continua with material and geometrical nonlinearities, is formulated in Section 3.5. Applications to a one-dimensional elastic/plastic wave propagation problem and a two-dimensional plane-stress beam bending problem are described in Section 3.6. The results and conclusions are presented in Section 3.7.

3.2 Probabilistic Finite Element Methods (PFEM) for Linear Continua

The linear finite element equations are:

$$\underset{\sim}{K}\,\underset{\sim}{d} = \underset{\sim}{F} \tag{3.2.1}$$

where the stiffness matrix is

$$\underset{\sim}{K} = \int_{\Omega} \underset{\sim}{B}^{T}\underset{\sim}{D}\,\underset{\sim}{B}\, d\Omega \tag{3.2.2}$$

The transpose is designated by a superscript "T"; the generalized gradient matrix, material response matrix, nodal displacement vector and nodal force vector are denoted by $\underset{\sim}{B}(\underset{\sim}{x})$, $\underset{\sim}{D}(\underset{\sim}{x},b)$, $\underset{\sim}{d}(b)$ and $\underset{\sim}{F}(b)$, respectively; $\underset{\sim}{x}$ are the spatial coordinates; Ω is the domain and $b(\underset{\sim}{x})$ is a random function. In this formulation, $b(\underset{\sim}{x})$ can be a random material property or a random load.

The basic idea of the "Second Moment Analysis" in PFEM is to expand, via Taylor Series, the $\underset{\sim}{d}$, $\underset{\sim}{D}$ and $\underset{\sim}{F}$ matrices about the mean value of b and to retain only up to second order terms. Equations will then be obtained for the mean values of the nodal displacements and the covariances of the nodal displacements in terms of the derivatives of the nodal displacements with respect to the random variables. Similarly, the mean and covariance of the element stresses and strains are obtained.

The random function $b(\underset{\sim}{x})$ is approximated using shape functions $N_i(\underset{\sim}{x})$ by

$$b(\underset{\sim}{x}) = \sum_{i=1}^{q} N_i(\underset{\sim}{x}) b_i \qquad (3.2.3a)$$

where b_i are the nodal values of $b(\underset{\sim}{x})$, that is the values of b at $\underset{\sim}{x}_i$, $i = 1, \ldots, q$.

To derive the PFEM matrix equations, the following notation will be used. For a given function g(b) and a small parameter ε:

$\bar{b}(\underset{\sim}{x}) = E[b(\underset{\sim}{x})]$	mean value of b, i.e. the expectation E[ ] of $b(\underset{\sim}{x})$
$db_1 = \varepsilon \Delta b_1 = \varepsilon(b_1 - \bar{b}_1)$	first order variation of b_1 about $\bar{b}_1$
$db_1 db_2 = \varepsilon^2 \Delta b_1 \Delta b_2$	second order variation of b_1 and b_2 about $\bar{b}_1$ and $\bar{b}_2$, respectively
$\bar{g}(\underset{\sim}{x}) = g(\underset{\sim}{x}, \bar{b}(\underset{\sim}{x}))$	value of g evaluated at $\bar{b}$
$\bar{g}_{b_1} = \frac{\partial g}{\partial b_1}$	partial derivative of g with respect to b_1 evaluated at $\bar{b}$
$\bar{g}_{b_1 b_2} = \frac{\partial^2 g}{\partial b_1 \partial b_2}$	mixed partial derivatives of g with respect to b_1 and b_2 evaluated at $\bar{b}$

The random function is defined by its expectation $\bar{b}(\underset{\sim}{x})$, coefficient of variation α and autocorrelation $R(b(x_i), b(x_j))$. The mean and variance are approximated by the same shape functions as b, so

$$E[b(\underset{\sim}{x})] = \sum_{i=1}^{q} N_i(\underset{\sim}{x}) E[b_i] \qquad (3.2.3b)$$

$$Var(b(\underset{\sim}{x})) = \sum_{i,j=1}^{q} N_i(\underset{\sim}{x}) N_j(\underset{\sim}{x}) \, Cov(b_i, b_j) \qquad (3.2.3c)$$

The matrices $\underset{\sim}{D}$, $\underset{\sim}{d}$ and $\underset{\sim}{F}$ are expanded about $\overline{b}$ via Taylor series:

$$\underset{\sim}{D} = \overline{\underset{\sim}{D}} + \sum_{i=1}^{q} \overline{\underset{\sim}{D}}_{b_i} db_i + \frac{1}{2} \sum_{i,j=1}^{q} \overline{\underset{\sim}{D}}_{b_i b_j} db_i db_j \qquad 3.(2.4)$$

$$\underset{\sim}{d} = \overline{\underset{\sim}{d}} + \sum_{i=1}^{q} \overline{\underset{\sim}{d}}_{b_i} db_i + \frac{1}{2} \sum_{i,j=1}^{q} \overline{\underset{\sim}{d}}_{b_i b_j} db_i db_j \qquad (3.2.5)$$

$$\underset{\sim}{F} = \overline{\underset{\sim}{F}} + \sum_{i=1}^{q} \overline{\underset{\sim}{F}}_{b_i} db_i + \frac{1}{2} \sum_{i,j=1}^{q} \overline{\underset{\sim}{F}}_{b_i b_j} db_i db_j \qquad (3.2.6)$$

Substituting Eqs. (3.2.4) through (3.2.6) into Eq. (3.2.1) and equating equal order terms, the zeroth, first and second order equations corresponding to Eq. (3.2.1) are:

Zeroth Order

$$\overline{\underset{\sim}{K}}\,\overline{\underset{\sim}{d}} = \overline{\underset{\sim}{F}} \qquad (3.2.7)$$

where

$$\overline{\underset{\sim}{K}} = \int_{\Omega} \underset{\sim}{B}^{T} \overline{\underset{\sim}{D}}\, \underset{\sim}{B}\, d\Omega \qquad (3.2.8)$$

First Order (ε terms)

$$\overline{\underset{\sim}{K}}\,\overline{\underset{\sim}{d}}_{b_i} = \overline{\underset{\sim}{F}}_{1i} \qquad i = 1, \ldots, q \qquad (3.2.9)$$

where

$$\overline{\underset{\sim}{F}}_{1i} = F_{b_i} - \int_{\Omega} \underset{\sim}{B}^T \overline{\underset{\sim}{D}}_{b_i} \underset{\sim}{B}\, \overline{\underset{\sim}{d}}\, d\Omega \tag{3.2.10}$$

Second Order (ε^2 terms)

$$\overline{\underset{\sim}{K}}\, \overline{\underset{\sim}{d}}_2 = \overline{\underset{\sim}{F}}_2 \tag{3.2.11}$$

where

$$\overline{\underset{\sim}{d}}_2 = \frac{1}{2} \sum_{i,j=1}^{q} \overline{\underset{\sim}{d}}_{b_i b_j} \Delta b_i \Delta b_j \tag{3.2.12}$$

and

$$\overline{\underset{\sim}{F}}_2 = \sum_{i,j=1}^{q} \{\frac{1}{2} \overline{\underset{\sim}{F}}_{b_i b_j} - \frac{1}{2}[\int_{\Omega} \underset{\sim}{B}^T \overline{\underset{\sim}{D}}_{b_i b_j} \underset{\sim}{B}\, \overline{\underset{\sim}{d}}\, d\Omega]$$

$$- [\int_{\Omega} \underset{\sim}{B}^T \overline{\underset{\sim}{D}}_{b_i} \underset{\sim}{B}\, \overline{\underset{\sim}{d}}_{b_j} d\Omega]\} \Delta b_i \Delta b_j \tag{3.2.13}$$

Once $\overline{\underset{\sim}{d}}$, $\overline{\underset{\sim}{d}}_{b_i}$ and $\overline{\underset{\sim}{d}}_2$ are obtained by solving Eqs. (3.2.7), (3.2.9) and (3.2.11), respectively, the mean and autocovariance matrices for the nodal displacement are given by

$$E[\underset{\sim}{d}] = \int_{-\infty}^{\infty} \underset{\sim}{d}(\underset{\sim}{b})\, f(\underset{\sim}{b})\, d\underset{\sim}{b} \tag{3.2.14}$$

and

$$\mathrm{Cov}(\underset{\sim}{d}^i, \underset{\sim}{d}^j) = \int_{-\infty}^{+\infty} (d^i - \overline{d}^i)(d^j - \overline{d}^j) f(\underset{\sim}{b}) d\underset{\sim}{b} \tag{3.2.15}$$

respectively, where f is the joint probability density function, d^i is the ith degree of freedom of $\underset{\sim}{d}$, and $\underset{\sim}{b}$ is the random-variable vector

$$\underset{\sim}{b} = (b_1, b_2, \ldots, b_q)^T \tag{3.2.16}$$

The second order estimate of the mean value of $\underset{\sim}{d}$ is obtained by employing Eq. (3.2.5) in Eq. (3.2.14) to give

$$E[\underset{\sim}{d}] = \overline{\underset{\sim}{d}} + \frac{1}{2}\{\sum_{i,j=1}^{q} \overline{\underset{\sim}{d}}_{b_i b_j} \mathrm{Cov}(b_i, b_j)\} \tag{3.2.17}$$

The covariance, $\mathrm{Cov}(b_i, b_j)$ is obtained from the given expectation $E[b(x)]$, coefficient of variation α and autocorrelation $R(b(x_i), b(x_j))$ as follows

$$\mathrm{Cov}(b_i, b_j) = [\mathrm{Var}(b(x_i))\mathrm{Var}(b(x_j))]^{1/2} R(b(x_i), b(x_j)) \tag{3.2.18}$$

where

$$\mathrm{Var}(b(x_i)) = \alpha^2 E[b(x_i)]^2 \tag{3.2.19}$$

Similarly, the first order accurate $\mathrm{Cov}(d^i, d^j)$, which is consistent with a second moment analysis, can be shown to be

$$\mathrm{Cov}(d^i, d^j) = \sum_{r,s=1}^{q} \overline{d^i}_{b_r} \overline{d^j}_{b_s} \mathrm{Cov}(b_r, b_s) \tag{3.2.20}$$

The strain and stress vectors for a typical element "e" are

$$\underset{\sim}{\varepsilon} = \underset{\sim}{B}(\underset{\sim}{x})\ \underset{\sim}{d}^{e} \tag{3.2.21}$$

and

$$\underset{\sim}{\sigma} = \underset{\sim}{D}(\underset{\sim}{x},b)\ \underset{\sim}{\varepsilon} \tag{3.2.22}$$

where $\underset{\sim}{d}^{e}$ is the element nodal displacement vector. Since $\underset{\sim}{B}$ is a deterministic function of $\underset{\sim}{x}$, the mean value and autocovariance of $\underset{\sim}{\varepsilon}$ can be similarly defined according to Eqs. (3.2.14) and (3.2.15), respectively. They are

$$E[\underset{\sim}{\varepsilon}] = \underset{\sim}{B}\ \overline{\underset{\sim}{d}}^{e} + \frac{1}{2}\{\sum_{i,j=1}^{q} \underset{\sim}{B}\ \overline{\underset{\sim}{d}}^{e}_{b_i b_j} \mathrm{Cov}(b_i,b_j)\} \tag{3.2.23}$$

and

$$\mathrm{Cov}(\underset{\sim}{\varepsilon}_e,\underset{\sim}{\varepsilon}_f) = \{\sum_{i,j=1}^{q} (\underset{\sim}{B}^{e}\overline{\underset{\sim}{d}}^{e}_{b_i})(\underset{\sim}{B}^{f}\overline{\underset{\sim}{d}}^{f}_{b_j})^{T}\mathrm{Cov}(b_i,b_j)\} \tag{3.2.24}$$

Employing Eq. (3.2.4) and the element counterpart of Eq. (3.2.5), the mean value and autocovariance of $\underset{\sim}{\sigma}$ can be shown to be

$$E[\underset{\sim}{\sigma}] = \overline{\underset{\sim}{D}}\ E[\underset{\sim}{\varepsilon}]$$

$$+ \{\sum_{i,j=1}^{q} [\overline{\underset{\sim}{D}}_{b_i}\underset{\sim}{B}\ \overline{\underset{\sim}{d}}^{e}_{b_j} + \frac{1}{2}\overline{\underset{\sim}{D}}_{b_i b_j}\underset{\sim}{B}\ \overline{\underset{\sim}{d}}^{e}]\mathrm{Cov}(b_i,b_j)\} \tag{3.2.25}$$

and

$$\mathrm{Cov}(\underset{\sim}{\sigma}_e,\underset{\sim}{\sigma}_f) = \{\sum_{i,j=1}^{q}[(\overline{\underset{\sim}{D}}^e\underset{\sim}{B}^e\overline{\underset{\sim}{d}}^e_{\underset{\sim}{b}_i})(\overline{\underset{\sim}{D}}^f\underset{\sim}{B}^f\overline{\underset{\sim}{d}}^f_{\underset{\sim}{b}_j})^T$$

$$+ (\overline{\underset{\sim}{D}}^e_{\underset{\sim}{b}_i}\underset{\sim}{B}^e\overline{\underset{\sim}{d}}^e)(\overline{\underset{\sim}{D}}^f_{\underset{\sim}{b}_j}\underset{\sim}{B}^f\overline{\underset{\sim}{d}}^f)^T + (\overline{\underset{\sim}{D}}^e\underset{\sim}{B}^e\overline{\underset{\sim}{d}}^e_{\underset{\sim}{b}_i})(\overline{\underset{\sim}{D}}^f_{\underset{\sim}{b}_j}\underset{\sim}{B}^f\overline{\underset{\sim}{d}}^f)^T$$

$$+ (\overline{\underset{\sim}{D}}^e_{\underset{\sim}{b}_i}\underset{\sim}{B}^e\overline{\underset{\sim}{d}}^e)(\overline{\underset{\sim}{D}}^f\underset{\sim}{B}^f\overline{\underset{\sim}{d}}^f_{\underset{\sim}{b}_j})^T]\mathrm{Cov}(b_i,b_j)\} \qquad (3.2.26)$$

respectively.

3.3 Transformation of the Full Covariance Matrix to a Diagonal Variance Matrix

It can be observed from Eqs. (3.2.7) through (3.2.13) that the determination of $\overline{\underset{\sim}{d}}$, $\overline{\underset{\sim}{d}}_{b_i}$ and $\overline{\underset{\sim}{d}}_2$ involve one factorization of $\overline{\underset{\sim}{K}}$ and q + 2 forward-reductions and back-substitutions. The latter operations consist of one solution to evaluate $\overline{\underset{\sim}{d}}$ (Eq. (3.2.7)); q solutions to evaluate $\overline{\underset{\sim}{d}}_{b_i}$ (Eq. (3.2.9)) and one more solution to evaluate $\overline{\underset{\sim}{d}}_2'$ (Eq. (3.2.11)) where $\overline{\underset{\sim}{d}}_2'$ is obtained by multiplying the joint probability density function with Eq. (3.2.11) and integrating over the domain of $\underset{\sim}{b}$ to yield

$$\overline{\underset{\sim}{K}}\,\overline{\underset{\sim}{d}}_2' = \overline{\underset{\sim}{F}}_2' \tag{3.3.1}$$

where

$$\overline{\underset{\sim}{d}}_2' = \frac{1}{2}\sum_{i,j=1}^{q} \overline{\underset{\sim}{d}}_{b_i b_j} \mathrm{Cov}(b_i, b_j) \tag{3.3.2}$$

and

$$\overline{\underset{\sim}{F}}_2' = \sum_{i,j=1}^{q} \{\frac{1}{2}\overline{\underset{\sim}{F}}_{b_i b_j} - \frac{1}{2}[\int_{\Omega} \underset{\sim}{B}^T \overline{\underset{\sim}{D}}_{b_i b_j} \underset{\sim}{B}\, \overline{\underset{\sim}{d}}\, d\Omega] - [\int_{\Omega} \underset{\sim}{B}^T \overline{\underset{\sim}{D}}_{b_i} \underset{\sim}{B}\, \overline{\underset{\sim}{d}}_{b_j} d\Omega]\}\mathrm{Cov}(b_i, b_j) \tag{3.3.3}$$

Hence, from Eq. (3.2.17), the mean value of $\underset{\sim}{d}$ is simply

$$E[\underset{\sim}{d}] = \overline{\underset{\sim}{d}} + \overline{\underset{\sim}{d}}_2' \tag{3.3.4}$$

Even though the above computations are compatible with the elemental discretization and nodal assembly procedures that characterize finite element theory and software, the number of matrix multiplications is proportional to $q(q + 1)/2$. This would be unacceptably expensive. The large number of computations arise from the double summations in i and j in Eq. (3.3.2) and (3.3.3). To remedy this situation, the covariance matrix $\mathrm{Cov}(b_i,b_j)$ is transformed to a diagonal variance matrix $\mathrm{Var}(c_i,c_j)$ such that

$$\mathrm{Var}(c_i,c_j) = 0 \qquad \text{for } i \neq j \tag{3.3.5}$$

and

$$\mathrm{Var}(c_i,c_j) = \mathrm{Var}(c_i) \qquad \text{for } i = j \tag{3.3.6}$$

Therefore, the number of matrix multiplications is proportional to q. The above involves the solution of the eigenproblem:

$$\underset{\sim}{G}\,\underset{\sim}{\psi} = \underset{\sim}{\psi}\,\underset{\sim}{\Lambda} \tag{3.3.7}$$

where the $\underset{\sim}{G}$ and $\underset{\sim}{\Lambda}$ matrices are used to denote $\mathrm{Cov}(b_i,b_j)$ and $\mathrm{Var}(c_i,c_j)$, respectively; and $\underset{\sim}{\psi}$ is a constant $q \times q$ fundamental matrix with the following properties:

$$\underset{\sim}{\psi}^T\underset{\sim}{\psi} = \underset{\sim}{\psi}\,\underset{\sim}{\psi}^T = \underset{\sim}{1} \tag{3.3.8}$$

$$\underset{\sim}{\Lambda} = \underset{\sim}{\psi}^T \underset{\sim}{G} \underset{\sim}{\psi} \tag{3.3.9}$$

and

$$\underset{\sim}{b} = \underset{\sim}{\psi}\, \underset{\sim}{c} \quad \text{or} \quad \underset{\sim}{c} = \underset{\sim}{\psi}^T \underset{\sim}{b} \tag{3.3.10}$$

$\underset{\sim}{1}$ is the q × q identity matrix and $\underset{\sim}{c}$ is a transformed q × 1 random variables vector.

With Eqs. (3.3.9) and (3.3.10), the mixed derivatives appearing in Eqs. (3.2.21) through (3.2.28), (3.3.2) and (3.3.3) reduce to second derivatives. For example, Eqs. (3.3.2) and (3.3.3) become:

$$\overline{\underset{\sim}{d}}_2' = \frac{1}{2} \sum_{i=1}^{q} \overline{\underset{\sim}{d}}_{c_i c_i} \mathrm{Var}(c_i) \tag{3.3.11}$$

and

$$\overline{\underset{\sim}{F}}_2' = \sum_{i=1}^{q} \{\frac{1}{2} \overline{\underset{\sim}{F}}_{c_i c_i} - \frac{1}{2}[\int_{\Omega} \underset{\sim}{B}^T \overline{\underset{\sim}{D}}_{c_i c_i} \underset{\sim}{B}\, \overline{\underset{\sim}{d}}\, d\Omega]$$

$$- [\int_{\Omega} \underset{\sim}{B}^T \overline{\underset{\sim}{D}}_{c_i} \underset{\sim}{B}\, \overline{\underset{\sim}{d}}_{c_i}\, d\Omega]\} \mathrm{Var}(c_i) \tag{3.3.12}$$

Analogous to modal analysis in structural dynamics problems, only a few modes (i.e. $\mathrm{Var}(c_i)$) are required to capture the major characteristics of the probabilistic distributions. However, the highest eigenvalues have to be employed. This is in contrast to the modal structural problem wherein the lowest eigenvalues are used.

3.4 Computational Procedures Using the Transformed Random Variables $\underset{\sim}{c}$

Assume that n highest $\mathrm{Var}(c_i)$ are adequate to characterize the probabilistic distribution. The discrete c_i are transformed according to

$$c_i = \sum_{j=1}^{q} \psi_{ji} b_j \qquad i = 1, \ldots, n \qquad (3.4.1)$$

and the mean and variance of $\underset{\sim}{c}$ are

$$E[\underset{\sim}{c}] = \underset{\sim}{\psi}^T E[\underset{\sim}{b}] \qquad (3.4.2)$$

and

$$\mathrm{Var}(\underset{\sim}{c}) = \text{diagonal terms of } \underset{\sim}{\Lambda} \qquad (3.4.3)$$

where

$$\underset{\sim}{\Lambda} = \underset{\sim}{\psi}^T \underset{\sim}{G}\, \underset{\sim}{\psi} \qquad (3.4.4)$$

The zeroth-order matrix equations to be solved are:

$$\overline{\underset{\sim}{K}}\, \overline{\underset{\sim}{d}} = \overline{\underset{\sim}{F}} \qquad (3.4.5)$$

The n first-order matrix equations to be solved are:

$$\overline{\underset{\sim}{K}}\ \overline{\underset{\sim}{d}}_{c_i} = \overline{\underset{\sim}{F}}_{i+2} \qquad i = 1, \ldots, n \qquad (3.4.6)$$

where

$$\overline{\underset{\sim}{F}}_{i+2} = \overline{\underset{\sim}{F}}_{c_i} - \left[\int_{\Omega} \underset{\sim}{B}^T \overline{\underset{\sim}{D}}_{c_i} \underset{\sim}{B}\ \overline{\underset{\sim}{d}}\ d\Omega\right] \qquad i = 1, \ldots, n \qquad (3.4.7)$$

The second-order matrix equations to be solved are:

$$\overline{\underset{\sim}{K}}\ \overline{\underset{\sim}{d}}_2 = \overline{\underset{\sim}{F}}_2^* \qquad (3.4.8)$$

where

$$\overline{\underset{\sim}{F}}_2^* = \sum_{i=1}^{n} \left\{\frac{1}{2}\overline{\underset{\sim}{F}}_{c_i c_i} - \frac{1}{2}\left[\int_{\Omega} \underset{\sim}{B}^T \overline{\underset{\sim}{D}}_{c_i c_i} \underset{\sim}{B}\ \overline{\underset{\sim}{d}}\ d\Omega\right]\right.$$

$$\left. - \left[\int_{\Omega} \underset{\sim}{B}^T \overline{\underset{\sim}{D}}_{c_i} \underset{\sim}{B}\ \overline{\underset{\sim}{d}}_{c_i}\ d\Omega\right]\right\} \mathrm{Var}(c_i) \qquad (3.4.9)$$

It is also interesting to note that Eqs. (3.4.5) through (3.4.9) can be put into the general form of

$$\underset{\sim}{K}\ \underset{\sim}{d} = \underset{\sim}{F} \qquad (3.4.10)$$

where $\underset{\sim}{K}$ is an $(n + 2) \times (n + 2)$ block lower triangular matrix of the form

$$\underset{\sim}{K} = \begin{bmatrix} \overline{\underset{\sim}{K}} & \underset{\sim}{0} & \underset{\sim}{0} & \cdot & \cdot & \underset{\sim}{0} & \underset{\sim}{0} \\ \overline{\underset{\sim}{K}}_{c_1} & \overline{\underset{\sim}{K}} & \underset{\sim}{0} & \cdot & \cdot & \underset{\sim}{0} & \underset{\sim}{0} \\ \overline{\underset{\sim}{K}}_{c_2} & \underset{\sim}{0} & \overline{\underset{\sim}{K}} & \cdot & \cdot & \underset{\sim}{0} & \underset{\sim}{0} \\ \cdot & \cdot & \cdot & \cdot & \cdot & \cdot & \cdot \\ \cdot & \cdot & \cdot & \cdot & \cdot & \cdot & \cdot \\ \overline{\underset{\sim}{K}}_{c_n} & \underset{\sim}{0} & \underset{\sim}{0} & \cdot & \cdot & \overline{\underset{\sim}{K}} & \underset{\sim}{0} \\ \overline{\underset{\sim}{K}}_{22} & \overline{\underset{\sim}{K}}_1 & \overline{\underset{\sim}{K}}_2 & \cdot & \cdot & \overline{\underset{\sim}{K}}_n & \overline{\underset{\sim}{K}} \end{bmatrix} \tag{3.4.11}$$

where $\overline{\underset{\sim}{K}}$, $\overline{\underset{\sim}{K}}_{c_i}$, $\overline{\underset{\sim}{K}}_i$ and $\overline{\underset{\sim}{K}}_{22}$ are

$$\overline{\underset{\sim}{K}} = \int_\Omega \underset{\sim}{B}^T \overline{\underset{\sim}{D}} \underset{\sim}{B} \, d\Omega \tag{3.4.12}$$

$$\overline{\underset{\sim}{K}}_{c_i} = \int_\Omega \underset{\sim}{B}^T \overline{\underset{\sim}{D}}_{c_i} \underset{\sim}{B} \, d\Omega \qquad i = 1, \ldots, n \tag{3.4.13}$$

$$\overline{\underset{\sim}{K}}_i = \int_\Omega \underset{\sim}{B}^T [\overline{\underset{\sim}{D}}_{c_i} \mathrm{Var}(c_i)] \underset{\sim}{B} \, d\Omega \qquad i = 1, \ldots, n \text{ no sum} \tag{3.4.14}$$

and

$$\overline{\underset{\sim}{K}}_{22} = \frac{1}{2} \int_\Omega \underset{\sim}{B}^T [\sum_{i=1}^{n} \overline{\underset{\sim}{D}}_{c_i c_i} \mathrm{Var}(c_i)] \underset{\sim}{B} \, d\Omega \tag{3.4.15}$$

Accordingly, $\underset{\sim}{d}$ and $\underset{\sim}{F}$ are n + 2 block vectors which are defined by

$$\underset{\sim}{d} = (\overline{\underset{\sim}{d}}, \overline{\underset{\sim}{d}}_{c_1}, \overline{\underset{\sim}{d}}_{c_2}, \ldots, \overline{\underset{\sim}{d}}_{c_n}, \overline{\underset{\sim}{d}}_2)^T \tag{3.4.16}$$

and

$$\underset{\sim}{F} = (\overline{\underset{\sim}{F}}, \overline{\underset{\sim}{F}}_{c_1}, \overline{\underset{\sim}{F}}_{c_2}, \cdots, \overline{\underset{\sim}{F}}_{c_n}, \overline{\underset{\sim}{F}}_2^{"})^T \tag{3.4.17}$$

where

$$\overline{\underset{\sim}{F}}_2^{"} = \frac{1}{2}\left[\sum_{i=1}^{n} \overline{\underset{\sim}{F}}_{c_i c_i} \mathrm{Var}(c_i)\right] \tag{3.4.18}$$

The mean and autocovariance matrices for the displacement are:

$$E[\underset{\sim}{d}] = \overline{\underset{\sim}{d}} + \overline{\underset{\sim}{d}}_2 \tag{3.4.19}$$

and

$$\mathrm{Cov}(d^i, d^i) = \sum_{j=1}^{n} \overline{d}^i_{c_j} \overline{d}^i_{c_j} \mathrm{Var}(c_j) \tag{3.4.20}$$

The mean and autocovariance matrices for the element strains are:

$$E[\underset{\sim}{\varepsilon}] = \underset{\sim}{B}\, \overline{\underset{\sim}{d}}^e + \underset{\sim}{B}\, \overline{\underset{\sim}{d}}^e_2 \tag{3.4.21}$$

and

$$\mathrm{Cov}(\underset{\sim}{\varepsilon}_e, \underset{\sim}{\varepsilon}_f) = \left\{\sum_{i=1}^{n} \left(\underset{\sim}{B}^e \overline{\underset{\sim}{d}}^e_{c_i}\right)\left(\underset{\sim}{B}^f \overline{\underset{\sim}{d}}^f_{c_i}\right)^T \mathrm{Var}(c_i)\right\} \tag{3.4.22}$$

Similarly, the mean and autocovariance matrices for the element stresses are:

$$E[\underset{\sim}{\sigma}] = \overline{\underset{\sim}{D}}\, E[\underset{\sim}{\varepsilon}]$$

$$+ \{ \sum_{i=1}^{n} [\overline{\underset{\sim}{D}}_{\underset{\sim}{c}_i} \underset{\sim}{B}\, \overline{\underset{\sim}{d}}^{e}_{\underset{\sim}{c}_i} + \frac{1}{2} \overline{\underset{\sim}{D}}_{\underset{\sim}{c}_i c_i} \underset{\sim}{B}\, \overline{\underset{\sim}{d}}^{e}] \mathrm{Var}(c_i)\} \tag{3.4.23}$$

and

$$\mathrm{Cov}(\underset{\sim}{\sigma}_e, \underset{\sim}{\sigma}_f) = \{ \sum_{i=1}^{n} [(\overline{\underset{\sim}{D}}^{e} \underset{\sim}{B}^{e} \overline{\underset{\sim}{d}}^{e}_{\underset{\sim}{c}_i})(\overline{\underset{\sim}{D}}^{f} \underset{\sim}{B}^{f} \overline{\underset{\sim}{d}}^{f}_{\underset{\sim}{c}_i})^T$$

$$+ (\overline{\underset{\sim}{D}}^{e}_{\underset{\sim}{c}_i} \underset{\sim}{B}^{e} \overline{\underset{\sim}{d}}^{e})(\overline{\underset{\sim}{D}}^{f}_{\underset{\sim}{c}_i} \underset{\sim}{B}^{f} \overline{\underset{\sim}{d}}^{f})^T$$

$$+ (\underset{\sim}{D}^{e} \underset{\sim}{B}^{e} \overline{\underset{\sim}{d}}^{e}_{\underset{\sim}{c}_i})(\overline{\underset{\sim}{D}}^{f}_{\underset{\sim}{c}_i} \underset{\sim}{B}^{f} \overline{\underset{\sim}{d}}^{f})^T$$

$$+ (\overline{\underset{\sim}{D}}^{e}_{\underset{\sim}{c}_i} \underset{\sim}{B}^{e} \overline{\underset{\sim}{d}}^{e})(\overline{\underset{\sim}{D}}^{f} \underset{\sim}{B}^{f} \overline{\underset{\sim}{d}}^{f}_{\underset{\sim}{c}_i})^T] \mathrm{Var}(c_i)\} \tag{3.4.24}$$

Remark 4.1 While the presentation of the PFEM solution algorithm via Eqs. (3.4.10) through (3.4.18) is quite elegant, these equations are not employed in practical computations since the formulations of $\overline{\underset{\sim}{K}}_{\underset{\sim}{c}_i}$, $\overline{\underset{\sim}{K}}_{\underset{\sim}{i}}$, $\underset{\sim}{K}_{22}$ and the triangulation of $\underset{\sim}{K}$ are unnecessary. Instead, the "sequential algorithms" given by Eqs. (3.4.5) through (3.4.9) are employed. It should be noted that only the $\overline{\underset{\sim}{K}}$ matrix needs to be formed and triangulated and $\overline{\underset{\sim}{F}}$, $\overline{\underset{\sim}{F}}_{i+2}$ and $\overline{\underset{\sim}{F}}_2$ are obtained by vector computations.

Remark 4.2 Once $\overline{\underset{\sim}{d}}$ is given by Eq. (3.4.5), the $\overline{\underset{\sim}{d}}_{\underset{\sim}{c}_i}$ as defined by Eqs. (3.4.6) and (3.4.7) are best obtained with parallel computations.

Remark 4.3 The matrices $\overline{\underset{\sim}{D}}_{\underset{\sim}{b}_i}$ and $\overline{\underset{\sim}{D}}_{\underset{\sim}{b}_i \underset{\sim}{b}_j}$ can be computed by direct differentiation or by the least-squares fit of the series Eq. (3.2.4) around $\overline{\underset{\sim}{b}}$. Once these matrices are obtained, the transformation Eqs. (3.4.1) and (3.4.2) can be employed to yield $\overline{\underset{\sim}{D}}_{\underset{\sim}{c}_i}$ and $\overline{\underset{\sim}{D}}_{\underset{\sim}{c}_i \underset{\sim}{c}_i}$. Similarly $\overline{\underset{\sim}{F}}_{\underset{\sim}{c}_i}$ and $\overline{\underset{\sim}{F}}_{\underset{\sim}{c}_i \underset{\sim}{c}_i}$ can be obtained.

Remark 4.4 The PFEM, as developed here, can incorporate smooth (C^o) shape functions in Eq. (3.2.4). However, this may result in more integration points in the evaluation of $\overline{\underset{\sim}{K}}_{\underset{\sim}{c}_i}$, $\overline{\underset{\sim}{K}}_{\underset{\sim}{i}}$ and $\overline{\underset{\sim}{K}}_{\underset{\sim}{22}}$ in Eqs. (3.4.13) through (3.4.15). To minimize computations, a super-element that spans several elements used for the displacement approximations and in which the shape function is a constant, is employed in the numerical examples studied here.

3.5 PFEM for Transient Analysis of Nonlinear Continua

The transient equations for the finite element model, which account for both geometrical and material nonlinearities, are:

$$\underset{\sim}{M}\,\underset{\sim}{a}(\underset{\sim}{b},t) + \underset{\sim}{f}(\underset{\sim}{d},\underset{\sim}{v},\underset{\sim}{b}) = \underset{\sim}{F}(\underset{\sim}{b},t) \tag{3.5.1}$$

where $\underset{\sim}{M}$ is the deterministic mass matrix; $\underset{\sim}{f}$ is the internal force vector; $\underset{\sim}{d}$, $\underset{\sim}{v}$ and $\underset{\sim}{a}$ are the displacement, velocity and acceleration vectors, respectively; $\underset{\sim}{F}$ is the external force; $\underset{\sim}{b}$ is the discretized random vector and t is the time. Following the same procedures outlined in the previous sections, the $\underset{\sim}{a}$, $\underset{\sim}{F}$ and $\underset{\sim}{f}$ vectors are expanded via Taylor series, however, total derivatives are applied to $\underset{\sim}{f}$. The second-order formulas for $\underset{\sim}{a}$, $\underset{\sim}{F}$ and $\underset{\sim}{f}$ are

$$\underset{\sim}{a} = \overline{\underset{\sim}{a}} + \sum_{i=1}^{q} \overline{\underset{\sim}{a}}_{b_i}\, db_i + \frac{1}{2} \sum_{i,j=1}^{q} \overline{\underset{\sim}{a}}_{b_i b_j}\, db_i db_j \tag{3.5.2}$$

$$\underset{\sim}{F} = \overline{\underset{\sim}{F}} + \sum_{i=1}^{q} \overline{\underset{\sim}{F}}_{b_i}\, db_i + \frac{1}{2} \sum_{i,j=1}^{q} \overline{\underset{\sim}{F}}_{b_i b_j}\, db_i db_j \tag{3.5.3}$$

and

$$\begin{aligned} \underset{\sim}{f} = \overline{\underset{\sim}{f}} &+ \sum_{i=1}^{q} \left[\overline{\underset{\sim}{f}}_{b_i} + \overline{\underset{\sim}{C}}\,\overline{\underset{\sim}{v}}_{b_i} + \overline{\underset{\sim}{K}}\,\overline{\underset{\sim}{d}}_{b_i}\right] db_i \\ &+ \sum_{i,j=1}^{q} \left[\frac{1}{2}\overline{\underset{\sim}{f}}_{b_i b_j} + \frac{1}{2}\overline{\underset{\sim}{C}}\,\overline{\underset{\sim}{v}}_{b_i b_j} + \frac{1}{2}\overline{\underset{\sim}{K}}\,\overline{\underset{\sim}{d}}_{b_i b_j}\right. \\ &\left. + \overline{\underset{\sim}{C}}_{b_i}\overline{\underset{\sim}{v}}_{b_j} + \overline{\underset{\sim}{K}}_{b_i}\overline{\underset{\sim}{d}}_{b_j}\right] db_i db_j \end{aligned} \tag{3.5.4}$$

where the tangential damping matrix and the tangential stiffness matrix are defined by

$$\underset{\sim}{C} = \frac{\partial \underset{\sim}{f}}{\partial \underset{\sim}{v}} \tag{3.5.5}$$

and

$$\underset{\sim}{K} = \frac{\partial \underset{\sim}{f}}{\partial \underset{\sim}{d}} \tag{3.5.6}$$

respectively. Using the above approximations in Eq. (5.1), the q + 2 solutions for $\underset{\sim}{d}$, $\underset{\sim}{v}$ and $\underset{\sim}{a}$ are:

Zeroth-Order Equation

$$\underset{\sim}{M}\,\overline{\underset{\sim}{a}} + \overline{\underset{\sim}{f}} = \overline{\underset{\sim}{F}} \tag{3.5.7}$$

First-Order Equations

$$\underset{\sim}{M}\,\overline{\underset{\sim}{a}}_{b_i} + \overline{\underset{\sim}{C}}\,\overline{\underset{\sim}{v}}_{b_i} + \overline{\underset{\sim}{K}}\,\overline{\underset{\sim}{d}}_{b_i} = \overline{\underset{\sim}{F}}_{i+2} \qquad i = 1, \ldots, q \tag{3.5.8}$$

and

$$\overline{\underset{\sim}{F}}_{i+2} = \overline{\underset{\sim}{F}}_{b_i} - \overline{\underset{\sim}{f}}_{b_i} \qquad i = 1, \ldots, q \tag{3.5.9}$$

Second-Order Equations

$$\underset{\sim}{M}\,\bar{\underset{\sim}{a}}_2 + \bar{\underset{\sim}{C}}\,\bar{\underset{\sim}{v}}_2 + \bar{\underset{\sim}{K}}\,\bar{\underset{\sim}{d}}_2 = \bar{\underset{\sim}{F}}_2 \tag{3.5.10}$$

where

$$\bar{\underset{\sim}{a}}_2 = \frac{1}{2}\sum_{i,j=1}^{q} \bar{\underset{\sim}{a}}_{b_i b_j}\,\mathrm{Cov}(b_i,b_j) \tag{3.5.11}$$

$$\bar{\underset{\sim}{v}}_2 = \frac{1}{2}\sum_{i,j=1}^{q} \bar{\underset{\sim}{v}}_{b_i b_j}\,\mathrm{Cov}(b_i,b_j) \tag{3.5.12}$$

$$\bar{\underset{\sim}{d}}_2 = \frac{1}{2}\sum_{i,j=1}^{q} \bar{\underset{\sim}{d}}_{b_i b_j}\,\mathrm{Cov}(b_i,b_j) \tag{3.5.13}$$

and

$$\bar{\underset{\sim}{F}}_2 = \sum_{i,j=1}^{q}\{\frac{1}{2}\bar{\underset{\sim}{F}}_{b_i b_j} - \frac{1}{2}\bar{\underset{\sim}{f}}_{b_i b_j} - \bar{\underset{\sim}{C}}_{b_i}\bar{\underset{\sim}{v}}_{b_j} - \bar{\underset{\sim}{K}}_{b_i}\bar{\underset{\sim}{d}}_{b_j}\}\mathrm{Cov}(b_i,b_j) \tag{3.5.14}$$

The computational effort in solving Eqs. (3.5.8) through (3.5.14) can be reduced significantly by transforming the full covariance matrix, $\mathrm{Cov}(b_i,b_j)$, to a diagonal variance matrix, $\mathrm{Var}(c_i)$. Since Eqs. (3.5.8) through (3.5.14) are linearized equations, the transformation procedures are parallel to those outlined in Sections 3 and 4. If n (recall $n < q$) highest $\mathrm{Var}(c_i)$ are used, the q + 2 block system becomes an n + 2 block system. These n + 2 blocks are:

$$\underset{\sim}{M}\,\bar{\underset{\sim}{a}} + \bar{\underset{\sim}{f}} = \bar{\underset{\sim}{F}} \tag{3.5.15}$$

$$\underset{\sim}{M}\,\bar{\underset{\sim}{a}}_{c_i} + \underset{\sim}{\bar{C}}\,\bar{\underset{\sim}{v}}_{c_i} + \underset{\sim}{\bar{K}}\,\bar{\underset{\sim}{d}}_{c_i} = \bar{\underset{\sim}{F}}_{i+2} \qquad i = 1, \ldots, n \qquad (3.5.16)$$

$$\underset{\sim}{M}\,\bar{\underset{\sim}{a}}_2 + \underset{\sim}{\bar{C}}\,\bar{\underset{\sim}{v}}_2 + \underset{\sim}{\bar{K}}\,\bar{\underset{\sim}{d}}_2 = \bar{\underset{\sim}{F}}_2 \qquad (3.5.17)$$

where

$$\bar{\underset{\sim}{F}}_{i+2} = \bar{\underset{\sim}{F}}_{c_i} - \bar{\underset{\sim}{f}}_{c_i} \qquad i = 1, \ldots, n \qquad (3.5.18)$$

and

$$\bar{\underset{\sim}{F}}_2 = \sum_{i=1}^{n} \{\frac{1}{2}\bar{\underset{\sim}{F}}_{c_i c_i} - \frac{1}{2}\bar{\underset{\sim}{f}}_{c_i c_i} - \underset{\sim}{\bar{C}}_{c_i}\bar{\underset{\sim}{v}}_{c_i} - \underset{\sim}{\bar{K}}_{c_i}\bar{\underset{\sim}{d}}_{c_i}\}\mathrm{Var}(c_i) \qquad (3.5.19)$$

Equations (3.5.15) through (3.5.19) are similar to those developed for the probabilistic dynamic response of a truss structure with uncorrelated random variables [15,16]. Therefore, the numerical solution algorithms given in [15,16] can be employed directly for the solutions of the above equations. Once $\bar{\underset{\sim}{a}}$, $\bar{\underset{\sim}{v}}$, $\bar{\underset{\sim}{d}}$, $\bar{\underset{\sim}{a}}_{c_i}$, $\bar{\underset{\sim}{v}}_{c_i}$, $\bar{\underset{\sim}{d}}_{c_i}$, $\bar{\underset{\sim}{a}}_2$, $\bar{\underset{\sim}{v}}_2$ and $\bar{\underset{\sim}{d}}_2$ are obtained, the mean and autocovariance matrices can be computed according to:

$$E[\underset{\sim}{d}] = \bar{\underset{\sim}{d}} + \bar{\underset{\sim}{d}}_2 \qquad (3.5.20)$$

$$E[\underset{\sim}{v}] = \bar{\underset{\sim}{v}} + \bar{\underset{\sim}{v}}_2 \qquad (3.5.21)$$

$$E[\underset{\sim}{a}] = \bar{\underset{\sim}{a}} + \bar{\underset{\sim}{a}}_2 \qquad (3.5.22)$$

and

$$\mathrm{Cov}(d^i,d^j) = \{\sum_{r=1}^{n} \bar{d}^i_{c_r} \bar{d}^j_{c_r} \mathrm{Var}(c_r)\} \tag{3.5.23}$$

$$\mathrm{Cov}(v^i,v^j) = \{\sum_{r=1}^{n} \bar{v}^i_{c_r} \bar{v}^j_{c_r} \mathrm{Var}(c_r)\} \tag{3.5.24}$$

$$\mathrm{Cov}(a^i,a^j) = \{\sum_{r=1}^{n} \bar{a}^i_{c_r} \bar{a}^j_{c_r} \mathrm{Var}(c_r)\} \tag{3.5.25}$$

3.6 Applications

The PFEM formulation developed in Sections 2 to 5 has been tested by studying two different applications. These are: (1) wave propagation in a one-dimensional elastic/plastic bar; and (2) static response of a two-dimensional plane stress elastic/plastic cantilever. In these numerical examples, the expectation, the spatial autocorrelation and the coefficient of variation of the random field b(x) are assumed as follows:

$$E[b(x_i)] = b_o(1.0 + \theta x_i/L) \tag{3.6.1}$$

and

$$R(b(x_i),b(x_j)) = \exp(-|x_i-x_j|/\lambda) \tag{3.6.2}$$

$$\alpha = 0.10 \tag{3.6.3}$$

where x_i, L, λ, and $b(x_i)$ denote the location, the length of the bar/beam, the correlation length and the random function at x_i, respectively. θ and b_o are constants. It is to be noted that the autocorrelation between any two points depends only on the interval between these points and not on their locations. The material in the bar/beam is assumed to be linear elastic and isotropic hardening, with the uniaxial yield stress as a Gaussian random field in the axial direction. As can be seen from Eqs. (3.6.1) and (3.6.2), the yield

stress is a linear function for the mean and an exponential function for the spatial autocorrelation.

The problem statement for the bar is depicted in Fig. 1. The random field is discretized so that q = NUMEL = 32. The probabilistic equations derived earlier are solved by the explicit predictor algorithm [15] with a slight numerical damping (γ = 0.55). A near-critical time step (Δt = .000455) is used to keep the number of time steps minimal, subject to the stability conditions.

In the case of the beam, the static response is calculated as a function of steadily increasing loading, by an implicit algorithm. The random field is discretized with 64 4-node 2D elements so that q = 16 (NUMEL = 64).

The mean and variance of the displacement at the free end of the bar, the variance and autocorrelation of the stress along the beam are computed using PFEM. These results are compared with Monte Carlo simulation (MCS) of 400 realizations with a first-order filter [5,9].

3.7 Results and Conclusions

The mean and the variance of the displacement at the free end of the bar, computed by PFEM and MCS, are compared in Figs. 2 and 3. The coefficient of variation of the displacement at the free end of the bar is found to be ~0.13 (the coefficient of variation of the yield stress is 0.10). The PFEM solutions compare very well with the MCS solutions. Although both methods compare very well in accuracy, the PFEM in this case needs much less computer time than the MCS. The convergence of the variance of displacement at the free end of the bar is plotted in Fig. 4, against the number of modes used in the PFEM computations. It is observed that only the largest 8 of the 32 eigenvalues (which correspond to the variance of the uncorrelated variables c_i) are sufficient, for an error less than 1%.

The variance of the stress at the fixed end of the beam, with increasing loading, is plotted in Fig. 5. The maximum coefficient of variation is found to be 0.09, and it occurs when the beam begins to yield, at the mean configuration. The PFEM variances are in excellent agreement with those of MCS. The autocorrelation of the stress along the length of the beam, with respect to the stress at the fixed end, is plotted in Fig. 6. As expected, the autocorrelation near the fixed end is ~1.0 and beyond that it decreases rapidly. The PFEM autocorrelation is in fairly good agreement with that of MCS. As in the case of the bar, only a few eigenvalues are found to be necessary. The largest 4 of the 16 eigenvalues are sufficient to ensure an error less than 5%.

Since the random field is handled by discretization, it is easy to

incorporate any specified mean, variance and autocorrelation structure in PFEM. As the stiffness matrix corresponding to the mean value of the random field appears in all the PFEM equations, the triangulation needs to be done only once and the computations are thereby reduced. The transformation of the correlated variables to a set of uncorrelated variables further reduces the computations as the covariance matrix is reduced from a full matrix to a diagonal matrix. However, to do this an eigenvalue problem of the covariance matrix needs to be solved. Numerical results obtained here suggest that a reduced set of the uncorrelated variables is sufficient to predict the response moments accurately. The PFEM essentially involve solution of a set of deterministic problems, and therefore, they are easily integrable into any FEM based code.

Elastic/Plastic Bar with End Load

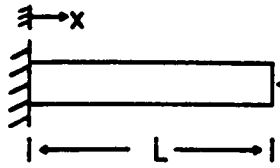

$A = 6.0$
$L = 1000.0$
$\rho = .00776$
$E = 30.X10^6$
$E_T = 30.X10^4$

Expectation of Yield Stress

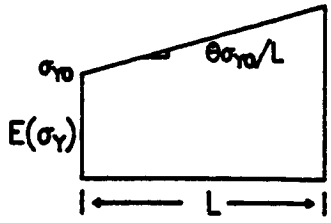

$\Theta = 0.1$
$\sigma_{Y0} = 25000.0$

Autocorrelation of Yield Stress

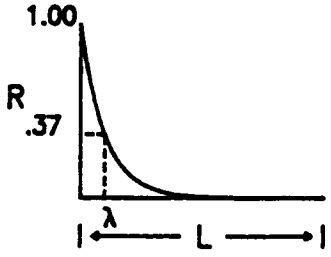

$\lambda = 0.1L$

Forcing Function

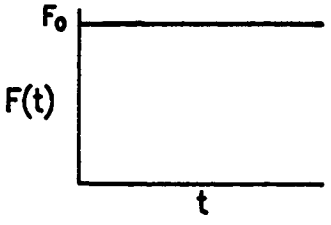

$F_0 = 25.X10^4$

Bar with Yield Stress as Random Field

Figure 1

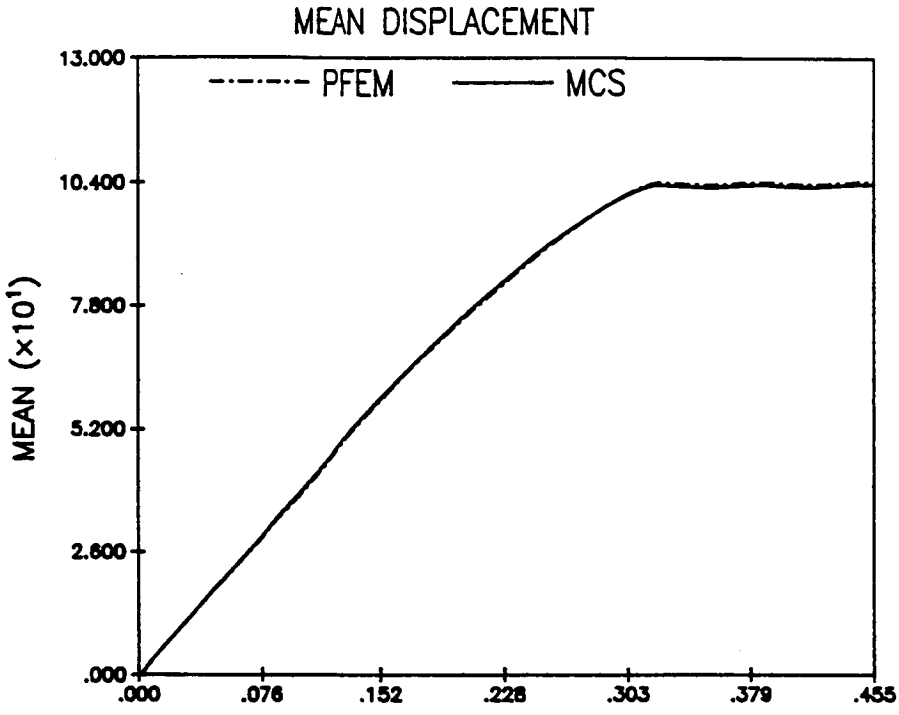

Figure 2

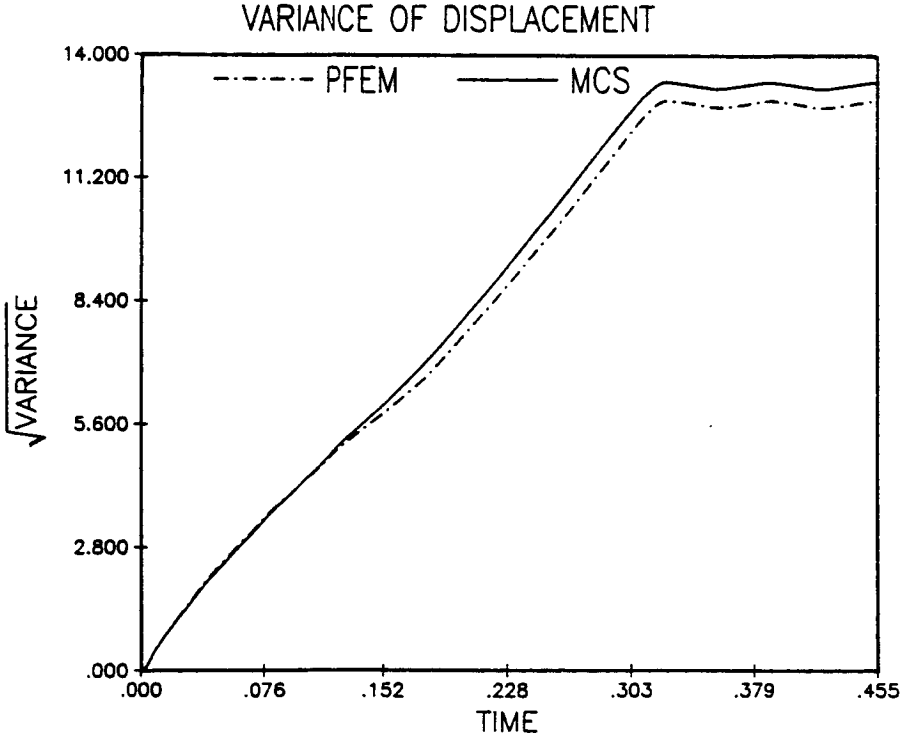

Figure 3

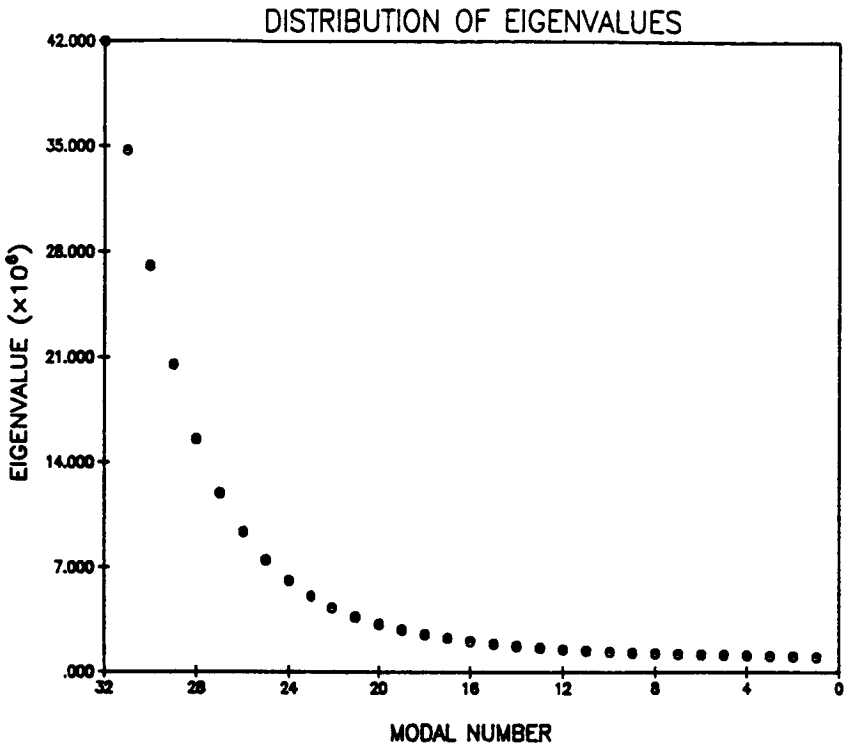

Figure 4a

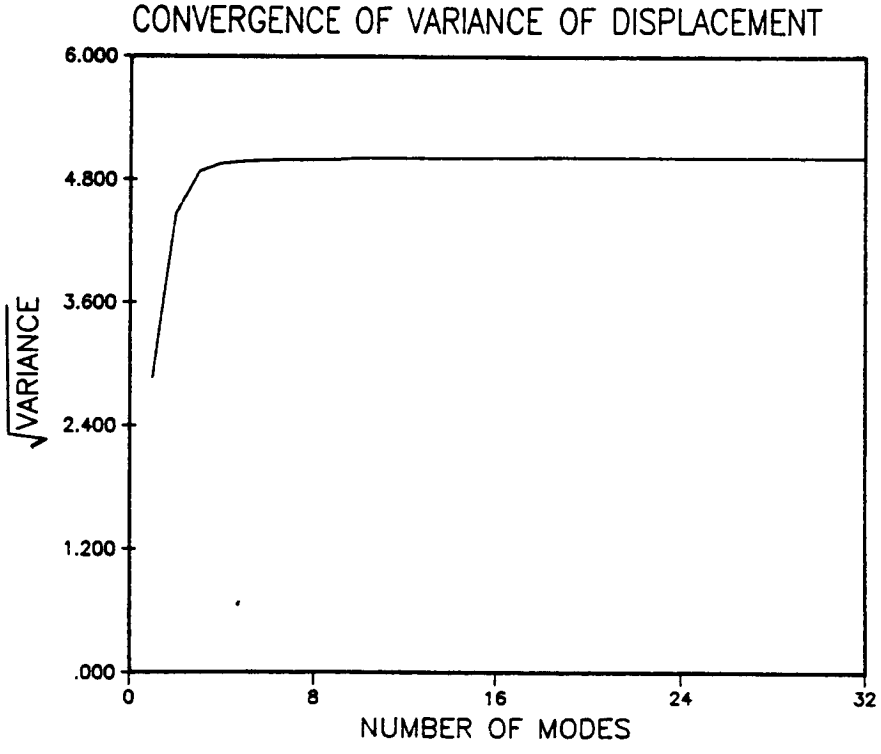

Figure 4b

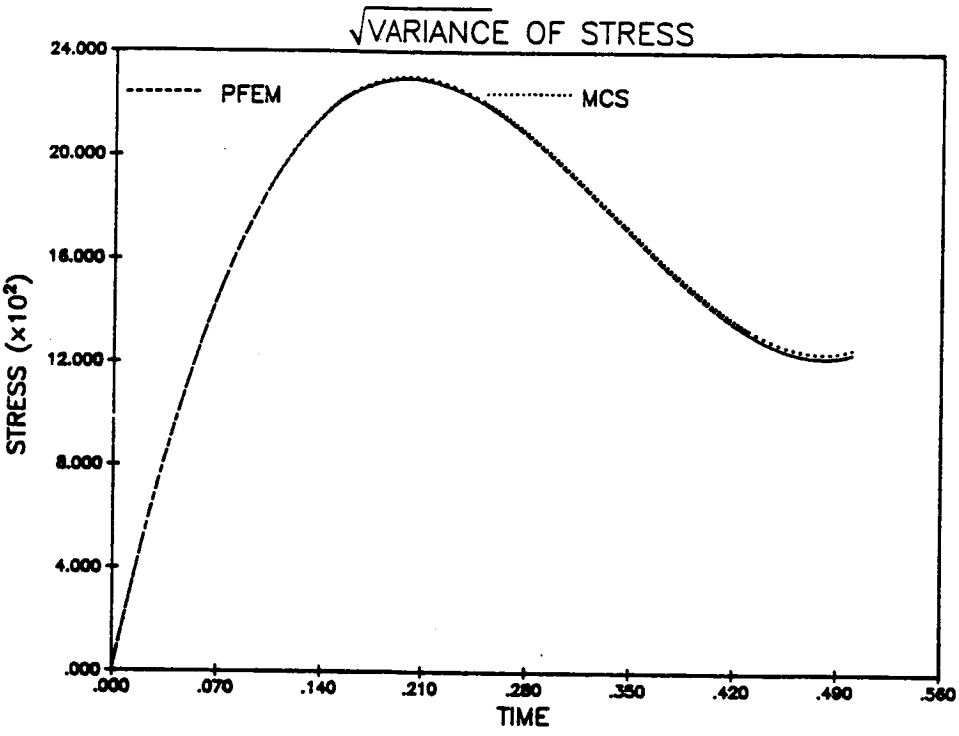

Figure 5

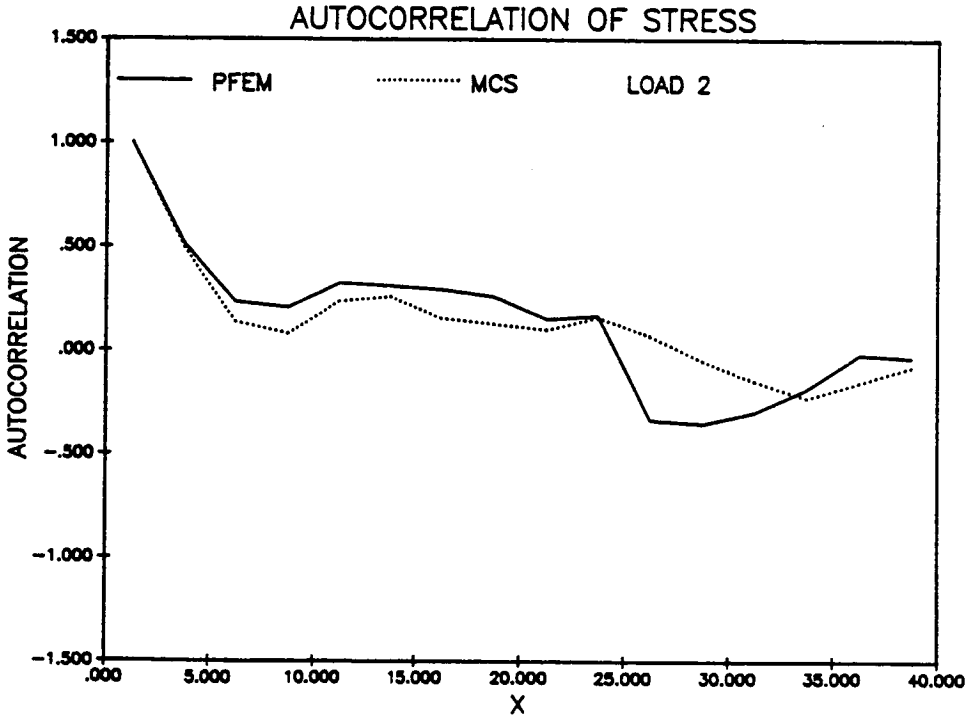

Figure 6

CHAPTER 4

PROBABILISTIC FINITE ELEMENT METHODS FROM VARIATIONAL PRINCIPLES

4.1 Introduction

Much research has been done in the recent years to quantify uncertainties in engineering systems and their combined effect on the response. Theoretically, these uncertainties are modeled as random fields or random variables governed by joint probability density or distribution functions. In practice, the exact joint probability density functions are not always available; only the first few moments such as the mean, variance and correlations are known. The effect of these uncertainties on the system is ideally evaluated by examining the probabilistic character of the response, such as the probability of the response exceeding allowable limits. These limits are referred to as the failure surfaces. Recent research in reliability is focused on developing efficient techniques for this purpose. In general, these techniques involve much computation and are subject to various restrictions on the nature of the failure criteria.

At the next level, estimates of response bounds, the level crossing rate or first passage time may be obtainable in some cases without extensive computations. At the easiest level of computation, the response statistics such as the mean, standard deviation and correlation coefficients are calculated [1,2]. These quantities are not only useful in themselves, but are also useful to calculate measures of reliability, e.g., the reliability index and reliability in terms of probability of survival [1-5]. In the past, the distribution functions for the

response were assumed and by using the response statistics, the probability of failure or survival was calculated [2]. Under a combination of uncertainties, the response distribution functions may be difficult to obtain.

More recently, second moment reliability techniques have been formulated in the space of the input uncertainties. Here, the non-normal uncertainties are transformed to normal variables and the failure surface is described in terms of the response quantities. Transformation to normal variables is done to make use of the special characteristics of normal distributions, such as rotational symmetry and rapid exponential decay of the density function. If the failure function is linear in terms of the response, the probability of failure is expressed in a straightforward manner in terms of the response statistics [2,3]. If the failure function is nonlinear, approximating it by a quadratic function yields accurate reliability values [5].

For analysis purposes, time-invariant and time-variant uncertainties need to be distinguished. In the latter the probabilistic features, such as density functions and statistics, vary with time. For example, in a static analysis of structures, only time-invariant uncertainties, such as experimentally determined material properties, may be present. Conversely, in the dynamic analysis of structures, the forces such as earthquake excitations, wind and wave forces, and jet noise excitation of aircraft panels are often treated as time-variant uncertainties. Compared to time-invariant uncertainties, these are very difficult to quantify exactly, and assumptions such as Gaussian density

functions, stationarity, ergodicity and white noise characteristics are common [6,7]. In structural mechanics, the characterization of time-variant uncertainties in excitations, particularly seismic loadings, is an area of active research [8-10,14,15]. Expressed mathematically, these are differential equations with stochastic excitations. For linear systems the problem is tractable because of the applicability of spectral decomposition and superposition techniques [6,7,11]. For nonlinear systems, techniques such as equivalent linearization have been adopted with success [6,12,13]. A concurrent, albeit less extensive, area of research in structural mechanics is the one that deals with stochastic coefficients of both types. Problems with time-variant, stochastic coefficients have proven to be the toughest to analyze and still are an active research area.

Apart from simulation techniques [2,16,17], a few non-statistical approaches are also currently available for solving problems with stochastic coefficients. These include numerical quadrature [18,19], second-moment analysis [20,21], the truncated hierarchy method [22], the method of moments [23], stochastic Green's function method [22], numerical solution of random integral equations [30,31] and the stochastic finite element method [29]. Merits and drawbacks of these and other methods are discussed in Refs. [24,26,29].

Recently, probabilistic finite element methods (PFEM) based on second-order perturbations have been formulated by the authors, for treating time-invariant, stochastic coefficients and excitations. These methods are based on second-moment techniques, so they are applicable

when the uncertainties are not too large and when the probabilistic density functions have decaying tails. Numerical results for various applications in trusses, bars, beams and plates have demonstrated the accuracy of PFEM, as compared with Monte Carlo simulation results [24-27]. These include both static and transient analyses of both linear and nonlinear structures, with random fields. Sample results for an elastoplastic cantilever beam with the uniaxial yield stress as a random field are given in Figs. 1a-1d [26]. The most appealing features about PFEM are its conceptual simplicity, ease of computer implementation, and computational efficiency. The special structure of the finite element equations, with features such as the symmetric stiffness matrices and the linear nature of the higher order equations, can be utilized to enhance the computational efficiency of the method for large-scale systems with many random variables. Compared to Monte Carlo simulations, computational requirements are often an order of magnitude smaller.

This paper focuses on the development of efficient and accurate methods for calculating the response statistics in structural mechanics, making use of finite element modeling and solution techniques. By developing the PFEM equations from a variational principle, the randomness in the shape of the domain and boundary conditions can be treated. The PFEM equations are derived for linear continua from the potential energy variational principle in the next section. In Section 4.3, the PFEM equations for nonlinear continua with large deformations are derived. It is shown that the final equations are similar to those

derived for the linear equations. Uncertainties arising from material and loads are accounted for in both formulations; randomness in the geometric properties such as shape is also included in the latter formulation. The PFEM equations are solved efficiently by numerical methods described in Section 4.4. The emphasis in this section is on numerical algorithms for computing the first and second order statistics of the displacement and stress and internal force. In Section 4.5, applications of PFEM to an elastoplastic plate with a hole and a turbine blade modeled by shell elements are studied. Results are summarized and discussed in section 4.6.

4.2 Development of PFEM for Linear Continua from the Potential Energy Variational Principle

The weak form which is obtained from the potential energy variational principle is:

$$\int_{\Omega} \delta u_{(i,j)} D_{ijk\ell} u_{(k,\ell)} d\Omega - \int_{\Omega} \delta u_i F_i d\Omega - \int_{\partial\Omega_h} \delta u_i h_i d\Gamma = 0 \qquad (4.2.1)$$

where the strain components are

$$\varepsilon_{ij} = u_{(i,j)} \stackrel{\text{def}}{=} \frac{1}{2}\left(\frac{\partial u_i}{\partial x_j} + \frac{\partial u_j}{\partial x_i}\right) \qquad \text{in } \Omega \qquad (4.2.2)$$

and the stress components are given by the linear stress-strain law

$$\sigma_{ij} = D_{ijk\ell}\varepsilon_{k\ell} \qquad \text{in } \Omega \qquad (4.2.3)$$

The traction and prescribed displacement boundary conditions are given by

$$\sigma_{ij} n_j = h_i \qquad \text{on } \partial\Omega_h \qquad (4.2.4)$$

and

$$u_i = g_i \qquad \text{on } \partial\Omega_g \qquad (4.2.5)$$

respectively. δu_i is an arbitrary test function which satisfies

$$\delta u_i = 0 \qquad \text{on } \partial\Omega_g \qquad (4.2.6)$$

Ω is the domain, $\partial\Omega_h$ and $\partial\Omega_g$ are the traction and prescribed displacement surfaces, respectively, which satisfy

$$\partial\Omega_h \cap \partial\Omega_g = \phi \qquad (4.2.7)$$

In the above equations: u_i are the components of the displacement, x_i are the spatial coordinates, n_j are the components of the normal vector; $D_{ijk\ell}$ are the components of the material response tensor; F_i, h_i and g_i are the components of the body force, the prescribed traction and the prescribed displacement, respectively. Repeated indices denote sums and a comma denotes partial differentiation.

The probabilistic potential energy variational principle (PPEVP), which is a combination of the potential energy variational principle and the second-order perturbation method (i.e., the second moment analysis), embeds the probabilistic distributions, as reflected in the mean and covariance of the material properties, domain, boundary conditions and loading, to yield the corresponding means and covariances of the response in the variational statement. The basic idea of the second-order perturbation method in PPEVP is to expand each random function about the mean value of the random field $b(\underset{\sim}{x})$, denoted by $\overline{b}(\underset{\sim}{x})$, and retain at most second order terms. That is, for a given small parameter ξ, representing the scale of randomness in $b(\underset{\sim}{x})$, the random function u_i is expanded about $\overline{b}$ via a second-order perturbation at a

given point $\underset{\sim}{x}$ by

$$u_i \simeq u_i^o + \xi u_i' + \xi^2 u_i'' \tag{4.2.8}$$

where u_i^o, u_i' and u_i'' are the zeroth, first and second order functions, respectively. Similar expansions are done for $D_{ijk\ell}$, F_i, h_i, n_j and g_i.

To simplify the subsequent development, the following abstract notations are introduced:

$$\langle \underset{\sim}{w}, \underset{\sim}{D}, \underset{\sim}{u} \rangle = \int_\Omega w_{(i,j)} D_{ijk\ell} u_{(k,\ell)} \, d\Omega \tag{4.2.9}$$

$$(\underset{\sim}{w}, \underset{\sim}{F}) = \int_\Omega w_i F_i \, d\Omega \tag{4.2.10}$$

$$(\underset{\sim}{w}, \underset{\sim}{h})_\partial = \int_{\partial\Omega_h} w_i h_i \, d\Gamma \tag{4.2.11}$$

Substituting the expanded functions into Eq. (4.2.1) and equating equal order terms, the zeroth, first and second order potential energy variational principles can be shown to be

Zeroth Order

$$\langle \delta\underset{\sim}{u}, \underset{\sim}{D}^o, \underset{\sim}{u}^o \rangle = (\delta\underset{\sim}{u}, \underset{\sim}{F}^o) + (\delta\underset{\sim}{u}, \underset{\sim}{h}^o)_\partial \tag{4.2.12}$$

First Order (ξ terms)

$$\langle \delta\underset{\sim}{u}, \underset{\sim}{D}^{o}, \underset{\sim}{u}' \rangle = (\delta\underset{\sim}{u}, \underset{\sim}{F}') + (\delta\underset{\sim}{u}, \underset{\sim}{h}')_{\partial} - \langle \delta\underset{\sim}{u}, \underset{\sim}{D}', \underset{\sim}{u}^{o} \rangle \qquad (4.2.13)$$

Second Order (ξ^2 terms)

$$\langle \delta\underset{\sim}{u}, \underset{\sim}{D}^{o}, \underset{\sim}{u}'' \rangle = (\delta\underset{\sim}{u}, \underset{\sim}{F}'') + (\delta\underset{\sim}{u}, \underset{\sim}{h}'')_{\partial} - \langle \delta\underset{\sim}{u}, \underset{\sim}{D}'', \underset{\sim}{u}^{o} \rangle - \langle \delta\underset{\sim}{u}, \underset{\sim}{D}', \underset{\sim}{u}' \rangle \qquad (4.2.14)$$

Remark 2.1 The arbitrary test function $\delta\underset{\sim}{u}$ satisfies $\delta\underset{\sim}{u} = \underset{\sim}{0}$ on the boundary ∂R_g.

Remark 2.2 All the functions with a superscript "o" are deterministic functions (i.e., evaluated at $\bar{b}$) whereas functions with superscripts "'" and '"' are random functions characterized by the random field $b(\underset{\sim}{x})$.

Remark 2.3 Equation (4.2.12) is the standard deterministic variational statement and therefore, the usual Galerkin finite element procedure can be employed directly. Once $\underset{\sim}{u}^{o}$ is determined from Eq. (4.2.12), the random functions $\underset{\sim}{u}'$ and $\underset{\sim}{u}''$ can be determined using Eqs. (4.2.13) and (4.2.14), sequentially.

It should be noted that the random functions $\underset{\sim}{D}'$, $\underset{\sim}{F}'$, $\underset{\sim}{h}'$ and $\underset{\sim}{g}'$ and the functions with the superscript '"' are, in general, described through spatial expectation and autocovariance functions. Therefore, in addition to the usual finite element approximation of the displacement field, the random field is also discretized with q shape functions. To incorporate the spatial expectation and autocovariance functions into the formulation, the discretized random variables b_K are expanded

about $\bar{b}_K$ via second moment methods. The first order variation at each point $\underset{\sim}{x}_K$ is denoted by $db_K = \xi \Delta b_K = \xi(b_K - \bar{b}_K)$.

For consistency with the finite element approximation and to assure the accuracy of the approximation of the random field, the random functions $\underset{\sim}{D}$, $\underset{\sim}{F}$, $\underset{\sim}{h}$ and $\underset{\sim}{g}$; which are, in general, functions of $\underset{\sim}{b}(\underset{\sim}{x})$ and $\underset{\sim}{x}$, are <u>first</u> discretized with the same q shape functions. For example, the finite element approximation of $\underset{\sim}{D}$, (the coefficient 1/2 has been added to the quadratic term (Eq. (4.2.18)) so that it is consistent with conventional descriptions of second moment analysis) is given by:

$$\underset{\sim}{D} \approx \underset{\sim}{D}^{o} + \xi \underset{\sim}{D}^{'} + \xi^2 \underset{\sim}{D}^{''} \tag{4.2.15}$$

or

$$\underset{\sim}{D} \approx \sum_{I=1}^{q} \Phi_I(\underset{\sim}{x}) \{ \underset{\sim}{D}_I^{o} + \xi \underset{\sim}{D}_I^{'} + \xi^2 \underset{\sim}{D}_I^{''} \} \tag{4.2.16}$$

where $\underset{\sim}{D}_I^{o}$ denotes the I^{th} nodal value of $\underset{\sim}{D}$ evaluated at $\bar{b}$, $\underset{\sim}{D}_I^{'}$ denotes the first order variation of $\underset{\sim}{D}(\underset{\sim}{x}_I, \bar{b})$ due to variations Δb_K, $\underset{\sim}{D}_I^{''}$ denotes the second order variation and $\Phi_I(\underset{\sim}{x})$ are the q shape functions. The random variables $\underset{\sim}{D}_I^{'}$ are then expanded in terms of the random variables b_K by

$$\underset{\sim}{D}_I^{'} = \sum_{K=1}^{q} (\underset{\sim}{D}_I^{'})_K \, \Delta b_K \tag{4.2.17}$$

$$\underset{\sim}{D}_I^{''} = \frac{1}{2} \sum_{K,L=1}^{q} (\underset{\sim}{D}_I^{''})_{KL} \, \Delta b_K \Delta b_L \tag{4.2.18}$$

respectively. The nodal values of $(\underset{\sim}{D}'_I)_K$ and $(\underset{\sim}{D}''_I)_{KL}$ can be obtained by partial differentiation or by a least-square fit. Similar definitions hold for $\underset{\sim}{F}$, $\underset{\sim}{h}$ and $\underset{\sim}{g}$.

The displacement is discretized similarly, however, with NUMEL elements and NUMNP nodes with each node having NDOF degrees of freedom, via (c.f. Eq. (4.2.8)), where

$$\underset{\sim}{u}^o = \sum_{A=1}^{NUMNP} N_A(\underset{\sim}{x})\underset{\sim}{d}^o_A \tag{4.2.19}$$

$$\underset{\sim}{u}' = \sum_{A=1}^{NUMNP} N_A(\underset{\sim}{x})\underset{\sim}{d}'_A \tag{4.2.20}$$

$$\underset{\sim}{u}'' = \sum_{A=1}^{NUMNP} N_A(\underset{\sim}{x})\underset{\sim}{d}''_A \tag{4.2.21}$$

and N_A are the displacement shape functions. The first and second order variations of $\underset{\sim}{d}'_A$ and $\underset{\sim}{d}''_A$ are defined by

$$\underset{\sim}{d}'_A = \sum_{K=1}^{q} (\underset{\sim}{d}'_A)_K \, \Delta b_K \tag{4.2.22}$$

and

$$\underset{\sim}{d}''_A = \frac{1}{2} \sum_{K,L=1}^{q} (\underset{\sim}{d}''_A)_{KL} \, \Delta b_K \Delta b_L \tag{4.2.23}$$

respectively.

Substituting the above Galerkin/finite element approximations into the zeroth, first and second order variational statements, the finite

element matrix equations can be obtained using Eqs. (4.2.19-21) and the arbitrariness of $\delta\underset{\sim}{d}$,

$$\delta\underset{\sim}{d} = (\delta d_1, \delta d_2, \ldots, \delta d_{NEQ})^T \tag{4.2.24}$$

It should be noted that only NEQ test functions are required since no test function is needed on the parametrized boundary ∂R_g; NEQ is the number of finite element equations to be solved.

Zeroth Order

$$\underset{\sim}{K}\,\underset{\sim}{d}^o = \underset{\sim}{f}^o \tag{4.2.25}$$

where

$$\underset{\sim}{K} = \{K_{AB}\} = \langle N_A, \underset{\sim}{D}^o, N_B \rangle \tag{4.2.26}$$

$$\underset{\sim}{f}^o = \{f_A^o\} = (N_A, \underset{\sim}{F}^o) + (N_A, \underset{\sim}{h}^o)_\partial$$

$$- \langle N_A, \underset{\sim}{D}^o, N_C \rangle g_C^o \tag{4.2.27}$$

$$\underset{\sim}{d}^o = \{d_B^o\} \tag{4.2.28}$$

where the subscript A takes the values of 1 to NEQ, B is summed from 1 to NEQ and C is summed from NEQ + 1 to NED; NED is equal to NDOF times

NUMNP.

First Order (for each Δb_K) $\quad K = 1, \ldots, q$

$$\underset{\sim}{K}\, \underset{\sim}{d}'_K = \underset{\sim}{f}'_K \tag{4.2.29}$$

where

$$\underset{\sim}{f}'_K = \{f'_A\}_K = (N_A, \underset{\sim}{F}'_K) + (N_A, \underset{\sim}{h}'_K)_\partial - \langle N_A, \underset{\sim}{D}'_K, \underset{\sim}{u}^o\rangle$$

$$- \langle N_A, \underset{\sim}{D}^o, N_C\rangle (g'_C)_K \tag{4.2.30}$$

and

$$\underset{\sim}{d}'_K = \{d'_B\}_K \tag{4.2.31}$$

Second Order (K and L are summed from 1 to q)

$$\underset{\sim}{K}\, \underset{\sim}{d}'' = \underset{\sim}{f}'' \tag{4.2.32}$$

where

$$\underset{\sim}{f}'' = \{f''_A\}_{KL}\, \Delta b_K \Delta b_L$$

$$= \{\tfrac{1}{2}(N_A, \underset{\sim}{F}''_{KL}) + \tfrac{1}{2}(N_A, \underset{\sim}{h}''_{KL})_\partial - \tfrac{1}{2}\langle N_A, \underset{\sim}{D}''_{KL}, \underset{\sim}{u}^o\rangle$$

$$- \langle N_A, \underset{\sim}{D}'_K, \underset{\sim}{u}'_L \rangle - \frac{1}{2} \langle N_A, \underset{\sim}{D}^o, N_C \rangle (g''_C)_{KL} \} \Delta b_K \Delta b_L \tag{4.2.33}$$

and

$$\underset{\sim}{d}'' = \frac{1}{2} \{d''_B\}_{KL} \Delta b_K \Delta b_L \tag{4.2.34}$$

The mean and autocovariance matrices for the nodal displacement are defined by

$$E[\underset{\sim}{d}] = \int_{-\infty}^{\infty} \underset{\sim}{d}(\underset{\sim}{b}) f(\xi, \underset{\sim}{b}) d\underset{\sim}{b} \tag{4.2.35}$$

and

$$Cov(d_{iA}, d_{jB}) = \int_{-\infty}^{\infty} (d_{iA} - \bar{d}_{iA})(d_{jB} - \bar{d}_{jB}) \, f(\xi, \underset{\sim}{b}) d\underset{\sim}{b} \tag{4.2.36}$$

respectively. f is the joint probability density function which is dependent on ξ. $\underset{\sim}{b}$ is the random-variable vector

$$\underset{\sim}{b} = (b_1, b_2, \ldots, b_q)^T \tag{4.2.37}$$

With Eq. (4.2.35), the second order accurate mean value of $\underset{\sim}{d}$ is shown to be

$$E[\underset{\sim}{d}] = \underset{\sim}{d}^o + \bar{\underset{\sim}{d}}'' \tag{4.2.38}$$

< 2

where $\underset{\sim}{\bar{d}}''$ is given by

$$\underset{\sim}{\bar{d}}'' = \frac{1}{2} \sum_{K,L=1}^{q} \underset{\sim}{d}''_{KL} \, \mathrm{Cov}(b_K, b_L) \tag{4.2.39}$$

From Eq. (4.2.36) the first-order autocovariance of the displacement can be shown to be

$$\mathrm{Cov}(d_{iA}, d_{jB}) = \sum_{K,L=1}^{q} (d'_{iA})_K (d'_{jB})_L \, \mathrm{Cov}(b_K, b_L) \tag{4.2.40}$$

To simplify the computational procedure of Eqs. (4.2.32-34), integrate Eq. (4.2.32) over the range of the random variables so that it is replaced by

$$\underset{\sim}{K} \, \underset{\sim}{\bar{d}}'' = \underset{\sim}{\bar{f}}'' \tag{4.2.41}$$

where $\underset{\sim}{\bar{d}}''$ is given in Eqs. (4.2.39) and $\underset{\sim}{\bar{f}}''$ is given by the right-hand side of Eq. (4.2.33) with $\Delta b_K \Delta b_L$ replaced by $\mathrm{Cov}(b_K, b_L)$.

4.3 PFEM for Nonlinear Continua with Large Deformations

In this section, the PFEM formulation for large deformations of hyperelastic materials in bodies of random shape is considered. The simplest form of the weak form for nonlinear elasticity with large deformations is:

$$\int_{\Omega} \delta\underset{\sim}{\varepsilon}^T \underset{\sim}{\sigma}\, d\Omega = \int_{\Omega} \delta\underset{\sim}{u}^T \underset{\sim}{F}\, d\Omega + \int_{\partial\Omega_h} \delta\underset{\sim}{u}^T \underset{\sim}{h}\, d\Omega \tag{4.3.1}$$

where $\underset{\sim}{\varepsilon}$, $\underset{\sim}{\sigma}$, $\underset{\sim}{F}$ and $\underset{\sim}{h}$ are the nonsymmetric measures of the strain, first Piola Kirchhoff stress, body force and traction, respectively; Ω and $\partial\Omega_h$ are the domain and natural boundary, respectively, in the initial configuration. Furthermore, the strain measure is given by

$$\underset{\sim}{\varepsilon} = \nabla\underset{\sim}{u} = \underset{\sim}{G} - \underset{\sim}{I} \tag{4.3.2}$$

where $\underset{\sim}{G}$ is the deformation gradient and $\underset{\sim}{I}$ is the identity matrix. The stress for a hyperelastic material is given by

$$\underset{\sim}{\sigma} = \underset{\sim}{\psi}(\underset{\sim}{G}) \tag{4.3.3}$$

where

$$\underset{\sim}{\psi} = \frac{\partial W}{\partial \underset{\sim}{G}} \tag{4.3.4}$$

and W is the strain energy density function. Randomness in material,

geometric properties and loads are represented by the random field $b(\underset{\sim}{x})$. To incorporate the random domain and boundaries into the formulation, Eq. (4.3.1) can be rewritten as

$$\int_R \delta\underset{\sim}{\varepsilon}^T \underset{\sim}{\sigma}\, J_v\, dR = \int_R \delta\underset{\sim}{u}^T \underset{\sim}{F}\, J_v\, dR + \int_{\partial R_h} \delta\underset{\sim}{u}^T \underset{\sim}{h}\, J_s\, dA \tag{4.3.5a}$$

employing the following mappings of the original domain Ω and boundary $\partial\Omega_h$ onto the reference domain R and boundary A:

$$d\Omega = J_v\, dR \tag{4.3.5b}$$

and

$$d\Gamma = J_s\, dA \tag{4.3.5c}$$

The displacement is approximated by a second order perturbation about the mean random field $\bar{b}$ at a given $\underset{\sim}{x}$:

$$\underset{\sim}{u} \approx \underset{\sim}{u}^o + \xi\underset{\sim}{u}' + \xi^2\underset{\sim}{u}'' \tag{4.3.6a}$$

where ξ represents the scale of randomness in $b(\underset{\sim}{x})$. Similarly, $\underset{\sim}{\varepsilon}$, $\underset{\sim}{F}$, $\underset{\sim}{h}$, J_v and J_s are expressed as second order perturbations. The stress is expanded as

$$\underset{\sim}{\sigma} \approx \underset{\sim}{\psi}^o + \xi(\underset{\sim}{\psi}' + \underset{\sim}{C}^o\underset{\sim}{\varepsilon}') + \xi^2(\underset{\sim}{\psi}'' + \underset{\sim}{C}'\underset{\sim}{\varepsilon}' + \underset{\sim}{C}^o\underset{\sim}{\varepsilon}'') \tag{4.3.6b}$$

where the first elasticity tensor is given by

$$\underset{\sim}{C} = \frac{\partial^2 W}{\partial \underset{\sim}{G} \partial \underset{\sim}{G}} \tag{4.3.6c}$$

The derivatives of nonlinear functions such as $\underset{\sim}{\psi}$ are given in Ref. [28]; however for nonlinear elasticity, the derivatives can be worked out explicitly. In addition, since the boundaries are parametrized, it is necessary to perturb the virtual strain in Eq. (4.3.5a) as this is a function of the domain geometry. Thus,

$$\delta\underset{\sim}{\varepsilon} = \delta\underset{\sim}{\varepsilon}^{o} + \xi\delta\underset{\sim}{\varepsilon}' + \xi^2\delta\underset{\sim}{\varepsilon}'' \tag{4.3.6d}$$

The randomness in domain and boundary geometry is taken care of by the Jacobians J_v and J_s, respectively, in Eq. (4.3.5a).

Substituting Eqs. (4.3.6a) through (4.3.6d) in Eq. (4.3.5a), the PFEM equations are obtained:

Zeroth Order

$$\int_R \delta\underset{\sim}{\varepsilon}^{oT}\underset{\sim}{\psi}^{o} J_v^{o}\, dR = \int_R \delta\underset{\sim}{u}^{T}\underset{\sim}{F}^{o} J_v^{o}\, dR + \int_{\partial R_h} \delta\underset{\sim}{u}^{T}\underset{\sim}{h}^{o} J_s^{o}\, dA \tag{4.3.7}$$

First Order

$$\int_R [\delta\underset{\sim}{\varepsilon}'^{T}\underset{\sim}{\psi}^{o} J_v^{o} + \delta\underset{\sim}{\varepsilon}^{oT}(\underset{\sim}{\psi}' + \underset{\sim}{C}^{o}\underset{\sim}{\varepsilon}')J_v^{o} + \delta\underset{\sim}{\varepsilon}^{oT}\underset{\sim}{\psi}^{o} J_v']\, dR$$

$$= \int_R [\delta \underset{\sim}{u}^T \underset{\sim}{F}' J_v^o + \delta \underset{\sim}{u}^T \underset{\sim}{F}^o J_v'] dR + \int_{\partial R_h} [\delta \underset{\sim}{u}^T \underset{\sim}{h}' J_s^o + \delta \underset{\sim}{u}^T \underset{\sim}{h}^o J_s'] dA \qquad (4.3.8)$$

Second Order

$$\int_R [\delta \underset{\sim}{\varepsilon}''^T \underset{\sim}{\psi}^o J_v^o + \delta \underset{\sim}{\varepsilon}'^T (\underset{\sim}{\psi}' + \underset{\sim}{C}^o \underset{\sim}{\varepsilon}') J_v^o + \delta \underset{\sim}{\varepsilon}'^T \underset{\sim}{\psi}^o J_v'$$

$$+ \delta \underset{\sim}{\varepsilon}^{oT} (\underset{\sim}{\psi}'' + \underset{\sim}{C}' \underset{\sim}{\varepsilon}' + \underset{\sim}{C}^o \underset{\sim}{\varepsilon}'') J_v^o + \delta \underset{\sim}{\varepsilon}^{oT} (\underset{\sim}{\psi}' + \underset{\sim}{C}^o \underset{\sim}{\varepsilon}') J_v' + \delta \underset{\sim}{\varepsilon}^{oT} \underset{\sim}{\psi}^o J_v''] dR$$

$$= \int_R [\delta \underset{\sim}{u}^T \underset{\sim}{F}'' J_v^o + \delta \underset{\sim}{u}^T \underset{\sim}{F}' J_v' + \delta \underset{\sim}{u}^T \underset{\sim}{F}^o J_v''] dR$$

$$+ \int_{\partial R_h} [\delta \underset{\sim}{u}^T \underset{\sim}{h}'' J_s^o + \delta \underset{\sim}{u}^T \underset{\sim}{h}' J_s' + \delta \underset{\sim}{u}^T \underset{\sim}{h}^o J_s''] dA \qquad (4.3.9)$$

It is noted that the test function $\delta \underset{\sim}{u}$ satisfies $\delta \underset{\sim}{u} = \underset{\sim}{0}$ on the parametrized prescribed displacement boundary ∂R_g and the intersection of the boundaries ∂R_h and ∂R_g is a null set.

Since Eq. (4.3.7) is the deterministic virtual work principle, standard techniques such as Newton Raphson iteration can be employed for its solution. After determining $\underset{\sim}{u}^o$, $\underset{\sim}{\varepsilon}^o$ and $\underset{\sim}{\psi}^o$ from Eq. (4.3.7), the random functions $\underset{\sim}{u}'$, $\underset{\sim}{\varepsilon}'$, $\underset{\sim}{\psi}'$ and $\underset{\sim}{u}''$, $\underset{\sim}{\varepsilon}''$, $\underset{\sim}{\psi}''$ can be determined from Eqs. (4.3.8) and (4.3.9), sequentially. It should be noted that the random functions $\underset{\sim}{\psi}'$, $\underset{\sim}{C}'$, $\underset{\sim}{F}'$, $\underset{\sim}{h}'$, J_s' and J_v' and the functions with the superscript '"' are, in general, given and described through the spatial expectation and autocovariance functions. Similar to the previous section, the random functions are discretized with q shape functions.

For example, the finite element approximation of the first

elasticity tensor, $\underset{\sim}{C}$, is given by:

$$\underset{\sim}{C} \simeq \underset{\sim}{C}^{o} + \xi \underset{\sim}{C}^{'} + \xi^2 \underset{\sim}{C}^{''} \tag{4.3.10a}$$

or

$$\underset{\sim}{C} \simeq \sum_{I=1}^{q} \Phi_I(\underset{\sim}{x}) \{ \underset{\sim}{C}_I^{o} + \xi \underset{\sim}{C}_I^{'} + \xi^2 \underset{\sim}{C}_I^{''} \} \tag{4.3.10b}$$

where $\underset{\sim}{C}_I^{o}$ denotes the I^{th} nodal value of $\underset{\sim}{C}$ evaluated at $\bar{b}$,

$$\underset{\sim}{C}_I^{'} = \sum_{M=1}^{q} (\underset{\sim}{C}_I^{'})_M \, \Delta b_M \tag{4.3.10c}$$

and

$$\underset{\sim}{C}_I^{''} = \frac{1}{2} \sum_{M,N=1}^{q} (\underset{\sim}{C}_I^{''})_{MN} \, \Delta b_M \Delta b_N \tag{4.3.10d}$$

respectively. Similar definitions hold for $\underset{\sim}{F}$, $\underset{\sim}{h}$, $\underset{\sim}{\psi}$, J_v and J_s.

Similarly, the displacement field is discretized, however with NUMEL elements and NUMNP nodes with each node having NDOF degrees of freedom (see Eqs. (4.2.8) and (4.2.19-23)).

The elemental strain is expressed as

$$\underset{\sim}{\varepsilon} = \underset{\sim}{B} \, \underset{\sim}{d} \tag{4.3.11}$$

where $\underset{\sim}{B}$ is the discretized gradient operator. The strain perturbation

is:

$$\underset{\sim}{\varepsilon} \approx \underset{\sim}{\varepsilon}^{o} + \xi\underset{\sim}{\varepsilon}' + \xi^2\underset{\sim}{\varepsilon}'' \tag{4.3.12}$$

or

$$\underset{\sim}{\varepsilon} \approx \underset{\sim}{B}^{o}\underset{\sim}{d}^{o} + \xi(\underset{\sim}{B}'\underset{\sim}{d}^{o} + \underset{\sim}{B}^{o}\underset{\sim}{d}') + \xi^2(\underset{\sim}{B}''\underset{\sim}{d}^{o} + \underset{\sim}{B}'\underset{\sim}{d}' + \underset{\sim}{B}^{o}\underset{\sim}{d}'') \tag{4.3.13a}$$

and from Eq. (4.4.3.6d)

$$\delta\underset{\sim}{\varepsilon} \approx \underset{\sim}{B}^{o}\delta\underset{\sim}{d}^{o} + \xi\underset{\sim}{B}'\delta\underset{\sim}{d}^{o} + \xi^2\underset{\sim}{B}''\delta\underset{\sim}{d}^{o} \tag{4.3.13b}$$

Substituting Eqs. (4.3.10) through (4.3.13) in Eqs. (4.3.7), (4.3.8) and (4.3.9) and using the arbitrariness of $\delta\underset{\sim}{d}^{o}$ the zeroth, first and second order equilibrium conditions are obtained, respectively.

Zeroth Order

$$\int_R \underset{\sim}{B}^{oT}\underset{\sim}{\psi}^{o}J_v^{o}\,dR = \int_R \underset{\sim}{N}^{T}\underset{\sim}{F}^{o}J_v^{o}\,dR + \int_{\partial R_h} \underset{\sim}{N}^{T}\underset{\sim}{h}^{o}J_s^{o}\,dA \tag{4.3.14}$$

First Order (for each b_M, M = 1, ..., q)

$$\underset{\sim}{K}\,\underset{\sim}{d}_M' = \underset{\sim}{f}_M' \tag{4.3.15a}$$

where

$$\underset{\sim}{f}'_M = \int_R \underset{\sim}{N}^T[\underset{\sim}{F}'_M J_v^o + \underset{\sim}{F}^o(J'_v)_M]dR + \int_{\partial R_h} \underset{\sim}{N}^T[\underset{\sim}{h}'_M J_s^o + \underset{\sim}{h}^o(J'_s)_M]dA$$

$$- \int_R \underset{\sim}{B}'^T \underset{\sim}{\psi}^o J_v^o \, dR - \int_R \underset{\sim}{B}^{oT}(\underset{\sim}{\psi}' + \underset{\sim}{C}^o \underset{\sim}{B}' \underset{\sim}{d}^o) J_v^o \, dR - \int_R \underset{\sim}{B}^{oT} \underset{\sim}{\psi}^o (J'_v)_M \, dR \quad (4.3.15b)$$

with

$$\underset{\sim}{C}^o = \underset{\sim}{D}^o + \underset{\sim}{T}^o \quad (4.3.15c)$$

resulting in

$$\underset{\sim}{K} = \underset{\sim}{K}_D + \underset{\sim}{K}_G \quad (4.3.15d)$$

where

$$\underset{\sim}{K}_D = \int_R \underset{\sim}{B}^{oT} \underset{\sim}{D}^o \underset{\sim}{B}^o J_v^o \, dR \quad (4.3.15e)$$

and

$$\underset{\sim}{K}_G = \int_R \underset{\sim}{B}^{oT} \underset{\sim}{T}^o \underset{\sim}{B}^o J_v^o \, dR \quad (4.3.15f)$$

where $\underset{\sim}{D}^o$ and $\underset{\sim}{T}^o$ represent the material response and initial stress matrices respectively. Explicit expressions of these matrices for a QBI element are given in Ref. [38].

Second Order (M and N are summed from 1 to q)

$$\underset{\sim}{K}\,\underset{\sim}{\ddot{d}} = \underset{\sim}{\ddot{f}} \tag{4.3.16a}$$

where

$$\begin{aligned}
\underset{\sim}{\ddot{f}} = \{ & \int_R \underset{\sim}{N}^T[\tfrac{1}{2}\,\underset{\sim}{\ddot{F}}_{MN} J_v^o + \underset{\sim}{F}'_M (J_v')_N + \tfrac{1}{2}\,\underset{\sim}{F}^o (\ddot{J}_v)_{MN}]\,dR \\
& + \int_{\partial R_h} \underset{\sim}{N}^T[\tfrac{1}{2}\,\underset{\sim}{\ddot{h}}_{MN} J_s^o + \underset{\sim}{h}'_M (J_s')_N + \tfrac{1}{2}\,\underset{\sim}{h}^o (\ddot{J}_s)_{MN}]\,dA \\
& - \int_R \underset{\sim}{B}'^T_M (\underset{\sim}{\psi}'_N + \underset{\sim}{C}^o \underset{\sim}{B}'_N \underset{\sim}{d}^o + \underset{\sim}{C}^o \underset{\sim}{B}^o \underset{\sim}{d}'_N) J_v^o \,dR - \int_R \underset{\sim}{B}'^T_M \underset{\sim}{\psi}^o (J_v')_N \,dR \\
& - \int_R \underset{\sim}{B}^{oT} (\tfrac{1}{2}\,\underset{\sim}{\ddot{\psi}}_{MN} + \underset{\sim}{C}'_M \underset{\sim}{B}'_N \underset{\sim}{d}^o + \underset{\sim}{C}'_M \underset{\sim}{B}^o \underset{\sim}{d}'_N + \tfrac{1}{2}\,\underset{\sim}{C}^o \underset{\sim}{\ddot{B}}_{MN} \underset{\sim}{d}^o + \underset{\sim}{C}^o \underset{\sim}{B}'_M \underset{\sim}{d}'_N) J_v^o \,dR \\
& - \int_R \underset{\sim}{B}^{oT} (\underset{\sim}{\psi}'_M + \underset{\sim}{C}^o \underset{\sim}{B}'_M \underset{\sim}{d}^o + \underset{\sim}{C}^o \underset{\sim}{B}^o \underset{\sim}{d}'_M)(J_v')_N \,dR \\
& - \int_R \tfrac{1}{2}\,\underset{\sim}{B}^{oT} \underset{\sim}{\psi}^o (\ddot{J}_v)_{MN} \,dR - \int_R \tfrac{1}{2}\,\underset{\sim}{\ddot{B}}^T_{MN} \underset{\sim}{\psi}^o J_v^o \,dR \} \Delta b_M \Delta b_N
\end{aligned} \tag{4.3.16b}$$

and

$$\underset{\sim}{\ddot{d}} = \tfrac{1}{2}\,\underset{\sim}{\ddot{d}}_{MN} \Delta b_M \Delta b_N \tag{4.3.16c}$$

Eqs. (4.3.14) through (4.3.16) are solved in sequence.

The second order accurate mean value of $\underset{\sim}{d}$ is

$$E[\underset{\sim}{d}] = \underset{\sim}{d}^{o} + \bar{\underset{\sim}{d}}^{"} \tag{4.3.17a}$$

where $\bar{\underset{\sim}{d}}^{"}$ is given by (c.f. the previous section)

$$\bar{\underset{\sim}{d}}^{"} = \frac{1}{2} \sum_{M,N=1}^{q} \underset{\sim}{d}^{"}_{MN} \, \mathrm{Cov}(b_M, b_N) \tag{4.3.17b}$$

and the first order accurate autocovariance of the displacement is

$$\mathrm{Cov}(d_{iA}, d_{jB}) = \sum_{M,N=1}^{q} (d'_{iA})_M (d'_{jB})_N \mathrm{Cov}(b_M, b_N) \tag{4.3.17c}$$

The mean and autocovariance matrices for the element strains can be obtained from the following:

$$E[\underset{\sim}{\varepsilon}] = \underset{\sim}{\varepsilon}^{o} + \bar{\underset{\sim}{\varepsilon}}^{"} \tag{4.3.18a}$$

where

$$\underset{\sim}{\varepsilon}^{o} = \underset{\sim}{B}^{o} \underset{\sim}{d}^{o} \tag{4.3.18b}$$

and $\bar{\underset{\sim}{\varepsilon}}^{"}$ is defined by

$$\bar{\underset{\sim}{\varepsilon}}^{"} = \sum_{M,N=1}^{q} \left[\frac{1}{2} \underset{\sim}{B}^{"}_{MN} \underset{\sim}{d}^{o} + \underset{\sim}{B}'_{M} \underset{\sim}{d}'_{N} + \frac{1}{2} \underset{\sim}{B}^{o} \underset{\sim}{d}^{"}_{MN}\right] \mathrm{Cov}(b_M, b_N) \tag{4.3.18c}$$

Thus,

$$\mathrm{Cov}(\underset{\sim}{\varepsilon}_i, \underset{\sim}{\varepsilon}_j) = \sum_{M,N=1}^{q} (\underset{\sim}{\varepsilon}'_i)_M (\underset{\sim}{\varepsilon}'_j)^{T}_N \mathrm{Cov}(b_M, b_N) \tag{4.3.18d}$$

with the definition

$$(\underset{\sim}{\varepsilon}_i')_M = (\underset{\sim}{B}_i')_M \underset{\sim}{d}_i^o + \underset{\sim}{B}_i^o (\underset{\sim}{d}_i')_M \qquad \begin{matrix} i = 1, \ldots, \text{NUMEL, no sum on i} \\ M = 1, \ldots, q \end{matrix} \tag{4.3.18e}$$

where subscript "i" denotes the i^{th} element and NUMEL is the total number of elements. Similarly, the mean first Piola-Kirchoff stress is:

$$E[\underset{\sim}{\sigma}] = \underset{\sim}{\sigma}^o + \bar{\underset{\sim}{\sigma}}'' \tag{4.3.19a}$$

where

$$\underset{\sim}{\sigma}^o = \underset{\sim}{\psi}^o \tag{4.3.19b}$$

and

$$\bar{\underset{\sim}{\sigma}}'' = \sum_{M,N=1}^{q} \left[\frac{1}{2} \underset{\sim}{\psi}_{MN}'' + \underset{\sim}{C}_M' \underset{\sim}{B}_N' \underset{\sim}{d}^o + \underset{\sim}{C}_M' \underset{\sim}{B}^o \underset{\sim}{d}_N' + \frac{1}{2} \underset{\sim}{C}^o \underset{\sim}{B}_{MN}'' \underset{\sim}{d}^o \right.$$

$$\left. + \underset{\sim}{C}^o \underset{\sim}{B}_M' \underset{\sim}{d}_N' + \frac{1}{2} \underset{\sim}{C}^o \underset{\sim}{B}^o \underset{\sim}{d}_{MN}'' \right] \mathrm{Cov}(b_M, b_N) \tag{4.3.19c}$$

and the stress autocovariance is defined by

$$\mathrm{Cov}(\underset{\sim}{\sigma}_i, \underset{\sim}{\sigma}_j) = \sum_{M,N=1}^{q} (\underset{\sim}{\sigma}_i')_M (\underset{\sim}{\sigma}_j')_N^T \mathrm{Cov}(b_M, b_N) \tag{4.3.19d}$$

with the definition

$$(\underset{\sim}{\sigma}_i')_M = (\underset{\sim}{\psi}_i')_M + \underset{\sim}{C}_i^o(\underset{\sim}{B}_i')_M\underset{\sim}{d}_i^o + \underset{\sim}{C}_i^o\underset{\sim}{B}_i^o(\underset{\sim}{d}_i')_M \qquad \begin{matrix} i = 1, \ldots, \text{NUMEL, no sum on } i \\ M = 1, \ldots, q \end{matrix}$$

(4.3.19e)

4.4 Computational Aspects of PFEM

4.4.1 Transformation of the Covariance Matrix

In linear problems, it can be observed from Eqs. (4.2.25), (4.2.29) and (4.2.41) that the determination of $\underset{\sim}{d}^{o}$, $\underset{\sim K}{d}'$ and $\underset{\sim}{\bar{d}}''$ involve one factorization of $\underset{\sim}{K}$ and q + 2 forward-reductions and back-substitutions. The latter operations consist of evaluation of $\underset{\sim}{d}^{o}$ in Eq. (4.2.25), q evaluations of $\underset{\sim K}{d}'$ in Eq. (4.2.29) and one more evaluation of $\underset{\sim}{\bar{d}}''$ in Eq. (4.2.41). Even though the above computations are compatible with the elemental discretization and nodal assembly procedures that characterize finite element theory and software, the number of matrix multiplications is proportional to q(q + 1)/2. This would be unacceptably expensive. The large number of computations arise from the double summations in i and j in Eq. (4.2.33). To remedy this situation, the covariance matrix $\mathrm{Cov}(b_i,b_j)$ is transformed to a diagonal variance matrix $\mathrm{Var}(c_i,c_j)$ such that

$$\mathrm{Var}(c_i,c_j) = 0 \qquad \text{for } i \neq j \qquad (4.4.1a)$$

and

$$\mathrm{Var}(c_i,c_j) = \mathrm{Var}(c_i) \qquad \text{for } i = j \qquad (4.4.1b)$$

Therefore, the number of matrix multiplications is now proportional to q. The above involves the solution of the eigenproblem

$$\underset{\sim}{G}\underset{\sim}{\psi} = \underset{\sim}{\psi}\underset{\sim}{\Lambda} \tag{4.4.1.2}$$

where G_{ij} and Λ_{ij} denote $\mathrm{Cov}(b_i,b_j)$ and $\mathrm{Var}(c_i,c_j)$, respectively, and $\underset{\sim}{\psi}$ is a constant transformation matrix with the following properties:

$$\underset{\sim}{\psi}^T\underset{\sim}{\psi} = \underset{\sim}{\psi}\underset{\sim}{\psi}^T = \underset{\sim}{1} \tag{4.4.1.3a}$$

$$\underset{\sim}{\Lambda} = \underset{\sim}{\psi}^T\underset{\sim}{G}\underset{\sim}{\psi} \tag{4.4.1.3b}$$

and

$$\underset{\sim}{b} = \underset{\sim}{\psi}\underset{\sim}{c} \quad \text{or} \quad \underset{\sim}{c} = \underset{\sim}{\psi}^T\underset{\sim}{b} \tag{4.4.1.4}$$

$\underset{\sim}{1}$ is the $q \times q$ identity matrix and $\underset{\sim}{c}$ is the transformed $q \times 1$ random variables vector. The mean and variance are

$$E[\underset{\sim}{c}] = \underset{\sim}{\psi}^T E[\underset{\sim}{b}] \tag{4.4.1.5}$$

and

$$\mathrm{Var}(\underset{\sim}{c}) = \text{diagonal terms of } \underset{\sim}{\Lambda} \tag{4.4.1.6}$$

With Eqs. (4.4.1.3b) and (4.4.1.4), the mixed derivatives appearing in Eq. (4.2.40) reduce to second derivatives, and the covariance matrix is replaced by the diagonal variance matrix in Eqs. (4.2.33) and

(4.2.40).

Analogous to modal analysis in structural dynamics problems, only a few modes n($n < q$) (i.e., Var(c_i)) are required to capture the major characteristics of the probabilistic distribution. However, the highest eigenvalues have to be employed. This is in contrast to the modal structural dynamics problem, wherein the lowest eigenvalues are used. As PFEM involves, essentially, a set of sensitivity equations with respect to $\underset{\sim}{c}$, recent techniques in design sensitivity analysis can be adapted easily. One such technique is the adjoint method in mechanical design [32-35]. In this method, the first and second order derivatives of the objective functions and constraints are calculated w.r.t. the design parameters, with minimal computations of the first and second order equations.

4.4.2 Adjoint Method in PFEM

Consider a typical function $\psi(\underset{\sim}{c},\underset{\sim}{d})$ involving the displacements $\underset{\sim}{d}$ and the random variables $\underset{\sim}{c}$. Chain differentiation yields

$$[\psi]_{c_i} = \psi_{c_i} + \underset{\sim}{\psi}_d^T \underset{\sim}{d}'_{c_i} \qquad i = 1, \ldots, n \qquad (4.4.2.1a)$$

where the subscript denotes the derivative with respect to c_i, and

$$\underset{\sim}{\psi}_d^T = (\psi_{d_1}, \ldots, \psi_{d_k}, \ldots, \psi_{d_{NEQ}}) \qquad (4.4.2.1b)$$

Substituting Eq. (4.2.29) in Eq. (4.4.2.1b), the explicit equation

$$[\psi]_{c_i} = \psi_{c_i} + \underset{\sim}{\psi}_d^T \underset{\sim}{K}^{-1} \underset{\sim}{f}_{c_i} \qquad i = 1, \ldots, n \qquad (4.4.2.2)$$

is obtained. Usually, in the direct method, the above equation is evaluated for each random variable c_i, involving 'n' solutions of the linear equation (4.4.2.2). In the adjoint method, $\underset{\sim}{\lambda}$ is selected to satisfy

$$\underset{\sim}{K}\,\underset{\sim}{\lambda} = \underset{\sim}{\psi}_d \qquad (4.4.2.3)$$

Then, Eq. (4.4.2.2) can be rewritten as

$$[\psi]_{c_i} = \psi_{c_i} + \underset{\sim}{\lambda}^T \underset{\sim}{f}_{c_i} \qquad i = 1, \ldots, n \qquad (4.4.2.4)$$

The adjoint problem, Eq. (4.4.2.3), is solved only once in this method. In the direct method, 'n' solutions of Eq. (4.2.29) are required. This is the advantage of the adjoint method over the direct method. Both methods require 'n' inner products with $\underset{\sim}{f}'_{c_i}$, in Eqs. (4.4.2.1) and (4.4.2.4), respectively. However, it has been shown that when the number of functions ψ is more than the number of random variables, the computational advantage of the adjoint method is lost [33,34]. By solving 'n' adjoint problems, the second order sensitivites can also be evaluated [33,34]. It should be noted that the adjoint method is applicable to nonlinear problems as well, as the first and second order equations are still linear.

4.4.3 Displacement Derivatives in PFEM

In mechanics, one is often interested in the response in only a portion of the entire domain. Stress concentrations, plastic flow and strain localization effects are some examples. Similarly, in probabilistic analysis, one is interested in the probability of failure, which usually initiates in a small domain. This translates into a few nodal displacements and element strains and stresses. In such cases, the adjoint methodology can be used to reduce the computations in PFEM equations for the evaluation of derivatives.

The adjoint method can be used to calculate the displacement derivatives of the k^{th} component of the displacement vector $\underset{\sim}{d}$, denoted by $d^{(k)}$. This is done by substituting

$$\psi = d^{(k)} \tag{4.4.3.1}$$

in Eq. (4.4.2.4). Thus,

$$[d^{(k)}]_{c_i} = d^{(k)}_{c_i} + \underset{\sim}{\lambda}^T \underset{\sim}{f}'_{c_i} \tag{4.4.3.2}$$

where $\underset{\sim}{\lambda}$ is obtained from the adjoint problem

$$\underset{\sim}{K}\,\underset{\sim}{\lambda} = d^{(k)}_{\underset{\sim}{d}} \quad . \tag{4.4.3.3}$$

Interestingly, the right hand side of Eq. (4.4.3.3) is a Boolean vector, with unit value at the k^{th} component. Therefore, the adjoint problem

for displacement derivatives can be interpreted as a linear structural problem with the same tangent stiffness and a unit load at the k^{th} position of the external force vector. The displacement covariance is then obtained from Eq. (4.2.39), where the derivatives are with respect to $\underset{\sim}{c}$ and the covariance matrix is replaced by the diagonal variance matrix (Eq. (4.4.1.6)).

In the direct method, the second-order term $\underset{\sim}{\bar{d}}''$ in Eq. (4.2.41) is obtained by a single solution, irrespective of the number of random variables c_i. This is because of the summation of the second-order displacement derivatives in Eq. (4.2.39).

In comparison, the adjoint method may require more computations to compute the second-order term $\underset{\sim}{\bar{d}}''$. This term requires the first derivatives of the displacements, over the entire domain. In such a scenario, the adjoint problem (cf. Eq. (4.4.3.3) has to be solved for each component of the displacement vector $\underset{\sim}{d}$, resulting in more computations. If the size of the vector $\underset{\sim}{d}$ is small when compared with the number of random variables c_i, the adjoint method will require fewer computations than the direct method. Thus, the selection of the adjoint method over the direct method depends on (i) the number of displacement components considered, (ii) the number of random variables c_i, $i = 1, \ldots, n$ and (iii) the size of the displacement vector $\underset{\sim}{d}$.

It is to be noted that the adjoint problem is always linear, irrespective of the primary problem. It has been noticed that the second-order term contributes very little to the mean displacement calculations [24-26]. If the second-order term is neglected, then the

adjoint method for the first-order mean and covariance would involve solutions of only two equations viz., Eqs. (4.2.29) and (4.4.3.3) and 'n' inner products with $\underset{\sim}{f}'_{c_i}$ in Eq. (4.4.3.2). The adjoint PFEM method for displacements is applicable to linear and nonlinear materials, with the use of stiffness and tangent stiffness matrices, respectively. The first order mean and covariance of displacements $d^{(k)}$, k = 1, ..., N where N is the number of displacements of interest, are

$$E[d^{(k)}] = d^{o(k)} \qquad k = 1, \ldots, N \qquad (4.4.3.4a)$$

$$Cov(d^{(k)},d^{(\ell)}) = \{ \sum_{r=1}^{q} [d^{(k)}]_{c_r} [d^{(\ell)}]_{c_r} Var(c_r)\} \qquad (4.4.3.4b)$$

4.4.4 Stress Derivatives in PFEM

The first derivative of the stresses with respect to the probabilistic variables, in any element, can be expressed in terms of the displacement derivatives in this element which are first calculated by the adjoint method. For a four node, 2D continuum element this requires the solution of eight adjoint problems. For linear materials, the stress derivatives with respect to the transformed vector $\underset{\sim}{c}$, in a given element are:

$$\underset{\sim}{\sigma}'_{c_i}\Big|_{\underset{\sim}{d}=\underset{\sim}{\bar{d}}} = \underset{\sim}{C}_{c_i}\underset{\sim}{B}^{o}\underset{\sim}{d}^{o} + \underset{\sim}{C}^{o}\underset{\sim}{B}_{c_i}\underset{\sim}{d}^{o} \qquad (4.4.4.1a)$$

resulting in

$$[\underset{\sim}{g}]_{c_i} = \underset{\sim}{g}'_{c_i}\Big|_{\underset{\sim}{d}=\underset{\sim}{d}^o} + \underset{\sim}{C}^o\underset{\sim}{B}^o\underset{\sim}{d}'_{c_i} \qquad (4.4.4.1b)$$

In the absence of random material properties, the first term in Eq. (4.4.4.1b) drops out and in the absence of random geometric properties, the second term drops out. In the case where only loads are random, both terms drop out.

For nonlinear materials, Eq. (4.4.4.1a) cannot be easily evaluated. One strategy is to replace these derivatives by their finite-difference counterparts [24]

$$\underset{\sim}{g}'_{c_i}\Big|_{\underset{\sim}{d}=\underset{\sim}{d}^o} \approx \frac{1}{2\Delta c_i}(\underset{\sim}{g}^{o+} - \underset{\sim}{g}^{o-})\Big|_{\underset{\sim}{d}=\underset{\sim}{d}^o} \qquad (4.4.4.2a)$$

with the definitions

$$\underset{\sim}{g}^{o+} = \underset{\sim}{g}(\underset{\sim}{c}^o + \Delta\underset{\sim}{c}_i) \qquad (4.4.4.2b)$$

$$\underset{\sim}{g}^{o-} = \underset{\sim}{g}(\underset{\sim}{c}^o - \Delta\underset{\sim}{c}_i) \qquad (4.4.4.2c)$$

and

$$\Delta\underset{\sim}{c}_i = (0, \ldots, \Delta c_i, \ldots, 0)^T \ . \qquad (4.4.4.2d)$$

The derivatives of the tangent constitutive matrix in Eqs. (4.3.16b) can also be approximated similarly. For a general nonlinear material, Eqs. (4.4.4.2b) and (4.4.4.2c) have to be evaluated by solution of the zeroth

order equation, with the appropriate values of $\underset{\sim}{c}$. However, for elastoplastic materials with random material properties, these quantities can be evaluated in the course of the zeroth order solution by the radial return algorithm [36]. Additional arrays to store the stresses in Eqs. (4.4.4.2) are all that is needed to achieve this. Essentially, the functional relationships

$$\underset{\sim}{\sigma}^{o+}_{t+\Delta t} = \underset{\sim}{g}(\underset{\sim}{\sigma}^{o+}_{t}, \underset{\sim}{d}^{o}_{t}, \Delta\underset{\sim}{c}_{t}) \tag{4.4.4.3a}$$

and

$$\underset{\sim}{\sigma}^{o-}_{t+\Delta t} = \underset{\sim}{g}(\underset{\sim}{\sigma}^{o-}_{t}, \underset{\sim}{d}^{o}_{t}, \Delta\underset{\sim}{c}_{t}) \tag{4.4.4.3b}$$

hold, for each c_i [37]. The subscripts 't' and 't+Δt' refer to two successive time steps, in the evolution of the stress history. The first order mean stress and covariance of stress are expressed as

$$E[\underset{\sim}{\sigma}] = \underset{\sim}{\sigma}^{o} \tag{4.4.4.4a}$$

and

$$Cov(\sigma^i,\sigma^j) = \{ \sum_{r=1}^{q} [\sigma^i]'_r [\sigma^j]'_r \, Var(c_r)\} \tag{4.4.4.4b}$$

where σ^i and σ^j are any two components of the elemental stress vector $\underset{\sim}{\sigma}$.

4.5 Applications

The usefulness of PFEM is demonstrated here by three applications. In the first two cases, the problem studied is an elastic-plastic plane continuum with a circular hole. In the first application (Fig. 2), the uniaxial yield stress and the uniform compressive load are assumed to be two independent stationary random fields, with an exponentially decaying correlation function. The load is discretized into 12 components, applied at the nodes, both for deterministic and random analyses. The yield stress is assumed to be radially correlated in an exponential manner (Fig. 2). The domain of the plate is divided into 15 ring-like bands and in these bands the mean yield stress is assumed constant in time and space. This results in 15 discretized random variables for the yield stress. The load is quasi-static and linearly increasing with time, with 8 load steps. The displacement and stress statistics are studied in each of these load steps.

The mean and variance of the compressive stress at load step 8, along the x-axis, are plotted in Figs. 3a and 3b, respectively. The elements near the hole are plastic at this load, as can be seen from Fig. 3a. The variance of the stress is maximum, therefore, near the hole and this is seen in Fig. 3b. These results compare very well with the Monte Carlo simulation (MCS) results. The coefficient of variance is 10% for the stress. The mean and variance of the stress near the hole (Point B) are plotted in Figs. 4a and 4b, respectively. The mean stress is plastic after the second load step. Thereafter, the mean

stress is almost constant and is equal to the uniaxial yield stress value, except for a slight hardening effect. The variance of stress rises rapidly when the yielding occurs (i.e., elastoplastic state of stress) and thereafter it rises gradually. The maximum coefficient of variation for the stress at Point B is 10%. The stress correlation along the x-axis, w.r.t. the stress at Point C, is plotted in Fig. 4c. Interestingly, the correlation is almost zero near the hole and there is inverse correlation near the fixed end of the plate (cf. Fig. 2). This suggests that the stresses in the plastic state are not correlated with the stress near Point C. This can be explained by the fact that beyond yielding the stress remains practically constant for this material because $E/E_T = 100$. Near the fixed end, the stress is almost zero and the negative correlation implies that this stress will statistically increase when the stress near point C decreases. By studying the effects of the two random fields separately, it is noticed that the random load effect in terms of the variance, is spread wider over the elements along the x-axis than the random material effect, and the effect is mainly near the hole. As is to be expected, the variance of the stress under the combined effect of the random material and random load is additive. Similarly, for the mean values of stress, the second order effect is additive.

The second example concerns the cyclic loading of the same plate with only the yield stress as the random field. Mechanical and aerospace components are usually subjected to thousands of cycles of stress, resulting in fatigue. The material properties usually show some

degradation with time in these components. A modest attempt is made here to see if there is a large variation of the response statistics after 3 cycles of loading and unloading. The mean and variance of the displacement at node A is plotted as functions of the load step in Fig. 5a. The mean displacement is sinusoidal, resembling closely the forcing function. The variance of the displacement is zero until the plate begins to yield in compression. After this, the variance jumps to a higher value and remains steady until the yielding in tension begins. At this point, there is a sharp drop in the displacement variance and after that the variance stays at a constant level. This phenomenon repeats every cycle. There seems to be a gradual buildup of the value of the displacement variance during every cycle, particularly under compression. The maximum coefficient of variation in these cycles is 2%.

The mean and variance of the stress at Point B are plotted in Fig. 5b. The mean stress is periodic, with a slight flattening at the top and bottom. This flat region corresponds to the plate yielding, in the mean sense. The variance of stress at Point B is periodic, and behaves similar to the displacement variance. The coefficient of variation is 10%.

The stress variance exhibits spikes whenever yielding is about to commence. The variance drops to a near zero level in these downward spikes. This phenomenon can be explained from the elastic-plastic behavior of the plate under stress reversal. To do this, three deterministic solutions of the stress in the plate are shown in Figs. 6a

and 6b at various loadsteps, under cyclic loading. These correspond to yield stress (σ_y) values of 26,000, 25,000 and 24,000 psi, respectively. During the first yielding, in compression, the magnitude of the stress for σ_y = 26,000 is maximum and this stress plot, in Fig. 6a, lies outermost. Before the next yielding in tension commences, there is a crossover of the three curves. This crossover is necessary because the magnitude of the stress at yield, for the highest yield stress value, is always the highest. The crossover repeats twice for each cycle of loading. This translates into a very small variance of stress near the crossover regions because the variation of stress w.r.t. the yield stress is near zero. The spikes in the displacement variance can also be explained similarly.

The third application studied is a turbine blade with random load along the edge, random yield stress and random length of the blade. The problem statement, along with the details of the random fields, are given in Fig. 7. The load is quasi-static and linearly increasing, with 15 load steps. The expectation and deviation of the displacement are plotted in Fig. 8a; the coefficient of variation is plotted in Fig. 8b. It is noticed that the first two steps are elastic and beyond that the blade starts yielding. Due to this yielding, the expectation is nearly flat beyond the second load step. In the elastic region, the maximum contribution for the deviation comes from the random load followed by the random length. In the elastoplastic region and beyond, the random yield stress affects the deviation most. The combined deviation has a maximum coefficient of variation of 13% and this occurs

just after the initiation of the yielding.

The stress statistics are plotted in Figs. 9a and 9b. The stress deviation is largely due to the random load in the elastic region, as in the case of displacement deviation; the effect of the random length is very small in both the elastic and plastic regions; the random yield stress causes the most deviation in the plastic region. The maximum coefficient of variation is 8%, at the last load step.

4.6 Conclusions

The PFEM techniques for linear and nonlinear materials, including elastoplastic materials, yield efficient and reliable statistics of the response quantities of interest. The direct solution of PFEM equations may require a substantial number of computations for large systems. By making use of features such as the eigenvalue orthogonalization and selection of only a few highest eigenvalues, the adjoint methodology, and superposition of random fields, these computations can be drastically reduced. The results obtained here show that the first and second order variances in response which are obtained by this form of the moment method agree well with Monte Carlo simulations when material properties such as the yield stress are random variables. The results also seem to suggest an increase in the response variance even with a small but steady degradation of material properties after several cycles. However, this needs to be investigated further. As discussed in the introduction, based on the response statistics, reliability measures can be calculated. In addition, the response gradients with respect to the random variables are calculated in the course of PFEM calculations. These are also useful in reliability calculations and probabilistic design.

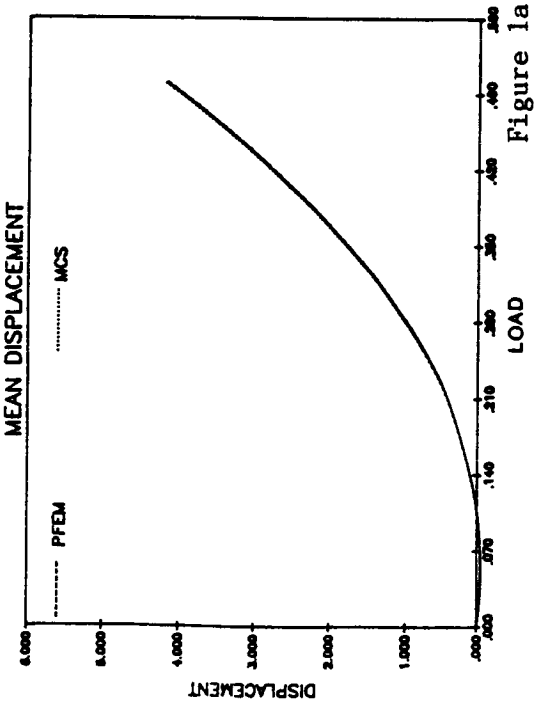

Figure 1a

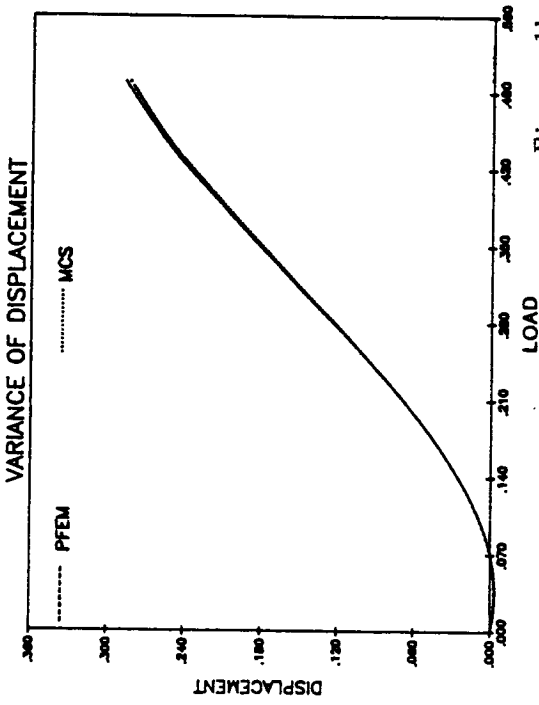

Figure 1b

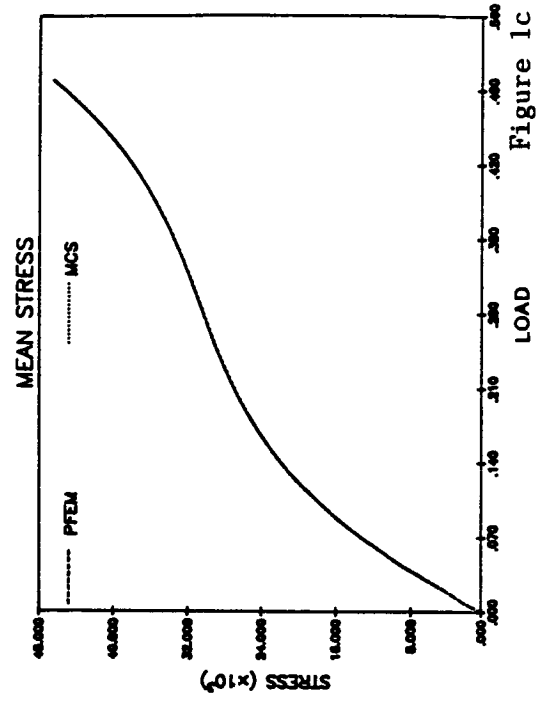

Figure 1c

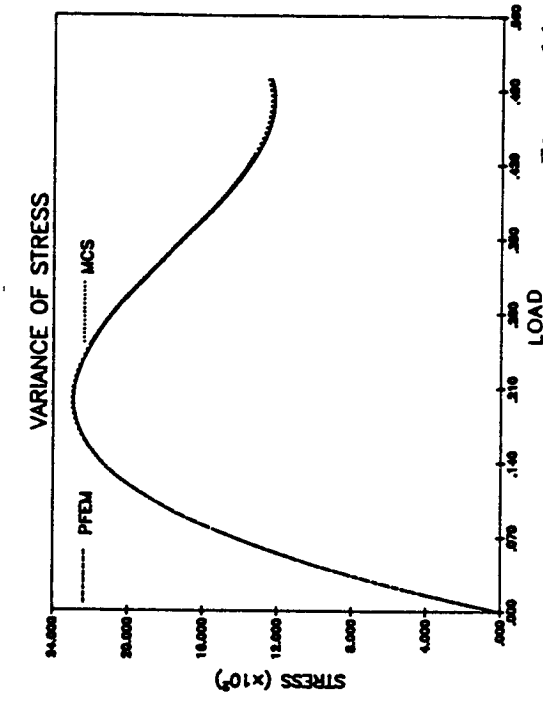

Figure 1d

Elastic/Plastic Plate with a Hole

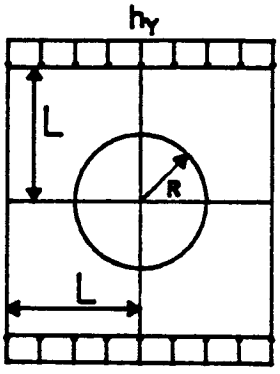

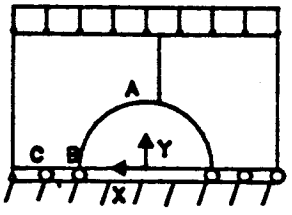

E $=30.X10^6$
E_T $=30.X10^4$
σ_Y $=25000.0$
(Isotropic Hardening)
ν $=0.3$
L $=6.0$, R $=3.0$

4 Node 2D Cont. Element
(Plane Stress)
784 Nodes, 720 Elements
Node 400 Point A
Element 15 Point B
Element 8 Point C

Random Load Characteristics

Size of Random Load Vector (q)= 12
Coefficient of Variation= 0.10
Correlation Length (λ)= 18.0

Load Steps	0001	0002	0003	0004	0005	0006	0007	0008
Mean Load (h_Y)	2000	4000	4100	4200	4300	4400	4500	4600

Random Material Characteristics

Size of Random Material Vector (q) = 15
Coefficient of Variation= 0.10
Correlation Length (λ)= 9.0
Mean Yield Stress= 25000.0

Spatial Correlation of Random Load and Yield Stress

$$R(x_i,x_j)=\exp(-ABS(x_i-x_j)/\lambda)$$

Problem Statement

Figure 2

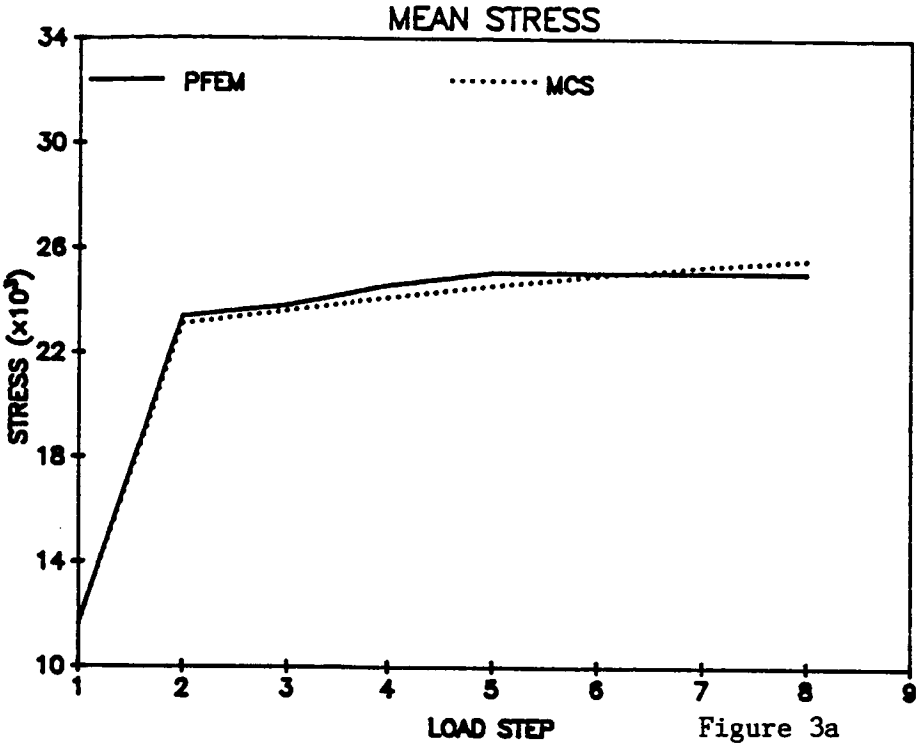

Figure 3a

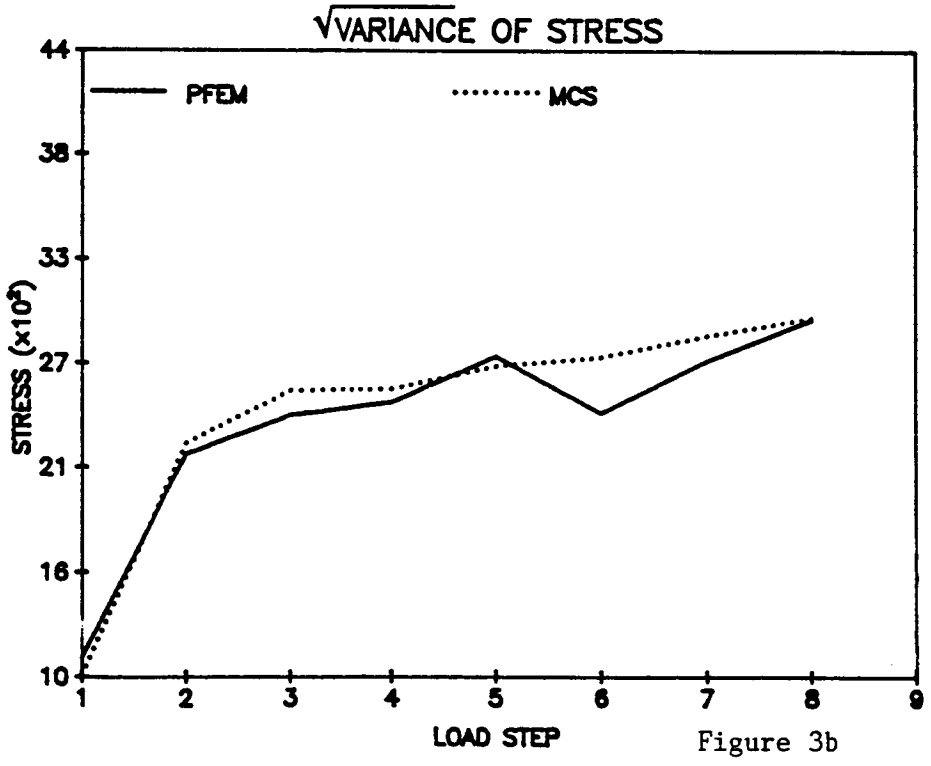

Figure 3b

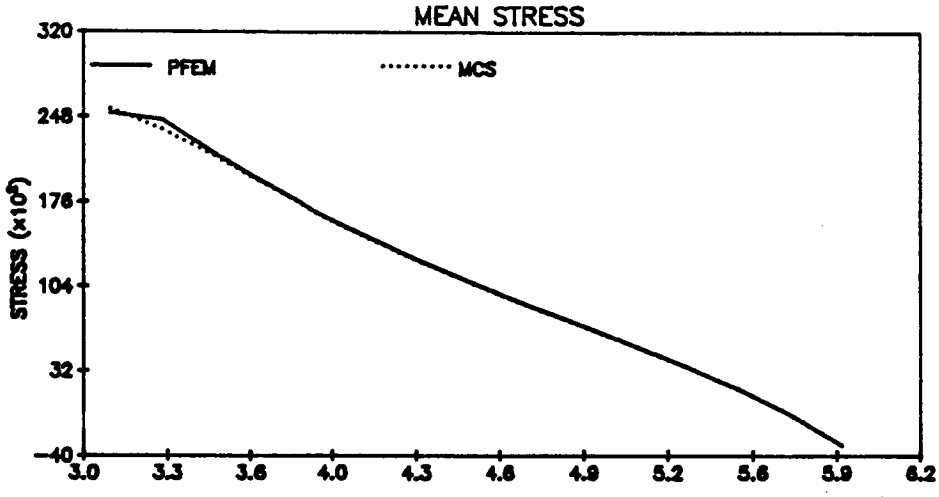

Figure 4a

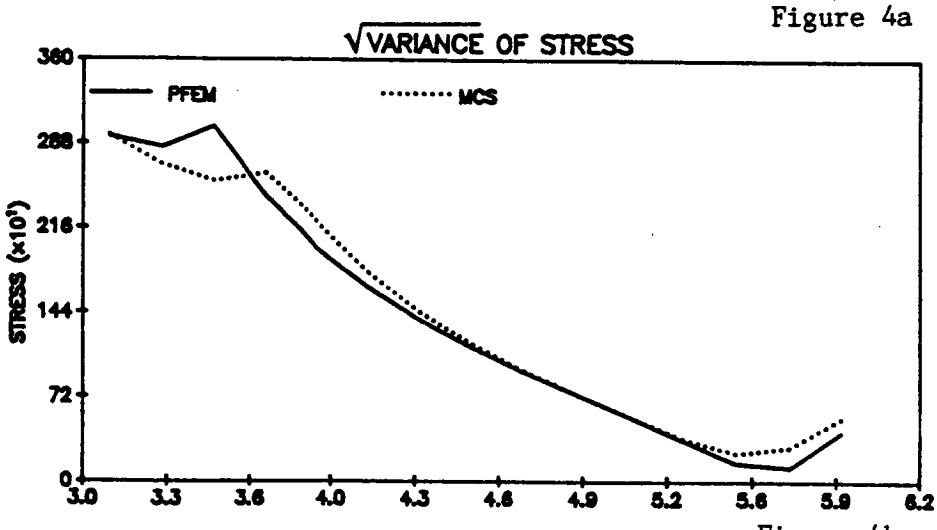

Figure 4b

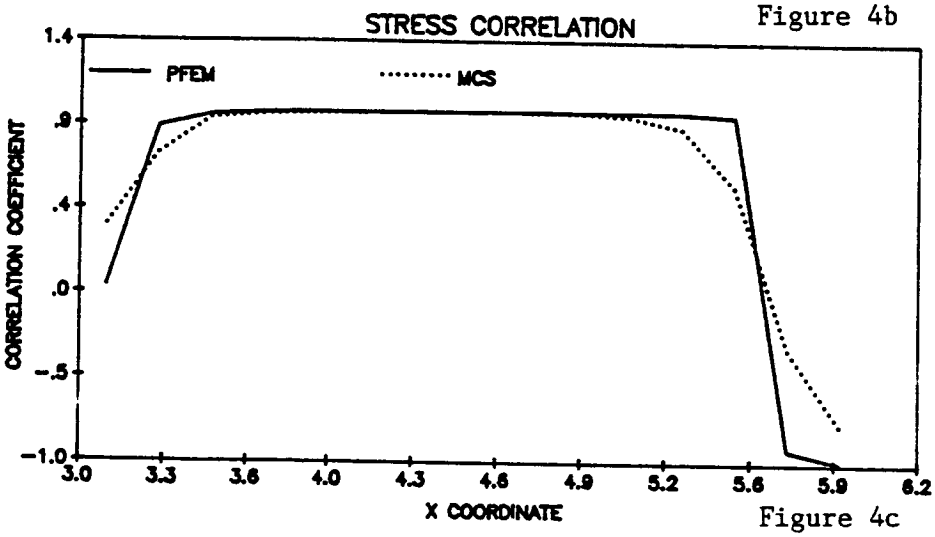

Figure 4c

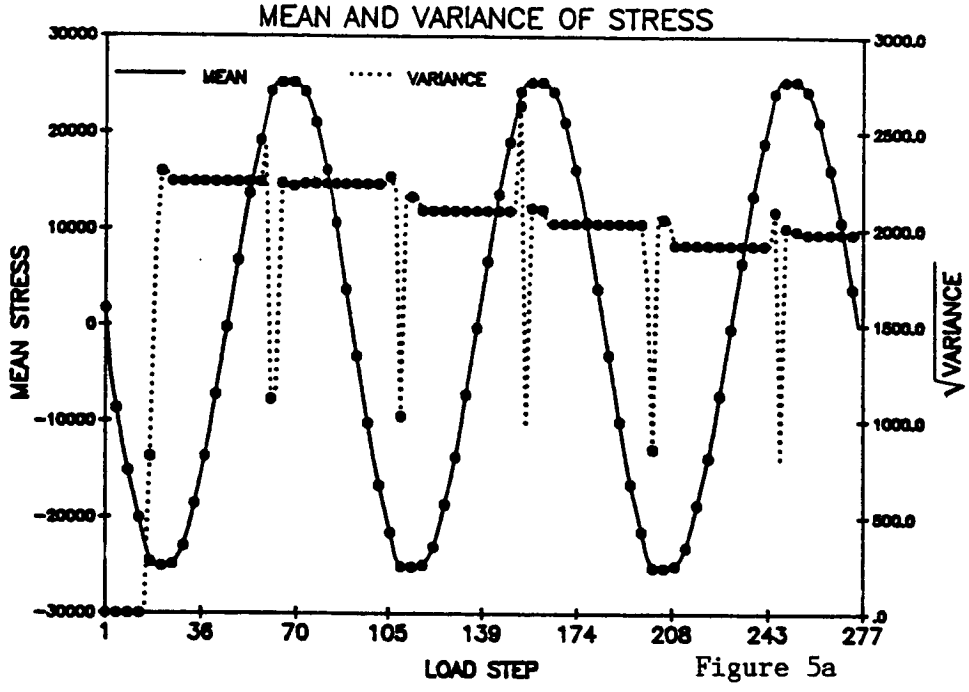

Figure 5a

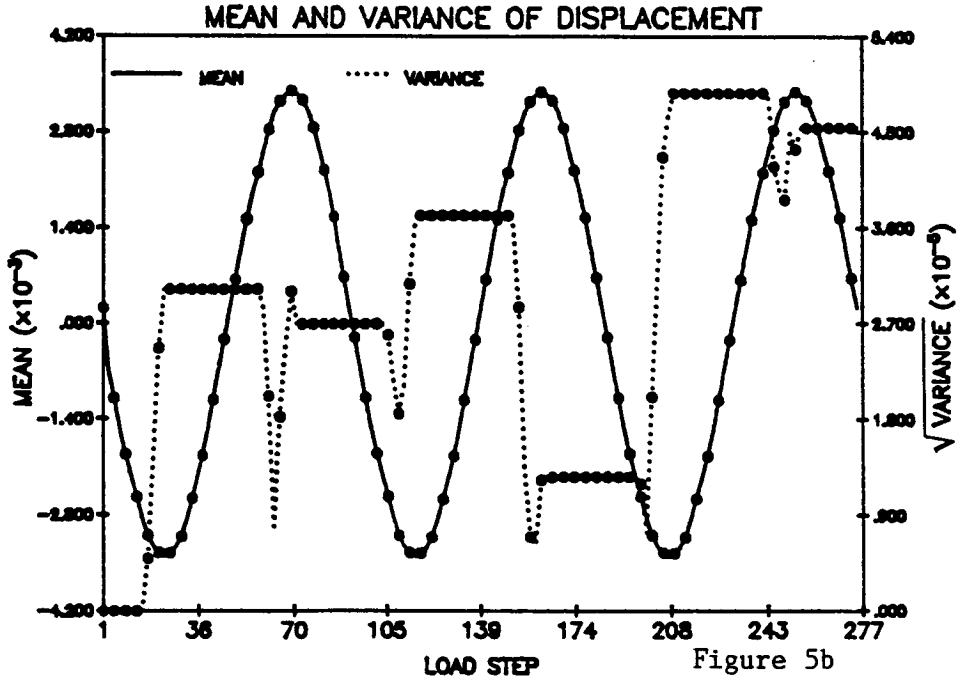

Figure 5b

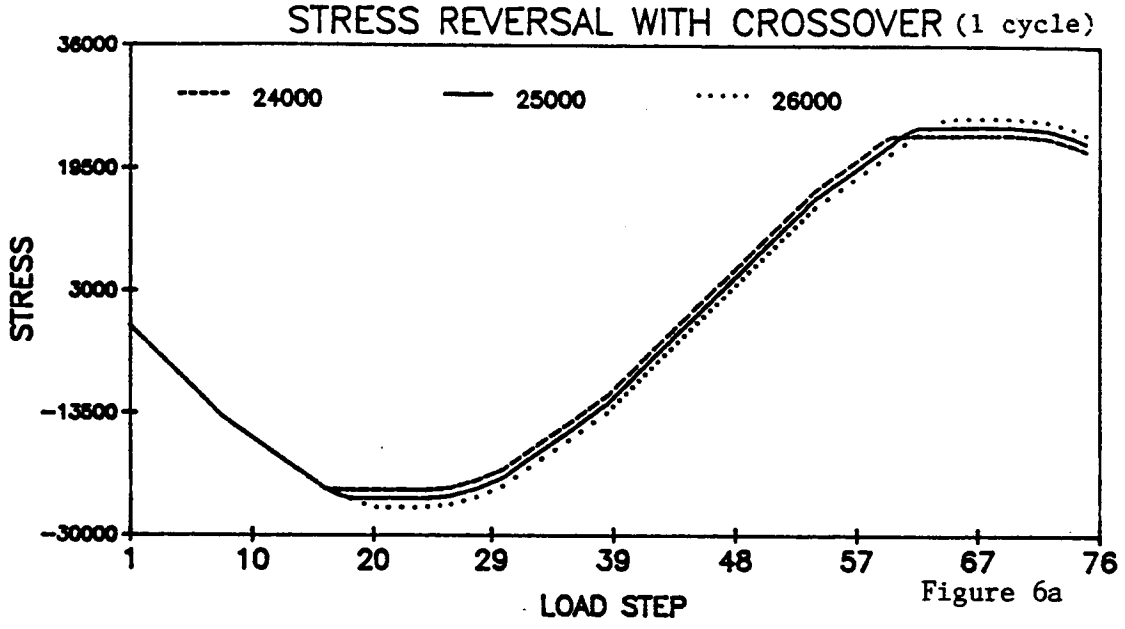

Figure 6a

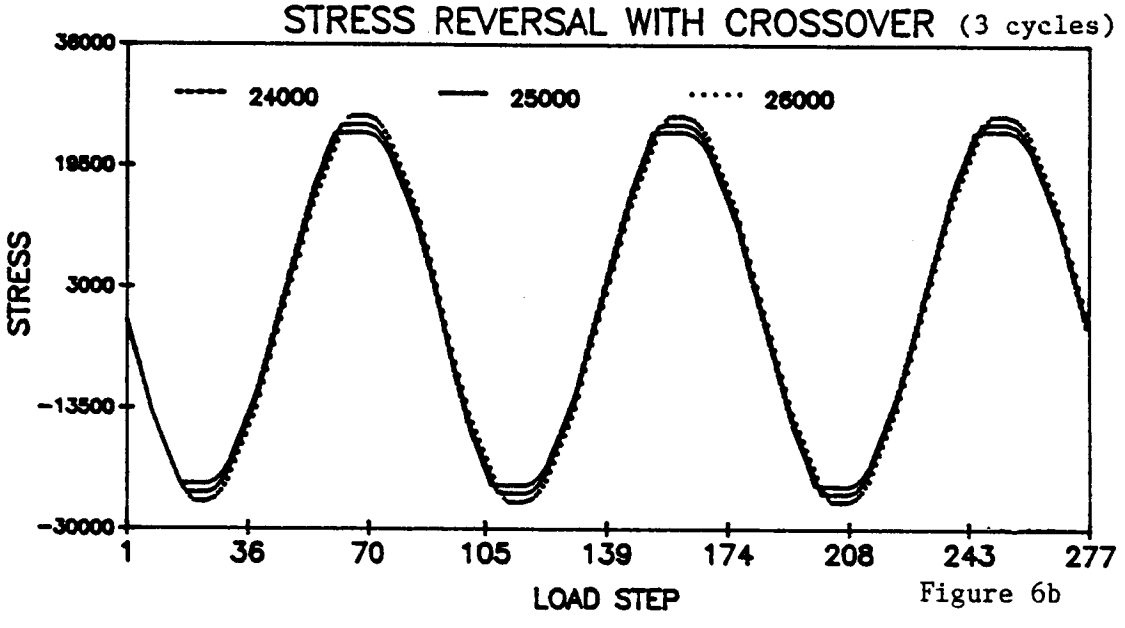

Figure 6b

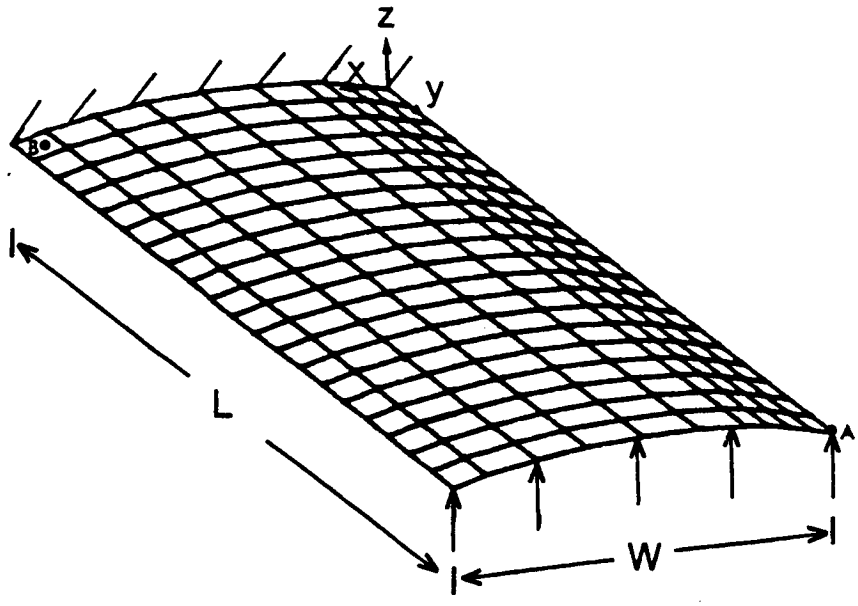

E =30.X10^6	4 Node Shell Element
E_T =30.X10^4	with SRI
σ_Y =25000.0	462 Nodes, 200 Elements
(Isotropic Hardening)	Disp. *Point A
ν =0.3	Stress *Point B
L =6.3, R =2.29	Maximum Thickness=.3

Random Load Characteristics

Size of Random Load Vector (q)= 10
Coefficient of Variation= 0.10
Correlation Length (λ)= 4W
Maximum Mean Load = 13.25

Random Material Characteristics

Size of Random Material Vector (q) = 20
Coefficient of Variation= 0.10
Correlation Length (λ)= 4L
Mean Yield Stress= 25000.0

Spatial Correlation of Random Load and Yield Stress

$R(x_i,x_j)=\exp(-ABS(x_i-x_j)/\lambda)$

Random Length

1 Variable, C.O.V = .02

Problem Statement

Figure 7

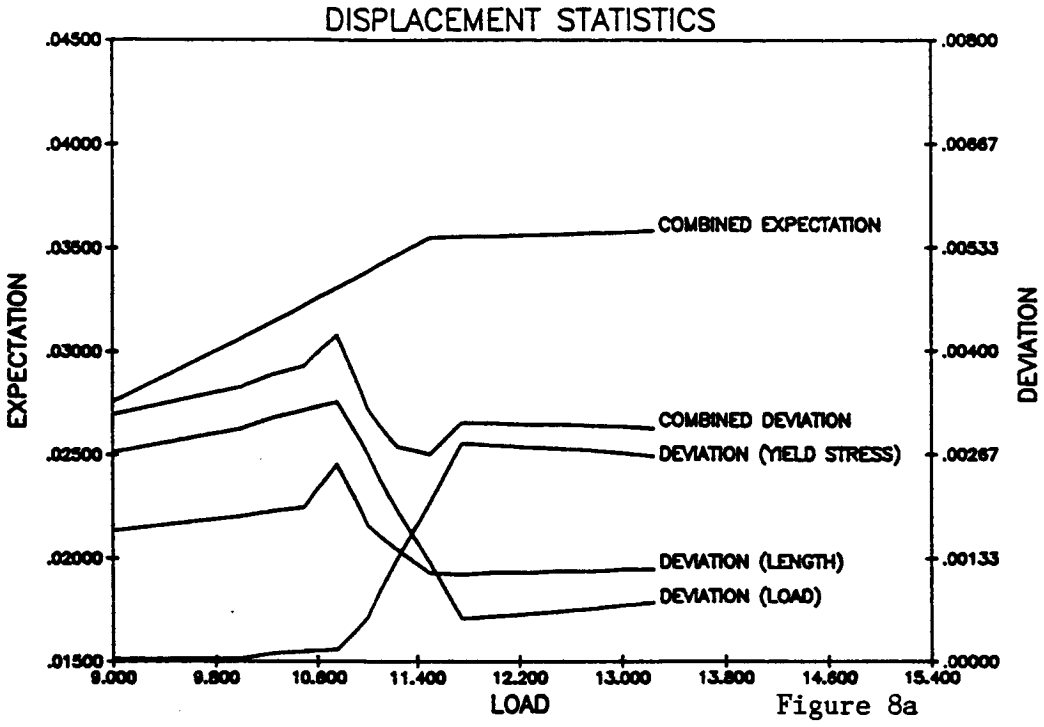

Figure 8a

Expectation and Coefficient of Variation of Displ.

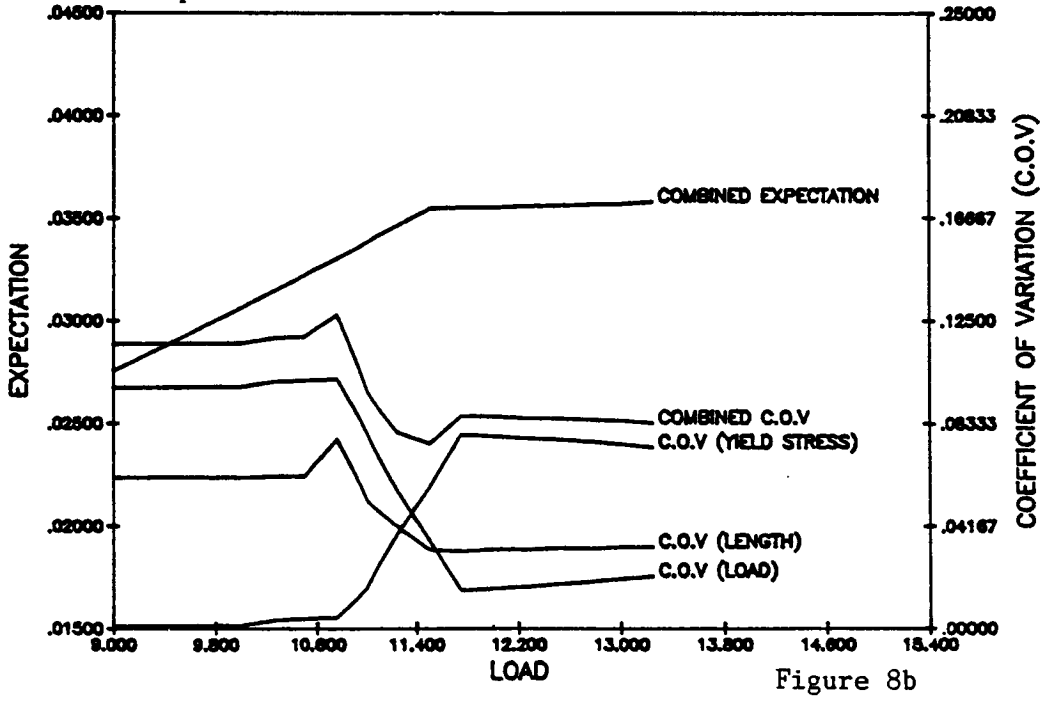

Figure 8b

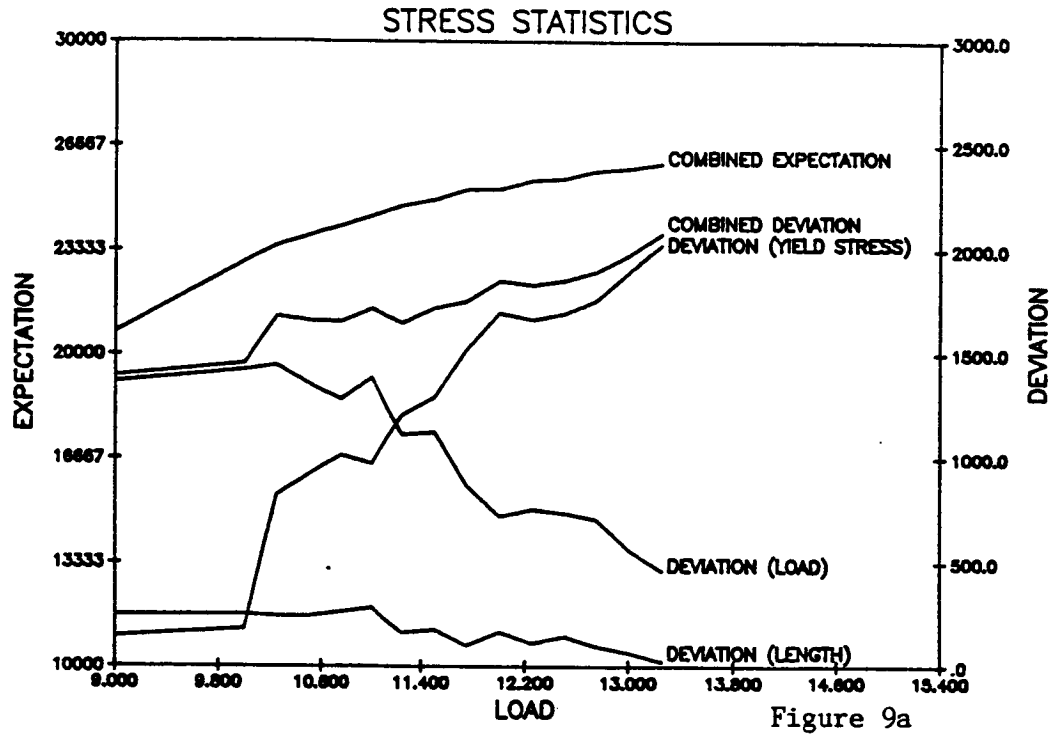

Figure 9a

Expectation and Coefficient of Variation of Stress

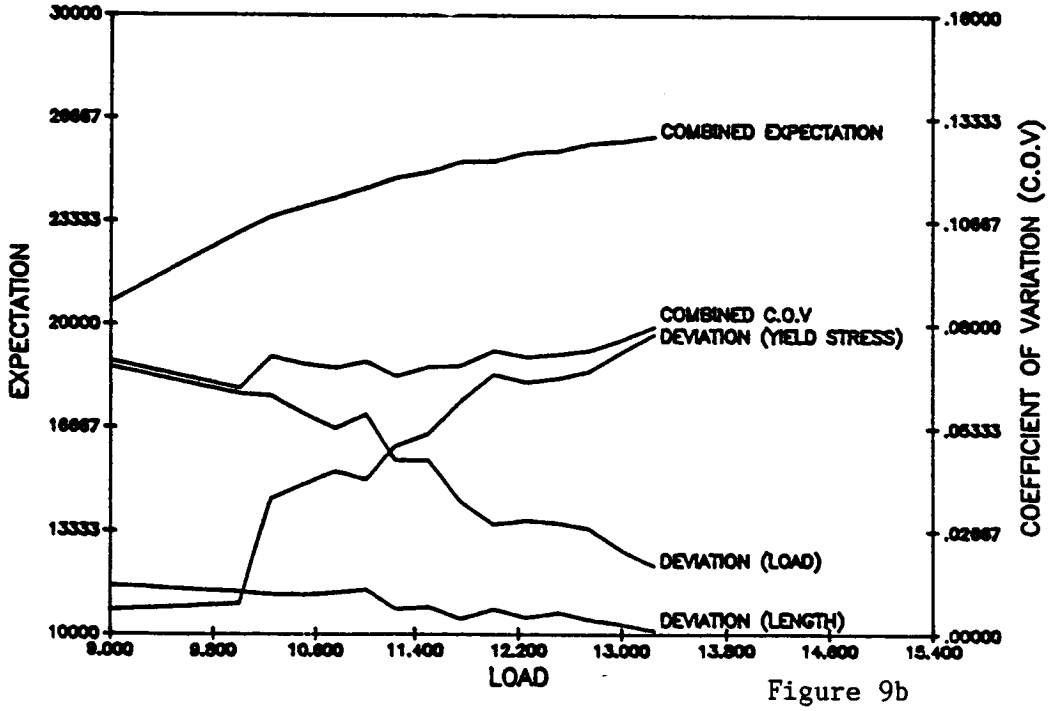

Figure 9b

CHAPTER 5

APPLICATIONS OF PROBABILISTIC FINITE ELEMENT METHODS IN ELASTIC/PLASTIC DYNAMICS

5.1 Introduction

Design methods for engineering problems are, in general, based on deterministic parameters. In practice there are often uncertainties associated with parameters such as: material and geometric properties, forces, and boundary conditions. Although, in most situations the uncertainties may be small, the combination of these can lead to large and unexpected excursions of the response, particularly in multi-component systems. In the context of failure and reliability analysis, this phenomenon is of obvious significance. In the past, problems with uncertainties have been studied to provide an insight of the statistical response variations, with methods like sampling [1-4], numerical integration [5,6], second-moment analysis [6,8] and stochastic finite element methods [6,9-12]. The choice of the appropriate method depends on the nature of the problem and this was briefly discussed by the authors in Refs. [12,13]. Typically, the uncertainties are modelled as random quantities governed by probability density functions, and that is also the case here.

A survey of the existing literature shows that, with the exception of the methods based on sampling, the other methods are limited to linear problems. Moreoever, techniques for handling random fields, where the randomness is spaced over the continua, are even scarcer. The authors have recently extended probabilistic finite element methods PFEM [13] to linear and nonlinear continua in both static and transient

settings.

A schematic of the PFEM is presented in Fig. 1a. In the PFEM [13], the random fields, characterized by the mean, variance and autocorrelation functions, are discretized to obtain the mean vector and the covariance matrix. For a correlated random field, the covariance matrix will be a full matrix and therefore it will require too many computations. To remedy this, the correlated vector is transformed to an uncorrelated vector by an eigenvalue orthogonalization procedure resulting in a diagonal covariance matrix, and therefore, fewer computations. This transformation procedure gives rise to a set of modes and corresponding eigenvalues. It is shown that only a few of these modes are sufficient to obtain a converged PFEM solution. Finally, the PFEM involves solution of a set of deterministic FEM equations to obtain the mean, variance and autocorrelation of the response.

In this paper, two applications of the PFEM in elastic/plastic dynamics with random material properties are studied in detail. The discretization of the random field depends on factors such as the inhomogeneity of the randomness and the extent of the spatial correlation. The necessary guidelines for the discretization are discussed in the next section. In Section 5.3, the choice of the number of modes necessary for a converged PFEM solution is discussed. The computational efficiency and accuracy of this method are compared with those of Monte Carlo simulation with a first-order filter [6,7] in Section 5.4, along with the conclusions.

5.2 Random Field Discretization

Let $b(\underset{\sim}{x})$ represent the random field. In PFEM, $b(\underset{\sim}{x})$ is approximated by discretization as

$$b(\underset{\sim}{x}) = \sum_{i=1}^{q} N_i(\underset{\sim}{x}) b_i \tag{5.2.1}$$

where $N_i(\underset{\sim}{x})$ represent the shape functions and b_i the discretized values of $b(\underset{\sim}{x})$ at x_i, $i = 1, \ldots, q$. It follows from Eq. (5.2.1) that

$$db(\underset{\sim}{x}) = \sum_{i=1}^{q} N_i(\underset{\sim}{x}) db_i \tag{5.2.2}$$

$$db^2(\underset{\sim}{x}) = \sum_{i,j=1}^{q} N_i(\underset{\sim}{x}) N_j(\underset{\sim}{x}) db_i db_j \tag{5.2.3}$$

where

$$db_i = b_i - \overline{b}_i \tag{5.2.4}$$

and $\overline{b}_i$ represent the mean values of b_i (also denoted by the expectation operator $E[\cdot]$). From Eq. (2.1) the expectation and the covariance of $b(\underset{\sim}{x})$ are, by definition,

$$E[b(\underset{\sim}{x})] = \int_{-\infty}^{+\infty} b(\underset{\sim}{x}) f(\underset{\sim}{b}) d\underset{\sim}{b} \tag{5.2.5}$$

$$= \sum_{i=1}^{q} N_i(\underset{\sim}{x}) E[b_i] \tag{5.2.6}$$

and

$$\mathrm{Cov}(b(\underset{\sim}{x}_k), b(\underset{\sim}{x}_\ell)) = \int_{-\infty}^{+\infty} (b(\underset{\sim}{x}_k) - \bar{b}(\underset{\sim}{x}_k))(b(\underset{\sim}{x}_\ell) - \bar{b}(\underset{\sim}{x}_\ell)) f(\underset{\sim}{b}) d\underset{\sim}{b} \tag{5.2.7}$$

$$= \sum_{i,j=1}^{q} N_i(\underset{\sim}{x}_k) N_j(\underset{\sim}{x}_\ell) \mathrm{Cov}(b_i, b_j) \tag{5.2.8}$$

where $f(\underset{\sim}{b})$ is the multivariate probability density function; $\underset{\sim}{x}_k$ and $\underset{\sim}{x}_\ell$ are any two points in the domain of $\underset{\sim}{x}$.

From second-moment analysis [6,8], the mean of any function $S(b(\underset{\sim}{x}), \underset{\sim}{x})$ at any point $\underset{\sim}{x}_k$, and the covariance of the function between any two points $\underset{\sim}{x}_k$ and $\underset{\sim}{x}_\ell$ can be written as

$$E[S_k] \cong \bar{S}_k + \frac{1}{2} \sum_{i,j=1}^{q} \frac{\partial^2 \bar{S}_k}{\partial b_i \partial b_j} \mathrm{Cov}(b_i, b_j) \tag{5.2.9}$$

and

$$\mathrm{Cov}(S_k, S_\ell) \cong \sum_{i,j=1}^{q} \left(\frac{\partial \bar{S}_k}{\partial b_i}\right)\left(\frac{\partial \bar{S}_\ell}{\partial b_j}\right) \mathrm{Cov}(b_i, b_j) \tag{5.2.10}$$

where

$$S_k = S(b(\underset{\sim}{x}), x_k) \tag{5.2.11}$$

and the superposed bar implies evaluation at $\underset{\sim}{\bar{b}}$. The error in Eqs. (5.2.9) and (5.2.10) arises from: (1) the truncation of higher order moments and (2) the discretization of the random field $b(\underset{\sim}{x})$ by the

finite vector $\underset{\sim}{b}$. If the randomness in $b(\underset{\sim}{x})$ is small, then the first error will be small for a smooth function and the second-moment analyis is applicable. The error due to discretization in Eqs. (5.2.6) and (5.2.8) can first be studied to provide an insight of the discretization accuracy.

The discretization error of the covariance field is defined by the L_2 norm

$$E^2 = \int_{\Omega} \left[\mathrm{Cov}_E(b(\underset{\sim}{x}_k), b(\underset{\sim}{x}_\ell)) - \mathrm{Cov}_D(b(\underset{\sim}{x}_k), b(\underset{\sim}{x}_\ell))\right]^2 d\Omega \tag{5.2.12}$$

where Cov_E and Cov_D represent the exact and discretized covariances. The exact covariance is calculated from the given function for the mean E[b], coefficient of variation α and the autocorrelation R as follows:

$$\mathrm{Cov}_E(b(\underset{\sim}{x}_k), b(\underset{\sim}{x}_\ell)) = \left[\mathrm{Var}(b(\underset{\sim}{x}_k))\mathrm{Var}(b(\underset{\sim}{x}_\ell))\right]^{1/2} R(b(\underset{\sim}{x}_k), b(\underset{\sim}{x}_\ell)) \tag{5.2.13}$$

where

$$\mathrm{Var}(b(\underset{\sim}{x}_k)) = (\alpha(b(\underset{\sim}{x}_k))E[b(\underset{\sim}{x}_k)])^2 \tag{5.2.14}$$

The discretized covariance between any two points $\underset{\sim}{x}_k$ and $\underset{\sim}{x}_\ell$ is obtained from:

$$\mathrm{Cov}_D(b(\underset{\sim}{x}_k), b(\underset{\sim}{x}_\ell)) = \sum_{i,j=1}^{q} N_i(\underset{\sim}{x}_k) N_j(\underset{\sim}{x}_\ell) \mathrm{Cov}(b_i, b_j) \tag{5.2.15}$$

and

$$\mathrm{Cov}(b_i,b_j) = \left[\mathrm{Var}(b_i)\mathrm{Var}(b_j)\right]^{1/2} R(b_i,b_j) \tag{5.2.16}$$

where b_i are the discretized points of $b(\underset{\sim}{x})$, corresponding to $\underset{\sim}{x}_i$, $i = 1, \ldots, q$. For a beam with a random field along the x-axis (Fig. 1b), the logarithmic plot of E against q is given in Fig. 2a, and the rate of convergence is found to be 1.325 for nearly all q between 4 and 64.

When the random field discretization is coupled with an FEM discretization, as in PFEM [13], q need not be equal to the number of finite elements NUMEL and the shape functions $N_i(\underset{\sim}{x})$ need not be the same as the finite element interpolants for the displacement field.

5.3 Transformation Procedure for Computational Efficiency

The mean and covariance can be obtained from Eqs. (5.2.11) and (5.2.12). However, the number of derivatives to be evaluated is proportional to $q(q+1)/2$. This arises from the double summations in i and j. To reduce the number of computations, the full covariance matrix $\mathrm{Cov}(b_i,b_j)$ is transformed to a diagonal variance matrix $\mathrm{Var}(c_i,c_j)$ such that

$$\mathrm{Var}(c_i,c_j) = 0 \qquad \text{for } i \neq j \tag{5.3.1}$$

and

$$\mathrm{Var}(c_i,c_j) = \mathrm{Var}(c_i) \qquad \text{for } i = j \tag{5.3.2}$$

Therefore, the number of derivative evaluations is proportional to q. The above is achieved through the eigenproblem:

$$\underset{\sim}{G}\underset{\sim}{\psi} = \underset{\sim}{\psi}\underset{\sim}{\Lambda} \tag{5.3.3}$$

where the $\underset{\sim}{G}$ and $\underset{\sim}{\Lambda}$ matrices denote $\mathrm{Cov}(b_i,b_j)$ and $\mathrm{Var}(c_i,c_j)$, respectively; $\underset{\sim}{\psi}$ is a constant $q \times q$ fundamental matrix with the following properties:

$$\underset{\sim}{\psi}^T\underset{\sim}{\psi} = \underset{\sim}{\psi}\underset{\sim}{\psi}^T = \underset{\sim}{1} \tag{5.3.4}$$

$$\underset{\sim}{\Lambda} = \underset{\sim}{\psi}^T \underset{\sim}{G} \underset{\sim}{\psi} \tag{5.3.5}$$

and

$$\underset{\sim}{b} = \underset{\sim}{\psi} \underset{\sim}{c} \quad \text{or} \quad \underset{\sim}{c} = \underset{\sim}{\psi}^T \underset{\sim}{b} \tag{5.3.6}$$

$\underset{\sim}{1}$ is the q × q identity matrix and $\underset{\sim}{c}$ is the transformed q × 1 vector of random variables.

With Eqs. (5.3.5) and (5.3.6), the mixed derivatives appearing in Eq. (5.2.11) reduce to second derivatives and $\text{Cov}(b_i, b_j)$ reduces to $\text{Var}(c_i)$:

$$E[S] = \bar{S} + \frac{1}{2} \sum_{i=1}^{q} \frac{\partial^2 \bar{S}}{\partial c_i^2} \text{Var}(c_i) \tag{5.3.7}$$

and

$$\text{Cov}(S_k, S_\ell) = \sum_{i=1}^{q} \left(\frac{\partial \bar{S}_k}{\partial c_i}\right)\left(\frac{\partial \bar{S}_\ell}{\partial c_i}\right) \text{Var}(c_i) \tag{5.3.8}$$

Thus, the discretized random vector $\underset{\sim}{b}$ is transformed to an uncorrelated random vector $\underset{\sim}{c}$, with the variance of $\underset{\sim}{c}$ as the eigenvalues of $\underset{\sim}{G}$ in Eq. (5.3.3).

In the numerical examples, an exponentially decaying autocorrelation in one-dimension is assumed with various correlation lengths 'λ' (i.e., the length at which the autocorrelation drops to 0.37, see Fig. 1b). It is observed that for one-dimensional random

fields, as λ increases from zero to a large value, the number of largest eigenvalues N, $N \leq q$ necessary to evaluate the mean and covariance in Eqs. (5.3.7) and (5.3.8) to a specified accuracy, decreases from q to 1. When λ is zero the random field is uncorrelated and all q eigenvalues are dominant. When the field is uncorrelated, all q random variables are necessary to represent the randomness of the field. As λ increases the number of dominant eigenvalues decreases. Eventually, for a very large λ the random field is closely correlated and there is just one dominant eigenvalue. When the field is closely correlated, only one random variable, corresponding to the largest eigenvalue, is sufficient to represent the randomness of the field.

This feature, when present, can easily be exploited to reduce the number of computations. The value of N can be chosen based on the distribution of the eigenvalues before solving the PFEM equations. The eigenvalues here can be interpreted as weighting factors for the corresponding mode shapes necessary to represent the covariance structure; a large eigenvalue means a dominant mode and vice versa. The eigenvalue distribution and the mode shapes are depicted in Figs. 2b, 3a and 3b, for a numerical example. Results of the eigenvalue distribution and selection of N, for a beam problem and a bar problem, are discussed in the next section.

5.4 Results and Discussion

(1) Elastic/Plastic Beam with Yield Stress as a Random Field

The problem statement is depicted in Fig. 1b. The yield stress is assumed to be a function of the position along the length of the beam only. The Gaussian random field, which is the yield stress, is discretized so that q = 16 (NUMEL = 64). 4-node continuum elements are employed. The coefficient of variation of the yield stress is assumed to be 0.10. The static response, as a function of the loading, is calculated by an implicit algorithm.

The mean displacement, the variance of the displacement, the mean bending stress and the variance of the bending stress are shown in Figs. 4a to 4d. The coefficient of variation of the displacement at the free end is found to be 0.069 and that of the stress at the fixed end is 0.087. The results are compared with those of a Monte Carlo simulation with 400 realizations and they are in excellent agreement.

The convergence of the random field discretization error, as defined in Eq. (5.2.13), is plotted in Fig. 2a. The rate of convergence is found to be 1.325. The eigenvalues of the covariance matrix are plotted in Fig. 2b. Based on the distribution, 4 out of the 16 largest eigenvalues were chosen. The mode-shapes, corresponding to these 4 largest and 4 smallest eigenvalues, are shown in Figs. 3a and 3b, respectively. The latter, clearly, play no role in representing a smooth autocorrelation, as is assumed here; if the field is highly uncorrelated these modes will be necessary. This resulted in a 95% accuracy in the variance of the stress at the wall (Fig. 2d).

The exact autocorrelation and the discretized autocorrelation for the Monte Carlo simulation of 400 realizations are compared in Fig. 2c; the autocorrelation is along the length of the beam, w.r.t. the yield stress at the wall. This amply demonstrates that this sample size would be sufficient to bring out the response correlation characteristics, and that the first-order filter captures the correlation characteristics quite well.

The spatial autocorrelation of the displacements at two different loads, along the length of the beam, are depicted in Figs. 5a and 5b. The spatial autocorrelation of the stresses along the length of the beam, at these loads, are depicted in Figs. 5c and 5d. The displacement autocorrelation is w.r.t. the free end displacement and the stress autocorrelation is w.r.t. the wall stress. In the first loading, 4 element layers (16 elements) near the fixed end are yielded and in the second loading 10 element layers (64 elements) are yielded. The displacements along the length of the beam show almost complete correlation with one another, irrespective of the correlation characteristics of the yield stress. The stresses, because of their direct dependence on the material properties, exhibit a varying autocorrelation along the length of the beam just like the random yield stress. Interestingly, the results of stress autocorrelation by PFEM and MCS are smooth and in good agreement in those elements that have yielded (in the mean sense) (Figs. 5c and 5d). In other elements the results show disagreement and oscillations in both PFEM and MCS results. In many of these elements, the mean stress is well below the

mean yield stress and so the randomness of the yield stress has a very insignificant effect on the stress values, as measured by the stress variances. Figs. 5c and 5d show that the stresses in the unyielded portion of the beam are highly uncorrelated to those in the yielded position. It is interesting to note that although the material law is highly nonlinear, the second order moment method which underlies PFEM agrees very well with Monte Carlo simulations.

(2) Elastic/Plastic Bar with Plastic Modulus as a Random Field

The problem statement is depicted in Fig. 6a. The plastic modulus E_T is assumed to be a Gaussian random field along the length of the bar. The material is assumed to be elastic-plastic with isotropic hardening. As can be seen from Fig. 6a, the yield stress is spatially a linear function for the mean and an exponential function for the autocorrelation. The coefficient of variation is assumed to be 0.10 and the random field is discretized so that q = NUMEL = 32. The probabilistic equations are solved by the explicit predictor algorithm [12] with a slight numerical damping ($\gamma = 0.55$). A near-critical time step ($\Delta t = 0.000455$) is used to keep the number of time steps minimal, subject to the stability conditions.

The mean and the variance of the displacement at the free end are shown in Figs. 6b and 6c. The coefficient of variation of the displacement at the free end is found to be ~0.05. The results are compared with those of a Monte Carlo simulation with 400 realizations and they are in excellent agreement. For both examples, the PFEM needed

much less computer time than the MCS. Also, only the largest 8 of the 32 eigenvalues are found to be sufficient to predict the displacement mean and covariance with a 99% accuracy.

In second moment PFEM, the superposition of the covariances of the response for two different, uncorrelated (to each other) random fields in a structure is the same as when both the random fields are present simultaneously. For example, the results of a bar with only the yield stress as the random field and those of the bar with only the plastic modulus as the random field can be superposed. The summed results will be the same as that of the bar with both the random fields present. When 'N' random fields are present, they are divided into 'n' groups ($n < N$) such that the fields within a group are correlated to one another and uncorrelated to those in the other groups. The PFEM results for each of these groups can then be simply summed, as in the case of 2 uncorrelated random fields. This is, of course, not possible in simulation where the entire calculations have to be repeated. For the purpose of probabilistic analysis in multi-component systems, this is an added advantage of PFEM over the simulation methods.

Schematic of PFEM

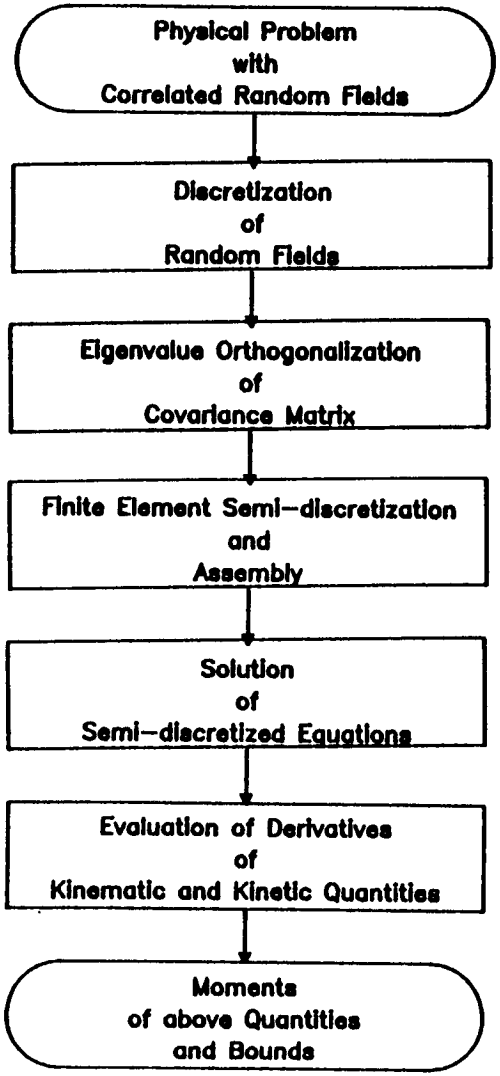

Figure 1a

Elastic/Plastic Cantilever Beam

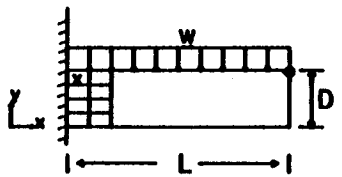

D =10.0
L =40.0
ρ =.00776
E =30.X10^6
E_T =30.X10^5
w_{max} =625.0

4X16 4-Node Continuum Elements
85 Nodes
Stress at x, Disp. at o Reported

Expectation of Yield Stress

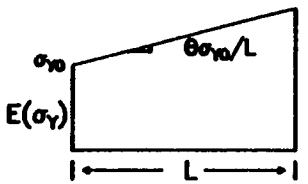

Θ =0.1
σ_{Y0} =25000.0

Autocorrelation of Yield Stress

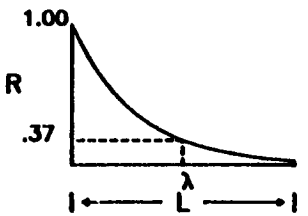

λ=0.5L

Problem 1

Figure 1b

Convergence of Yield Stress Covariance

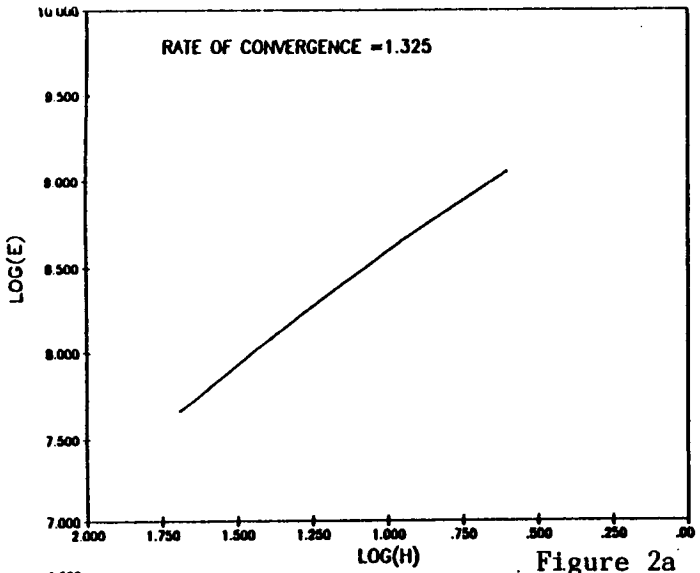

Figure 2a

Distribution of Eigenvalues of Yield Stress

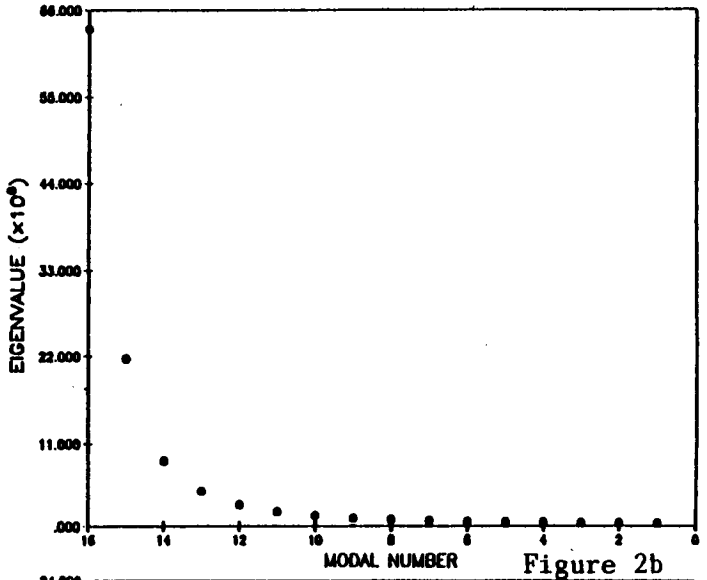

Figure 2b

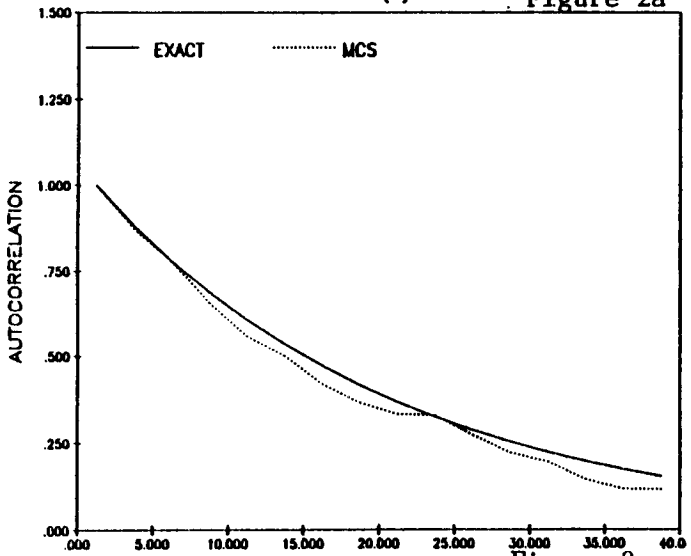

Figure 2c

Autocorrelation of Yield Stress by MCS

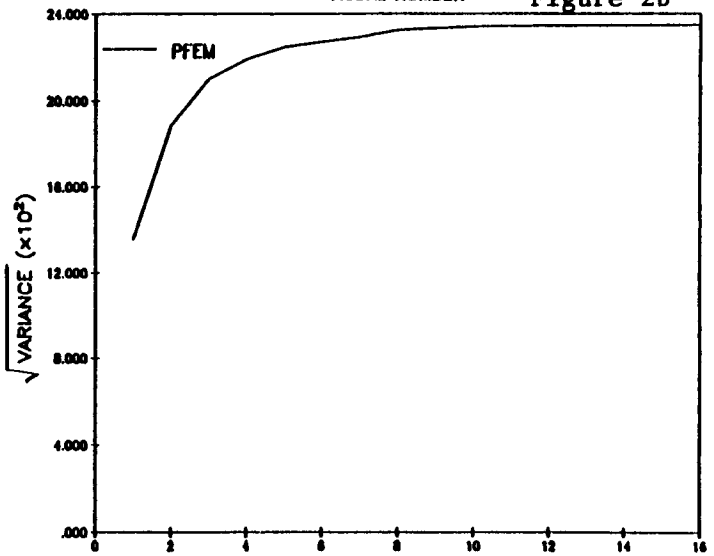

Figure 2d

Convergence of Variance of Stress

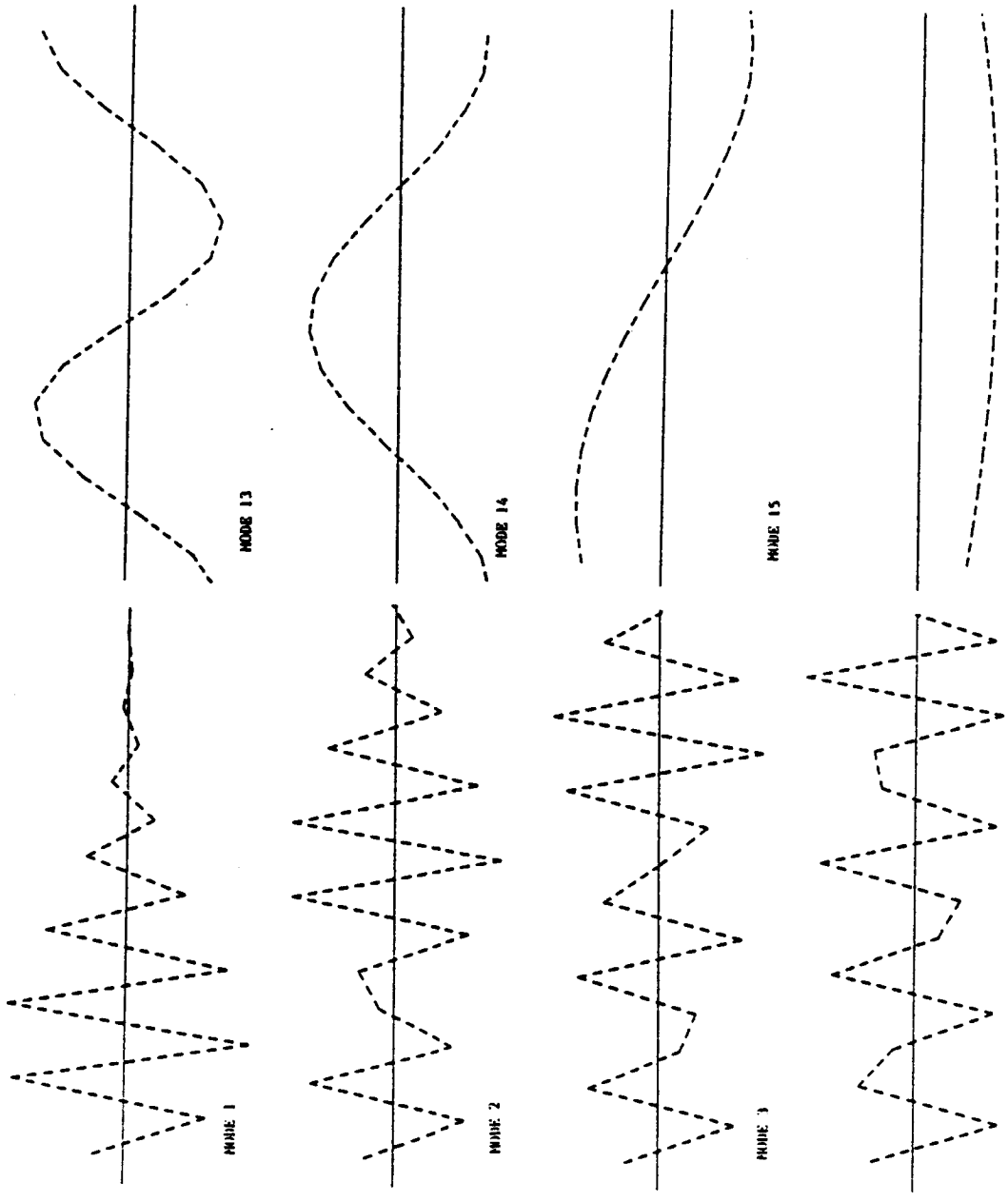

Some Negligible Modes

Figure 3a

Most Dominant Modes

Figure 3b

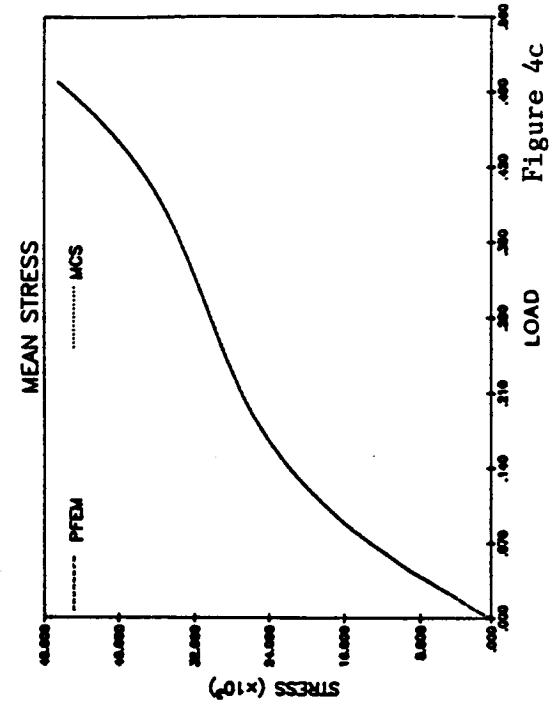

Figure 4c

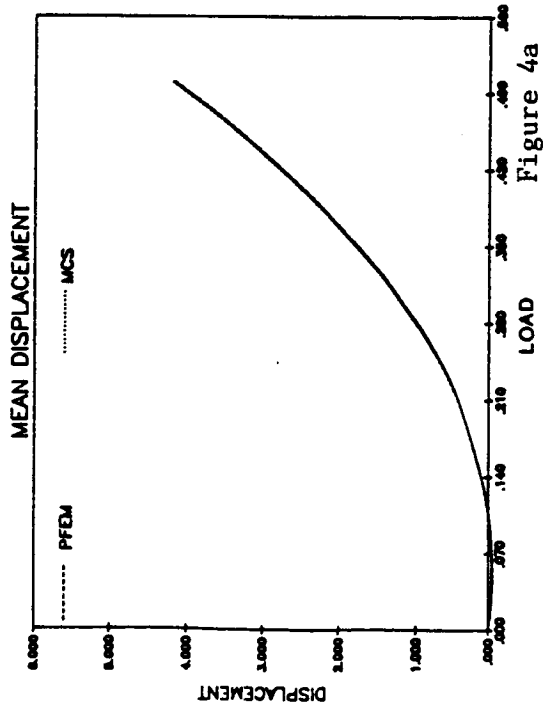

Figure 4a

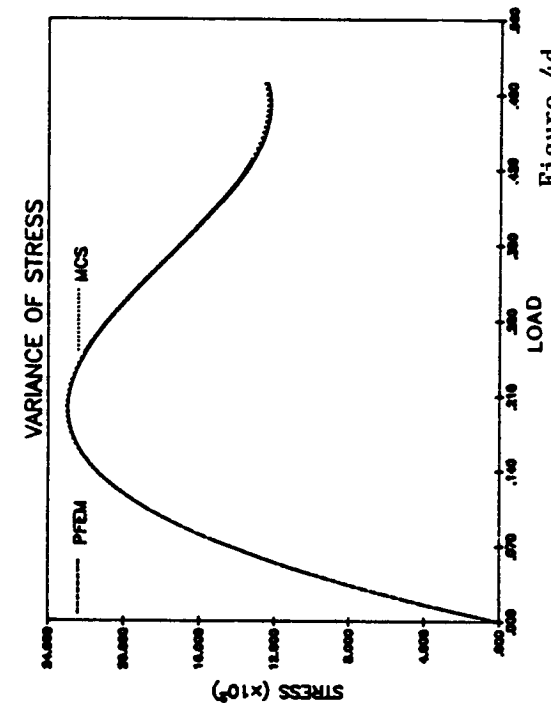

Figure 4d

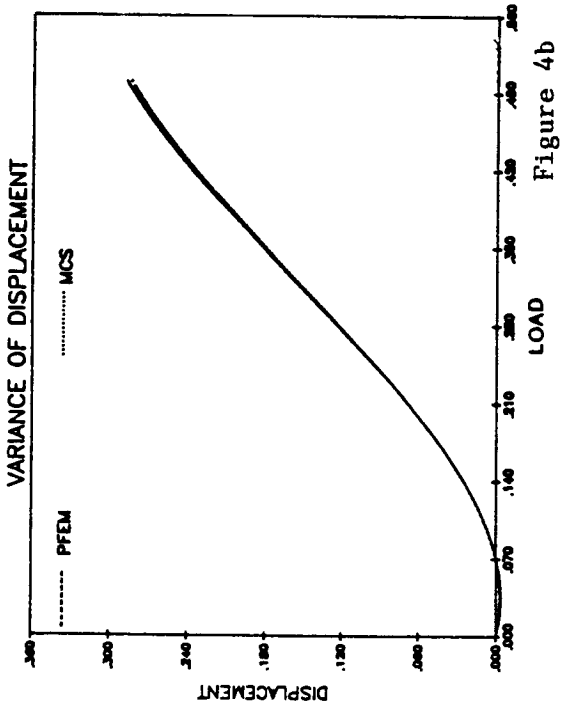

Figure 4b

Autocorrelation of Displacement (Load 1)

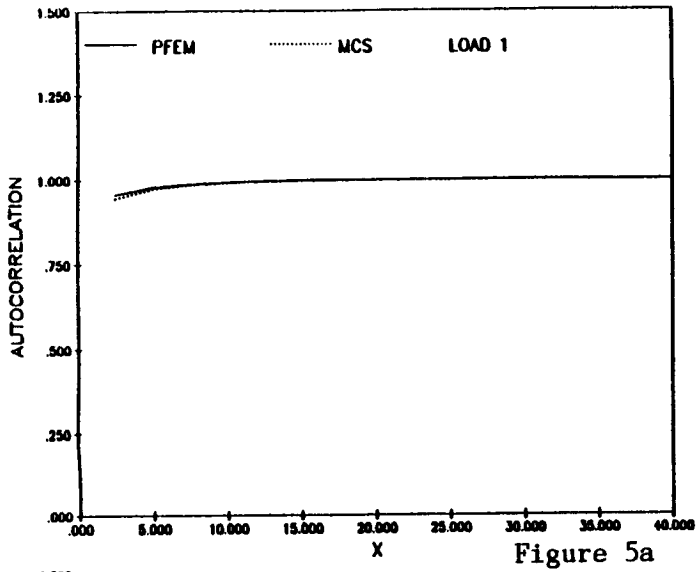

Figure 5a

Autocorrelation of Stress (Load 2)

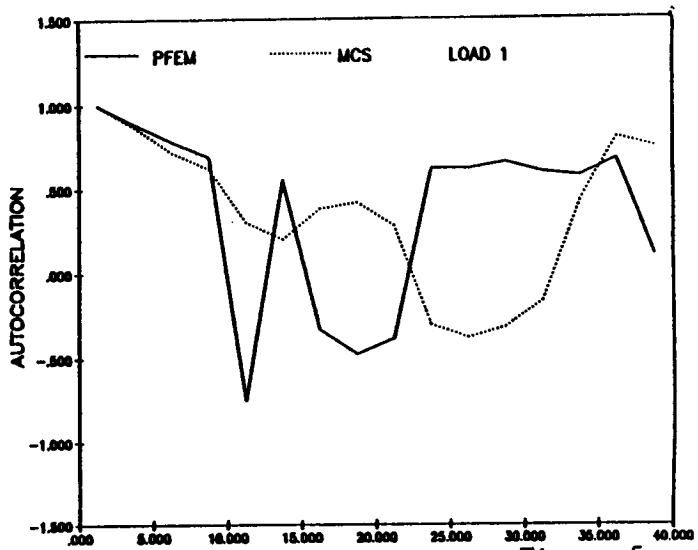

Figure 5c

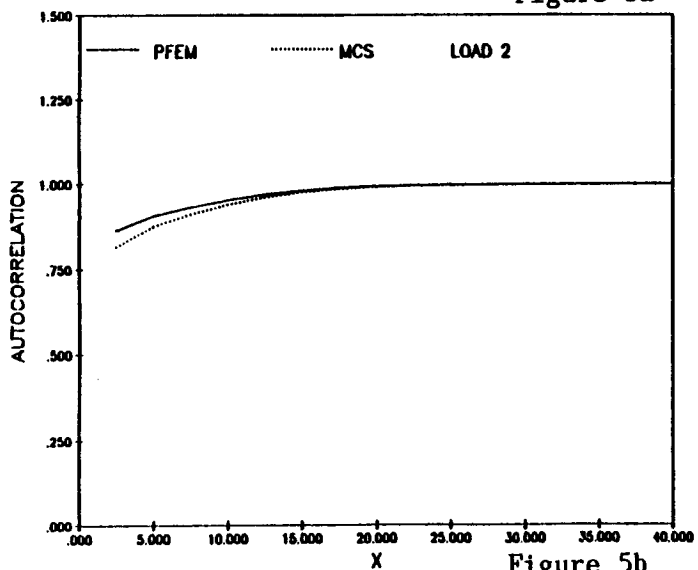

Figure 5b

Autocorrelation of Displacement (Load 2)

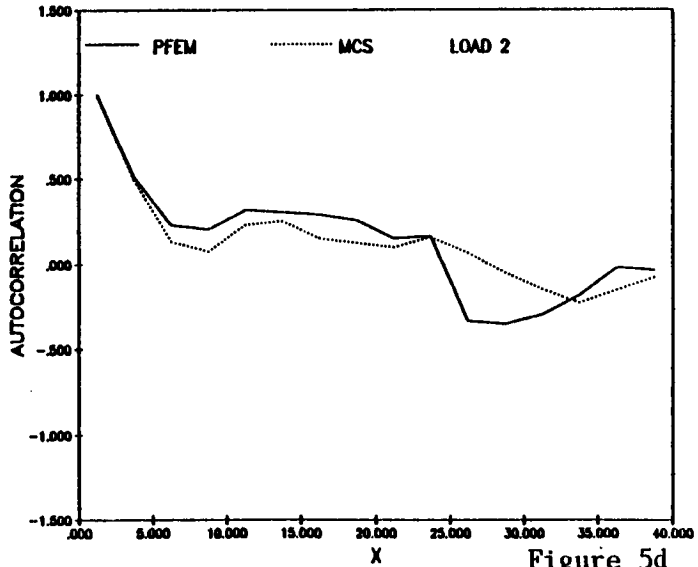

Figure 5d

Autocorrelation of Stress (Load 2)

Elastic/Plastic Bar with End Load

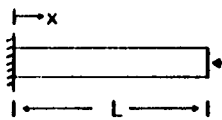

A =6.0
L =1000.0
ρ =.00776
E =30.X10^6
σ_Y=25000.0

Expectation of Plastic Modulus

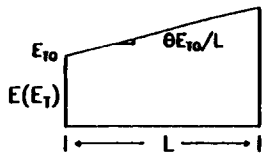

Θ =0.1
E_{TO} =30.X10^4

Autocorrelation of Plastic Modulus

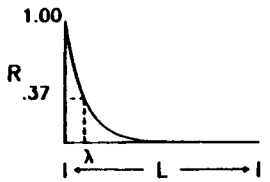

λ=0.1L

Forcing Function

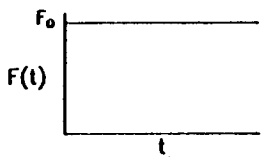

F_o=25.X10^4

Problem 2

Figure 6a

Comparison of Mean Displacement

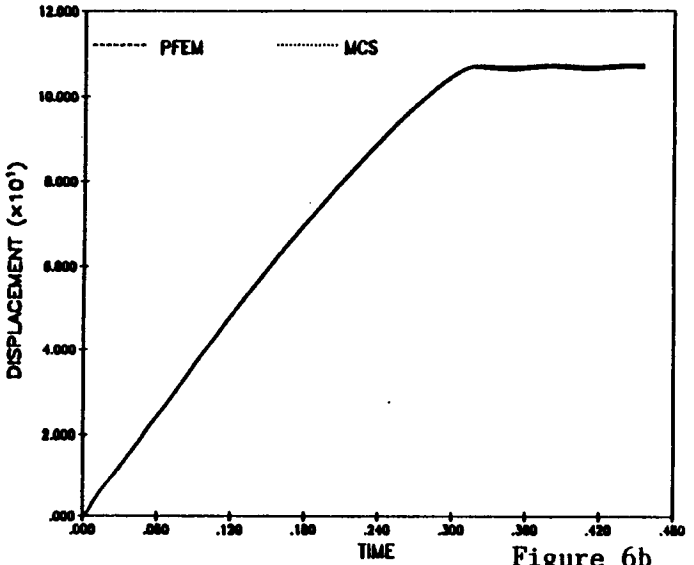

Figure 6b

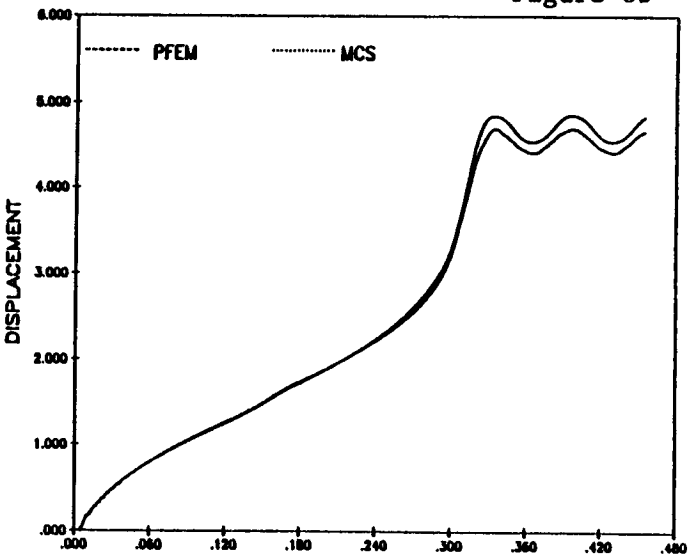

Figure 6c

Comparison of Variance of Displacement

CHAPTER 6

SUMMARY AND CONCLUSIONS

The theme of this study was to develop and apply efficient probabilistic finite element methods for various classes of problems in structural and solid mechanics. In nonlinear problems the main issue addressed was the evaluation of the higher order derivatives of the stresses and the internal nodal forces with respect to the random variables (Chapter 2). It was shown that finite-differencing was a fairly accurate way of approximating these derivatives. Applications in truss structures were studied and the results agree with those of Monte Carlo simulation and Hermite-Gaussian quadrature. It was also discovered that the higher-order equations involve secular terms which caused the solutions to deteriorate with time. Damping did not mitigate the problem and other remedies were suggested to eliminate secular terms. Secular terms, however, do not arise when only the external forces are random. The spatial discretization procedure of the random field resulting in the mean vector and the covariance matrix was outlined in Chapter 3, along with a simple check on the discretization accuracy. The popular eigenvalue transformation technique to obtain a vector of uncorrelated variables has also been implemented in PFEM. This reduced the computations from a quadratic to a linear dependence on the number of random variables. Furthermore, it was observed that a reduced set of the uncorrelated variables was sufficient to model the randomness. Each variable represented a mode of correlation and depending on the strength of correlation adequate number of modes had to

be included. In general, the higher the correlation the lesser was the number of modes that were required. The eigenvalues of the transformation were weighting factors in the superposition of modes. Whereas in Chapters 2 and 3 the PFEM equations were derived from the equations of motion, it was demonstrated in Chapter 4 that they can be quite as easily derived from variational principles. For linear continua, the equations were derived from the potential energy variational principle and for nonlinear continua undergoing large deformation the corresponding equations were derived from the principle of virtual work with appropriate stress and strain measures. Also, for elastoplastic materials, a direct method of evaluating the stress derivatives was outlined. An important advantage in deriving the PFEM equations from variational principles is the ease of incorporating the random geometry.

Various applications were studied in truss structures, bar, beams and plates and the results compare favorably with those of Monte Carlo simulation. It was noticed that the second order terms have negligible contribution to the mean response. It was also noticed that the strength of correlation did not affect the magnitude of the response moments appreciably. However, this may not be the case when the structural reliability has to be calculated. With the use of adjoint method it was demonstrated that the response moments can be selectively computed in a desired portion of the structure. Some applications in elastic-plastic dynamics were studied in detail in Chapter 5. Most uncertainties seem to linearly affect the response (i.e., a 10% c.o.v.

of a random property gives to not more than 10% c.o.v. of the displacement or stress). It was also noticed the displacements in any structure were always perfectly correlated regardless of the correlation level among the random variables. This was not the case for stresses, however. Unlike stress, which can exhibit sudden variation in a structure as in stress concentration, the displacement field in a structure is a smooth function by nature. Alternatively, from the finite element context, the external force is obtained by integrating the stresses over the domain and then the displacements are obtained. This integration process results in a smooth displacement field.

Based on the work in this research, the following suggestions are made for further work:

1. Methodologies for modeling mixed random boundary conditions, with PFEM. Direchlet and Neumann boundary conditions, with random magnitudes, can be easily incorporated in PFEM as random external forces. However, mixed boundary conditions are not so easily modeled. Example: A beam may not be fully clamped or fixed.
2. Second-moment based reliability techniques are available for mostly linear systems. The major issue in nonlinear systems is the computation of the response gradients. By incorporating some of the techniques outlined in this report, this computation may be done, accurately and efficiently. In limited situations, the response moments themselves may be used to calculate reliability.
3. As PFEM involves solution of a set of independent first-order equations, in addition to the zeroth and the second-order equations,

the first order equations can be processed in parallel. The solution sequence would be: solution of the zeroth-order equation first, parallel solution of the first-order equations next and finally the solution of a single second-order equation. In solving the higher order equations, the already decomposed stiffness matrix can be made use of.

REFERENCES

CHAPTER 1

1. Lin, Y. K., "Probabilistic Theory of Structural Dynamics," McGraw-Hill, 1967.

2. Ang, A. H. S. and Tang, W. H., "Probability Concepts in Engineering Planning and Design," Volume I, Basic Principles, John Wiley and Sons, 1975.

3. Vanmarcke, E., "Random Fields, Analysis and Synthesis," MIT Press, Second Printing, 1984.

4. Breiman, L., "Probability and Stochastic Processes: With a View Toward Applications," Houghton-Mifflin Company, Boston, 1969.

5. Caughey, T. K., "Nonlinear Theory of Random Vibrations," Advances in Applied Mechanics, 11, C. S. Yih, ed., Academic Press, New York, 209-253, 1971.

6. Ma, F., "Extension of Second Moment Analysis to Vector-Valued and Matrix-Valued Functions," in preparation.

7. Ma, F., "Approximate Analysis of Linear Stochastic Systems with Colored Multiplicative Noise," to be published in International Journal of Engineering Science.

CHAPTER 2

1. Haftka, R. T., "Techniques for Thermal Sensitivity Analysis," International Journal for Numerical Methods in Engineering, 17, 71-80, 1981.

2. Liu, W. K. and Belytschko, T., Progress Report to NASA - "Variational Approach to Probabilistic Finite Elements," December 1984.

3. Newmark, N. M., "A Method of Computation for Structural Dynamics," Journal of Engineering Mechanics Division, ASCE, 85, 67-94, 1959.

4. Liu, W. K., Belytschko, T. and Zhang, Y. F., "Implementation and Accuracy of Mixed-Time Implicit-Explicit Methods for Structural Dynamics," Computers & Structures 19 (4), 521-530, 1984.

5. Liu, W. K., Belytschko, T. and Mani, A., "Probabilistic Finite Elements for Transient Analysis," presented at the ASME Winter Annual Meeting, Miami, November 1985.

CHAPTER 3

1. McKay, M. D., Beckman, R. J., Conover, W. J., "A Comparison of Three Methods for Selecting Values of Input Variables in the Analysis of Output from a Computer Code," Technometoics, Vol. 21, No. 2, May 1979.

2. Tocher, K. D., "The Art of Simulation," Van Nostrand, 1963.

3. Raj, Des., "Sampling Theory," McGraw-Hill, 1968.

4. Larson, H. J., "Probabilistic Models in Engineering Sciences," V1-2, John Wiley, 1979.

5. Ang, A. H. S. and Tang, W. K., "Probability Concepts in Engineering Planning and Design," Volume I, Basic Principles, John Wiley and Sons, 1975.

6. Vanmarcke, E., "Random Fields, Analysis and Synthesis," MIT Press, Second Printing, 1984.

7. Lin, Y. K., "Probabilistic Theory of Structural Dynamics," McGraw-Hill, 1967.

8. Rosenblatt, M., "Remarks on a Multivariate Transformation, Annals of Mathematical Statistics, Vol. 23, No. 3, September 1952, pp. 470-472.

9. Ma, F. and Wei, M. S., "On the Synthesis of Porous Random Fields for Groundwater Flow," Computer-Aided Engineering, ASME PVP-Vol. 98-5, pp. 237-242, 1985.

10. Gorman, M., "Structural Resistance Moments by Quadratures," Structural Safety, 2, pp. 73-81, 1984.

11. Contreras, H., "The Stochastic Finite-Element Method," Computers & Structures, Vol. 12, pp. 341-348, 1980.

12. Lawrence, M. A. and Ang, A. H. S., "A Galerkin-Based Stochastic Finite Element Method," Abstract presented at ASME/ASCE Meeting, June 24-26, 1985, Albuquerque, New Mexico.

13. Nakagiri, S., Hisada, T. and Toshimitsu, K., "Stochastic Time-History Analysis of Structural Vibration with Uncertain Damping," ASME, PVP-Vol. 93, pp. 109-120, June 1984.

14. Cornell, C. A., "First Order Analysis of Model and Parameter Uncertainty," Int. Sym. on Uncertainties in Hydodogic and Water Resource Systems, Univ. of Arizona, Tucson, 1972.

15. Liu, W. K., Belytschko, T. and Mani, A., "Probabilistic Finite Element Methods in Nonlinear Structural Dynamics," to appear in Computer Methods in Applied Mechanics and Engineering.

16. Liu, W. K., Belytschko, T. and Mani, A., "A Computational Method for the Determination of the Probabilistic Distribution of the Dynamic Response of Structures," Computer-Aided Engineering, ASME PVP-Vol. 98-5, pp. 243-248, 1985.

17. Ma, F., "Approximate Analysis of Linear Stochastic Systems with Colored Multiplicative Noise," to be published in Int. Jour. of Eng. Sci.

CHAPTER 4

1. Ditlevsen, O., Reliability, Theory and its Application in Structural and Soil Mechanics, Christensen, P. T., ed., Martinus Nijhoff Publishers, Boston, 1983.

2. Ang, A. H. S. and Tang, W. K., Probability Concepts in Engineering Planning and Design, Volumes I and II, Wiley, 1984.

3. Hasofer, A. M. and Lind, N. C., "An Exact and Invariant First Order Reliability Format," Journal of Engineering Mechanics Division, ASCE, Vol. 100, EM1, pp. 111-121, 1974.

4. Rackwitz, R. and Fiessler, B., "Structural Reliability Under Combined Random Load Sequences," Journal of Computers and Structures, Vol. 9, pp. 489-494, 1978.

5. Wirsching, P. M. and Wu, Y. T., "Advanced Reliability Methods for Structural Evaluation," Advances in Aerospace Structural Analysis, Burnside, O. H. and Parr, C. H., eds., pp. 75-85, WAM, ASME, Miami Beach, 1985.

6. Caughey, T. K., "Nonlinear Theory of Random Vibrations," Advances in Applied Mechanics, Vol. 11, Yih, C. S., ed., Academic Press, New York, pp. 209-253, 1971.

7. Lin, Y. K., Probabilistic Theory of Structural Dynamics, McGraw-Hill, New York, 1967.

8. Kiureghian, A. D., "Structural Response to Stationary Excitation," Journal of Engineering Mechanics Division, ASCE, Vol. 106, No. EM6, pp. 1195-1213, 1980.

9. Adomian, G., Stochastic Systems, Academic Press, New York, 1983.

10. Shinozuka, M., "Basic Analysis of Structural Safety," Journal of the Structural Division, ASCE, Vol. 109, No. 3, pp. 721-740, 1983.

11. Igusa, T. and Kiureghian, A. D., "Modal Decomposition Method for Stationary Response of Nonclassically Damped Systems," Earthquake Engineering and Structural Dynamics, Vol. 12, No. 1, pp. 121-136, 1984.

12. Spanos, P. T. D. and Iwan, W. D., "On the Existence and Uniqueness of Solutions Generated by Equivalent Linearization," International Journal of Nonlinear Mechanics, Vol. 13, pp. 71-78, 1978.

13. Spanos, P. T. D., "Stochastic Linearization in Structural Dynamics," Applied Mechanics Review, Vol. 34, No. 1, pp. 1-8, 1981.

14. Baber, T. T. and Wen, Y. K., "Stochastic Response of Multi-Story Yielding Frames," Earthquake Engineering and Structural Dynamics, Vol. 10, pp. 403-416, 1982.

15. Sues, R. M., Wen, Y. K. and Ang, A. H. S., "Stochastic Evaluation of Seismic Structural Performance," Journal of the Structural Division, ASCE, Vol. 111, No. 6, pp. 1204-1219, 1985.

16. Tocher, K. D., The Art of Simulation, Van Nostrand, 1963.

17. Raj, Des., Sampling Theory, McGraw-Hill, 1968.

18. McKay, M. D., Beckman, R. J. and Conover, W. J., "A Comparison of Three Methods for Selecting Values of Input Variables in the Analysis of Output from a Computer Code," Technometrics, Vol. 21, No. 2, 1979.

19. Gorman, M., "Structural Resistance Moments by Quadratures," Structural Safety, 2, pp. 73-81, 1984.

20. Ma, F., "Approximate Analysis of Linear Stochastic Systems with Colored Multiplicative Noise," Int. Jour. of Eng. Sci., Vol. 24, pp. 19-34, 1986.

21. Nakagiri, S., Hisada, T. and Toshimitsu, K., "Stochastic Time-History Analysis of Structural Vibration with Uncertain Damping," ASME, PVP-Vol. 93, pp. 109-120, 1984.

22. Soong, T. T., Random Differential Equations in Science and Engineering, Academic Press, New York, 1973.

23. Lax, M. D., "The Method of Moments for Linear Random Boundary Value Problems," SIAM Journal of Applied Mechanics, Vol. 31, No. 1, 1976.

24. Liu, W. K., Belytschko, T. and Mani, A., "Probabilistic Finite Element Methods for Nonlinear Structural Dynamics," Computer Methods in Applied Mechanics and Engineering, Vol. 56, pp. 61-81, 1986.

25. Liu, W. K., Belytschko, T. and Mani, A., "Random Field Finite Elements," International Journal of Numerical Methods in Engineering, Vol. 23, pp. 1831-1845, 1986.

26. Liu, W. K., Belytschko, T. and Mani, A., "Applications of Probabilistic Finite Element Methods in Elastic/Plastic Dynamics," Journal of Engineering for Industry, ASME, Vol. 109, pp. 2-8, 1987.

27. Liu, W. K., Besterfield, G. and Belytschko, T., "A Variational Approach to Probabilistic Finite Element Methods," submitted to Journal of Engineering Mechanics Division, ASCE, 1987.

28. Liu, W. K., Belytschko, T., Besterfield, G. H. and Mani, A., "Probabilistic Finite Elements and Potential Applications to Fractures," presented at the 4th Army Conference on Applied Mathematics and Computing, May 27-30, 1986.

29. Lawrence, M. A., "A Basis Random Variable Approach to Stochastic Finite Elements," to appear in International Journal of Numerical Methods in Engineering.

30. Szopa, J., "Response of Stochastic Linear System," Journal of Engineering Mechanics Division, ASCE, Vol. 107, No. EM1, pp. 1-11, 1981.

31. Tsokos, C. P. and Padgett, W. J., Random Integral Equations with Applications to Stochastic Systems, Springer-Verlag, Berlin, Germany, 1971.

32. Haug, E. J., Arora, J. S. and Feng, T. T., "Sensitivity Analysis and Optimization of Structures for Dynamic Response," ASME J. Mech. Design, Vol. 100, No. 2, pp. 311-318, 1978.

33. Arora, J. S. and Haug, E. J., "Methods of Design Sensitivity Analysis in Structural Optimization," AIAA J., Vol. 17, No. 9, pp. 970-974, 1979.

34. Haftka, R. T., "Second Order Sensitivity Derivatives in Structural Analysis," AIAA J., Vol. 20, No. 12, pp. 1765-1766, 1982.

35. Ryu, Y. S., Maririan, M., Hu, C. C. and Arora, J. S., "Structural Design Sensitivity Analysis of Nonlinear Response," Computers and Structures, Vol. 21, No. 1/2, pp. 245-255, 1985.

36. Krieg, R. D. and Key, S. W., "Implementation of a Time Independent Plasticity Theory into Structural Computer Programs," Constitutive Equations in Viscoplasticity: Computational and Engineering Aspects, AMD 20, ASME, New York, 1976.

37. Liu, W. K., "Development of Finite Element Procedures for Fluid-Structure Interaction," National Technical Information Service Report NTIS-PB82-147984, 1982.

38. Liu, W. K., Belytschko, T. and Chen, J. S., "Nonlinear Versions of Flexurally Superconvergent Elements," to appear in Computer Methods in Applied Mechanics and Engineering.

CHAPTER 5

1. Tocher, K. D., "The Art of Simulation," Van Nostrand, 1963.

2. Raj, Des., "Sampling Theory," McGraw-Hill, 1968.

3. Larson, H. J., "Probabilistic Models in Engineering Sciences," Vl-2, John Wiley, 1979.

4. McKay, M. D., Beckman, R. J. and Conover, W. J., "A Comparison of Three Methods for Selecting Values of Input Variables in the Analysis of Output from a Computer Code," Technometrics, Vol. 21, No. 2, May 1979.

5. Gorman, M., "Structural Resistance Moments by Quadratures," Structural Safety, 2, pp. 73-81, 1984.

6. Ang, A. H. S. and Tang, W. K., "Probability Concepts in Engineering Planning and Design," Volumes I and II, Basic Principles, John Wiley and Sons, 1984.

7. Lin, Y. K., "Probabilistic Theory of Structural Dynamics," McGraw-Hill, 1967.

8. Ma, F., "Approximate Analysis of Linear Stochastic Systems with Colored Multiplicative Noise," Int. Jour. of Eng. Sci., Vol. 24, pp. 19-34, 1986.

9. Contreras, H., "The Stochastic Finite-Element Method," Computers & Structures, Vol. 12, pp. 341-348, 1980.

10. Lawrence, M. A. and Ang, A. H. S., "A Galerkin-Based Stochastic Finite Element Method," Abstract presented at ASME/ASCE Meeting, June 24-26, 1985, Albuquerque, New Mexico.

11. Nakagiri, S., Hisada, T. and Toshimitsu, K., "Stochastic Time-History Analysis of Structural Vibration with Uncertain Damping," ASME, PVP-Vol. 93, pp. 109-120, June 1984.

12. Liu, W. K., Belytschko, T. and Mani, A., "Probabilistic Finite Element Methods in Nonlinear Structural Dynamics," to appear in Computer Methods in Applied Mechanics and Engineering.

13. Liu, W. K., Belytschko, T. and Mani, A., "Random Field Finite Elements," to appear in International Journal of Numerical Methods in Engineering.

APPENDICES

1. Krieg, R. D. and Key, S. H., "Implementation of a Time Independent Plasticity Theory into Structural Computer Programs," Constitutive Equations in Viscoplasticity: Computational and Engineering Aspects, AMD 20, ASME, New York, 1976.

2. Liu, W. K., "Development of Finite Element Procedures for Fluid-Structure Interaction," National Technical Information Service Report NTIS-PB82-147984, 1982.

APPENDIX A: REVIEW OF MONTE CARLO SIMULATION METHODS AND HERMITE-GAUSS QUADRATURE SCHEMES

A.1 Monte Carlo Simulation Methods

Various Monte Carlo Simulation techniques are now available. In our analysis, the "simple" Monte Carlo method is used. The important feature about the Monte Carlo method is its flexibility. In other words, the computational procedures are the same irrespective of whether the model is linear or nonlinear so long as the solution can be obtained from the governing equation.

The main idea behind Monte Carlo simulation methods is to randomly generate values of the random variables subject to the probability density function and to calculate the output corresponding to these values. From this set of output, the probabilistic distribution properties, such as the mean and variance, are statistically estimated.

In the analysis of the two degrees of freedom probabilistic system, a normal random generator is used. This normal random number generator, RANF, is available on the Northwestern University CDC system. It has been well tested and for large sample size, the distribution is close to normal. This "closeness" can also be estimated by the so called Central Limit Theorem, which states as follows: "if a population has a finite variance σ^2 and mean value μ, then the distribution of the sample mean approaches the normal distribution with variance σ^2/n and mean μ as the sample size n increases." The sample size used in this analysis is 400. Both the spring constants K_1 and K_2 are randomly generated and the corresponding displacement solutions are calculated using the exact

deterministic solutions.

A.2 Implicit Time Integration with Hermite Gauss Quadrature Scheme

Let us consider a linear two degrees of freedom probabilistic system

$$\underset{\sim}{M}\,\underset{\sim n+1}{a} + \underset{\sim}{K}\,\underset{\sim n+1}{d} = \underset{\sim n+1}{F} \tag{A.2.1}$$

where

$$\underset{\sim}{M} = \begin{bmatrix} m_1 & 0 \\ 0 & m_2 \end{bmatrix} \; ; \quad \underset{\sim}{K} = \begin{bmatrix} K_1+K_2 & -K_2 \\ -K_2 & K_2 \end{bmatrix} \; ; \quad \underset{\sim}{F} = \begin{Bmatrix} 0 \\ F(t) \end{Bmatrix} \tag{A.2.2}$$

n is the time step number and the initial conditions $\underset{\sim o}{d}$, $\underset{\sim o}{v}$ and $\underset{\sim o}{a}$ are given. At each time step n, Eq. (A.1) is solved by the Newmark-β algorithm with $\beta = 0.25$, $\gamma = 0.5$ and $\Delta t = 0.02\ T_{min}$ where T_{min} is the smallest fundamental period. The finite difference matrix equation can be shown to be

$$\underset{\sim}{K}^{eff}\,\underset{\sim n+1}{d} = \underset{\sim}{F}^{eff} \tag{A.2.3}$$

where

$$\underset{\sim}{K}^{eff} = \underset{\sim}{M} + \beta\Delta t^2 \underset{\sim}{K} \tag{A.2.4}$$

$$\underset{\sim}{F}^{eff} = \beta\Delta t^2 \underset{\sim}{F}_{n+1} + \underset{\sim}{M}\, \underset{\sim}{\tilde{d}}_{n+1} \tag{A.2.5}$$

$$\underset{\sim}{\tilde{d}}_{n+1} = \underset{\sim}{d}_n + \Delta t\, \underset{\sim}{v}_n + (\tfrac{1}{2} - \beta)\, \Delta t^2\, \underset{\sim}{a}_n \tag{A.2.6}$$

and

$$\underset{\sim}{\tilde{v}}_{n+1} = \underset{\sim}{v}_n + \Delta t\, (1 - \gamma)\, \underset{\sim}{a}_n \tag{A.2.7}$$

Once $\underset{\sim}{d}_{n+1}$ is determined from Eq. (A.2.3), i.e.,

$$\underset{\sim}{d}_{n+1} = (\underset{\sim}{K}^{eff})^{-1}\, \underset{\sim}{F}^{eff} \tag{A.2.8}$$

$\underset{\sim}{a}_{n+1}$ and $\underset{\sim}{v}_{n+1}$ can be determined as follows

$$\underset{\sim}{a}_{n+1} = (\underset{\sim}{d}_{n+1} - \underset{\sim}{\tilde{d}}_{n+1})/\beta\Delta t^2 \tag{A.2.9}$$

and

$$\underset{\sim}{v}_{n+1} = \underset{\sim}{\tilde{v}}_{n+1} + \gamma\Delta t\, \underset{\sim}{a}_{n+1} \tag{A.2.10}$$

The solution procedures are then repeated with n replaced by n + 1 until $n\Delta t$ greater or equal to a desired time. Since K_1 and K_2 are random variables, therefore, $\underset{\sim}{d}_{n+1}$ by Eq. (A.8) is "implicitly" a

function of K_1 and K_2. Using the basic definitions of mean and variance, the expected value of $\underset{\sim}{d}_{n+1}$ is

$$E[\underset{\sim}{d}_{n+1}] = \int_{-\infty}^{+\infty} \int_{-\infty}^{+\infty} \underset{\sim}{d}_{n+1}(K_1, K_2)\, f_{K_1}(K_1)\, f_{K_2}(K_2)\, dK_1\, dK_2 \qquad (A.2.11)$$

where $f_{K_1}(K_1)$ and $f_{K_2}(K_2)$ are the probability density functions for K_1 and K_2 respectively. In writing Eq. (A.2.11), the assumption that K_1 is uncorrelated to K_2 has been employed. Once the expected value is evaluated, the variance of $\underset{\sim}{d}_{n+1}$ can then be computed according to

$$Var(\underset{\sim}{d}_{n+1}) = E[\underset{\sim}{d}^2_{n+1}] - (E[\underset{\sim}{d}_{n+1}])^2 \qquad (A.2.12)$$

The Hermite Gauss Quadrature scheme is to approximate the double integrals which appears in Eq. (A.2.11) by

$$E[\underset{\sim}{d}_{n+1}] = \sum_{i=1}^{n1} \sum_{j=1}^{n2} w_i\, w_j\, \underset{\sim}{d}_{n+1}(K_1^i, K_2^j)\, f_{K_1}(K_1^i)\, f_{K_2}(K_2^j) \qquad (A.2.13)$$

where n1 and n2 are the number of integration points for K_1 and K_2 respectively, w_i and w_j are their corresponding weights. As might be figured from above equation, if the number of random variables is m, the number of simulations N is

$$N = n1 * n2 * .... * nm \qquad (A.2.14)$$

and N grows exponentially. Therefore, unless the number of random

variables is small, this method is not recommended. However, if a physical situation dictates that some of the random variables can be excluded in the calculations, N can then be reduced significantly. Under this circumstance, the Hermite Gauss Quadrature Scheme can be an efficient and accurate method. An example of this practical situation has been demonstrated in Chapter 2, Section 4. In the analysis of the ten-bar structure, it was predetermined that only four of the ten bars will yield and the yield stresses are chosen as normal random variables.

If 3 points are used in evaluating each normally distributed K_i in Eq. (A.2.13), the weight and quadrature points are

$$w_i = (1/6,\ 4/6,\ 1/6) \tag{A.2.15a}$$

and

$$K_i = (\mu - 3\sigma\ ,\ \mu\ ,\ \mu + 3\sigma) \tag{A.2.15b}$$

respectively. And for this "bias" integration procedure, the number of simulations required (for each time step n) is

$$N = 3 * 3 * 3 * 3 = 81 \tag{A.2.16a}$$

Whereas, if one cannot observe apriori that six of the ten bars will not yield, the number of simulations required becomes

$$N = 3^{10} = 59049 \qquad \text{(A.2.16b)}$$

which makes this a handicapped method.

APPENDIX B: RESONANT EXCITATION OF RESPONSE SENSITIVITIES

The equation of motion and the sensitivity equation for a single-degree-of-freedom spring-mass-damper system are

$$M \ddot{x} + C \dot{x} + K x = F(t) \tag{B.1}$$

$$M \frac{\partial \ddot{x}}{\partial b} + C \frac{\partial \dot{x}}{\partial b} + K \frac{\partial x}{\partial b} = \hat{F}(t) \tag{B.2}$$

where

$$\hat{F}(t) = \frac{\partial F}{\partial b} - \frac{\partial M}{\partial b} \ddot{x} - \frac{\partial C}{\partial b} \dot{x} - \frac{\partial K}{\partial b} x \tag{B.3}$$

M, C, K are assumed to be dependent on the parameter b; we are interested in the sensitivity of the response x(t) to this parameter b. Let F(t) be such that x(t) is stable. Under this condition it is shown below that the response sensitivity $\frac{\partial x}{\partial b}$ is resonantly excited.

The damped natural frequencies of the system Eq. (B.1) and the sensitivity Eq. (B.2) are the same. The excitation $\hat{F}(t)$ involves x, $\dot{x}$ and $\ddot{x}$ in Eq. (B.2) and is, therefore, a resonant excitation. Thus approximations for x(t), such as

$$x(b_o + \Delta b, t) \approx x(b_o, t) + \left(\frac{\partial x}{\partial b}\right)_{b=b_o} \Delta b + \frac{1}{2} \left(\frac{\partial^2 x}{\partial b^2}\right)_{b=b_o} \Delta b^2 \tag{B.4}$$

at b_o for any small interval Δb, are valid only for a short duration and the accuracy deteriorates rapidly thereafter.

Since the PFEM equations (2.7) in Chapter 2 use the first and second-order response sensitivities, they are valid for a short duration only. A similar phenomenon is also observed in the transient response of nonlinear structures. A possible explanation for this phenomenon is that the time 't' has a multiplying effect on the interval 'Δb' in the second and third terms in Eq. (B.4) and this results in the deteriorating accuracy. However, the PFEM equations developed in Section 2 of Chapter 2 are suitable for application when one is interested in a short-time history e.g., the response due to an impulsive load.

APPENDIX C: NUMERICAL ALGORITHM FOR STRESS AND DISPLACEMENT DERIVATIVES

For materials with random elastoplastic properties, such as yield stress or plastic modulus, the finite-difference based derivatives (Eq. (4.4.15b), Chapter 4) can be evaluated explicitly without recourse to the solution of the equilibrium equation at each finite-differencing point; the stiffness matrix, corresponding to the mean configuration of the random properties, needs to be decomposed only once. This configuration is represented by the vector $\underset{\sim}{c}$ of size q. Subsequently, the displacement derivatives can be calculated by forward reduction and back substitution in Eq. (4.3.15a), Chapter 4. These computations are done in conjunction with the radial return method proposed in Ref. [1] and as implemented in Ref. [2].

For each element integration point, for every equilibrium iteration 'ν' in a given load step 'm', the following quantities are stored:

$\overline{\underset{\sim}{\tau}}^{\nu}$: stress

$\overline{\underset{\sim}{\alpha}}^{\nu}$: center of the von Mises yield surface

$\overline{k}^{\nu}$: radius of the yield surface

$\overline{\underset{\sim}{C}}_T$: tangent constitutive matrix

where the superposed "—" implies quantities evaluated at $\overline{\underset{\sim}{c}}$.

FLOWCHART

Part I Radial return for mean stresses and diplacements

Begin loop on load steps, m

⋮

Begin loop on iterations, ν

⋮

Begin loop on elements

⋮

Begin loop on integration points

a) Pick up $\overline{\underset{\sim}{c}}^{\nu}$, $\overline{\underset{\sim}{\alpha}}^{\nu}$, $\overline{k}^{\nu}$, $\overline{\underset{\sim}{C}}_T$

b) Compute the elastic trial stress increment $\Delta\overline{\underset{\sim}{\tau}}^{\nu}$ and update the stress to obtain the elastic trial stress $\overline{\underset{\sim}{\tau}}^{\nu+1}_{trial}$: $\overline{\underset{\sim}{\tau}}^{\nu+1}_{trial} = \overline{\underset{\sim}{\tau}}^{\nu} + \Delta\overline{\underset{\sim}{\tau}}^{\nu}$

c) Compute: $\overline{\underset{\sim}{\sigma}}^{\nu+1}_{trial}$ = deviatoric part of $(\overline{\underset{\sim}{\tau}}^{\nu+1}_{trial} - \underset{\sim}{\alpha}^{\nu})$ (C.1)

d) Compute: $\overline{\phi} = 3\overline{J}_2 - (\overline{k}_n)^2$ (C.2)

where $\overline{J}_2$ is the second invariant of stress and $\overline{\phi}$ is the yield function.

e) If $\overline{\phi} < 0$, $\overline{\underset{\sim}{\tau}}^{\nu+1} = \overline{\underset{\sim}{\tau}}^{\nu+1}_{trial}$; go to step h. (C.3)

If $\overline{\phi} > 0$, compute the plastic strain increment $\Delta\overline{d}^p$:

$$\Delta\overline{d}^p = (\sqrt{3\overline{J}_2} - \overline{k}^{\nu})/(3G + B) \quad (C.4)$$

where G and B are the shear modulus and plastic modulus, respectively. 'B' is further defined as:

$$B = \frac{EE_T}{E-E_T} \quad (C.5)$$

where E and E_T are the elastic and tangent moduli, respectively.

f) compute:

$$\Delta s = 3G\,\Delta\overline{d}^p\sqrt{3\overline{J}_2} \quad (C.6)$$

$$\Delta\alpha = (1 - \beta)B\,\Delta\overline{d}^p/\sqrt{3\overline{J}_2} \quad (C.7)$$

g) Correct stresses by radial return:

$$\overline{\underset{\sim}{\tau}}^{\nu+1} = \overline{\underset{\sim}{\tau}}^{\nu+1}_{trial} - \Delta s\,\overline{\underset{\sim}{\sigma}}^{\nu+1}_{trial} \quad (C.8)$$

$$\overline{\underset{\sim}{\alpha}}^{\nu+1} = \overline{\underset{\sim}{\alpha}}^{\nu} + \Delta\alpha\,\overline{\underset{\sim}{\sigma}}^{\nu+1}_{trial} \quad (C.9)$$

$$\overline{k}^{\nu+1} = \overline{k}^{\nu} + \beta B\,\Delta\overline{d}^p \quad (C.10)$$

h) Compute the tangent constitutive matrix $\overline{\underset{\sim}{C}}_T$ and assemble the tangent stiffness matrix

⋮

End loop on integration points

⋮

End loop on elements

⋮

End loop on iterations until equilibrium is satisfied. The stresses, strains and displacements, $\overline{\underset{\sim}{\tau}}_{m+1}$, $\overline{\underset{\sim}{\varepsilon}}_{m+1}$ and $\overline{\underset{\sim}{d}}_{m+1}$ are obtained from the final iteration.

⋮

Part II Displacement derivatives

The following quantities are also stored for each element integration point, in a given load step m, for each 'i' representing a random variable c_i:

$\underset{\sim}{\tau}_m^{+i}$, $\underset{\sim}{\tau}_m^{-i}$: stresses, near the mean $\overline{\underset{\sim}{c}}$

$\underset{\sim}{\alpha}_m^{+i}$, $\underset{\sim}{\alpha}_m^{-i}$: yield surface centers near the mean $\overline{\underset{\sim}{c}}$

k_m^{+i}, k_m^{-i}: yield surface radii, near the mean $\overline{\underset{\sim}{c}}$.

$\underset{\sim}{C}_T^{+i}$, $\underset{\sim}{C}_T^{-i}$: tangent constitutive matrices, near the mean $\overline{\underset{\sim}{c}}$,

where

$$\underset{\sim}{c}^{+i} = \bar{\underset{\sim}{c}} + (0, \ldots, \Delta c^i, \ldots, 0)^T \tag{C.11}$$

$$\underset{\sim}{c}^{-i} = \bar{\underset{\sim}{c}} - (0, \ldots, \Delta c^i, \ldots, 0)^T \tag{C.12}$$

and

$$\Delta \underset{\sim}{c}^i = \beta \bar{c}^i \quad , \quad 0.01 < \beta < 0.05 \tag{C.13}$$

Begin loop on 'i' for each random variable

⋮

Begin loop on elements

⋮

Begin loop on integration points

⋮

i) Compute the strain increment $\Delta\bar{\underset{\sim}{\varepsilon}}_m$ as

$$\Delta\bar{\underset{\sim}{\varepsilon}}_m = \bar{\underset{\sim}{\varepsilon}}_{m+1} - \bar{\underset{\sim}{\varepsilon}}_m \tag{C.14}$$

ii) Pick up $\underset{\sim}{\tau}_m^{+i}$, $\underset{\sim}{\alpha}_m^{+i}$, k_m^{+i}, $(\underset{\sim}{C}_T^{+i})_m$

iii) Compute the elastic trial stress $(\underset{\sim}{\tau}_{m+1}^{+i})^{trial}$

iv) Repeat steps (c) through (h) to finally obtain
$\underset{\sim}{\tau}_{m+1}^{+i}$, $\underset{\sim}{\alpha}_{m+1}^{+i}$, k_{m+1}^{+i}, $(\underset{\sim}{C}_T^{+i})_{m+1}$

v) Pick up $\underset{\sim}{\tau}_m^{-i}$, $\underset{\sim}{\alpha}_m^{-i}$, k_m^{-i}, $(C_T)_m^{-i}$ and repeat steps (iii) and (iv) to also obtain $\underset{\sim}{\tau}_{m+1}^{-i}$, $\underset{\sim}{\alpha}_{m+1}^{-i}$, $\underset{\sim}{k}_{m+1}^{-i}$, $(\underset{\sim}{C}_T^{-i})_{m+1}$

vi) Compute and store the first order finite-difference derivatives:

$$\frac{\partial \bar{\underset{\sim}{\tau}}_{m+1}}{\partial c_i} \approx \frac{\overset{+i}{\underset{\sim}{\tau}}_{m+1} - \overset{-i}{\underset{\sim}{\tau}}_{m+1}}{2\Delta c_i} \tag{C.15}$$

and

$$\frac{\partial \bar{\underset{\sim}{C}}_T}{\partial c_i} \approx \frac{\overset{+i}{\underset{\sim}{C}}_T - \overset{-i}{\underset{\sim}{C}}_T}{2\Delta c_i} \tag{C.16}$$

vii) Compute and assemble the forcing term $\underset{\sim}{f}_i'$ in Eq. (4.3.15b), Chapter 4; note that

$$\underset{\sim}{\psi}' = \frac{\partial \bar{\underset{\sim}{\tau}}_{m+1}}{\partial c_i} \tag{C.17}$$

in the equation.

End loop on integration points

⋮

End loop on elements

viii) Solve Eq. (4.3.15a), Chapter 4 to obtain the displacement derivatives $\frac{\partial \underset{\sim}{d}_{m+1}}{\partial c_i}$ and store.

Part III Stress derivatives

Begin loop on elements

⋮

Begin loop on integration points

ix) Compute stress derivatives as:

$$\left[\bar{\underset{\sim}{\tau}}_{m+1}\right]_{c_i} = \frac{\partial \bar{\underset{\sim}{\tau}}_{m+1}}{\partial c_i} + \bar{\underset{\sim}{C}}_T \bar{\underset{\sim}{B}} \left(\frac{\partial \underset{\sim}{d}_{m+1}}{\partial c_i}\right) \tag{C.18}$$

```
End loop on integration points
          :
          :
End loop on elements
          :
          :
End loop on random variables
          :
          :
End loop on load steps
```